11th ACES International Workshop

Marlborough Convention Centre

28 February – 3 March, 2023

Workshop Abstracts

Multi-physics *and* data-driven earthquake-tsunami modeling

Gabriel, A.-A.[1,2]

1. *Scripps Institution of Oceanography, UCSD, La Jolla, CA, USA*
2. *Ludwig-Maximilians-Universität München, Munich, Germany*

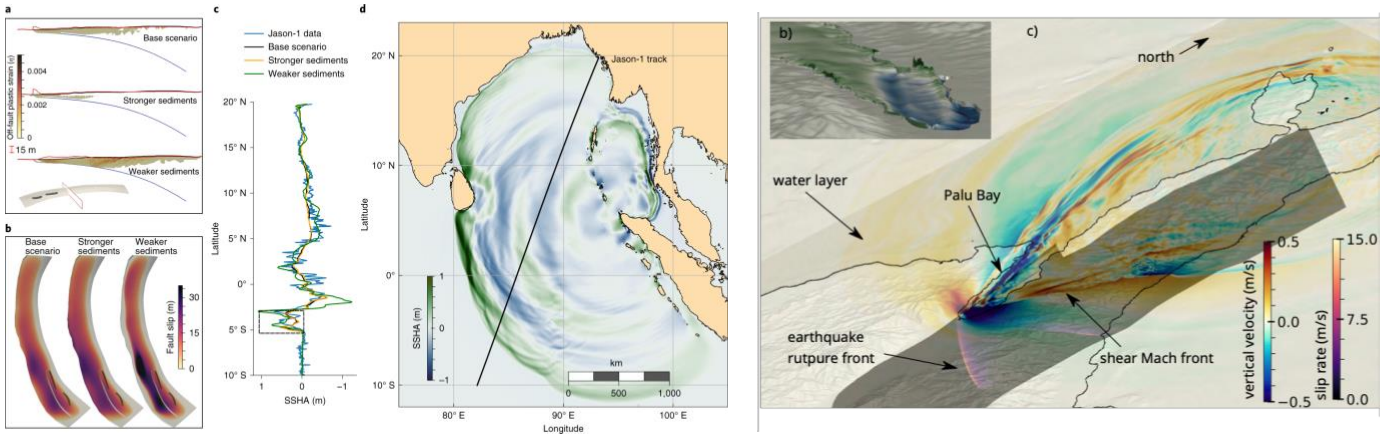

Figure 1. Left: Off-fault yielding and time-dependent tsunami generation in data-constrained and physics-based, linked earthquake dynamic rupture and tsunami simulations of the 2004 Sumatra events *[Ulrich et al., 2022]*. Right: 3D fully coupled acoustic-elastic simulation with gravity of the 2018 Sulawesi supershear earthquake and local tsunami in Palu Bay *(Krenz et al., 2021)*.

Determining the dynamics that control earthquakes and tsunami generation is critical to mitigate cascading geo-hazards but is impeded by structural complexity, large spatio-temporal scales and scarce or asymmetric instrumental coverage. I will demonstrate how to unify and verify the required initial conditions for geometrically complex, multi-physics earthquake–tsunami modelling from interdisciplinary geophysical observations [*Ulrich et al., 2022*]. Our 3D physics-based and data-driven numerical models can constrain the effects of fault geometries, tectonic loading, rigidity variations with depth, sediment strength on earthquake and tsunami dynamics verified by observables. In large-scale computational models of the 2004 Sumatra–Andaman earthquake and Indian Ocean tsunami we reconcile near- and far-field seismic, geodetic, geological, and tsunami observations and reveal tsunamigenic trade-offs between slip to the trench, splay faulting and bulk yielding of the accretionary wedge.

I will next present new highly scalable 3D fully-coupled earth and ocean modelling (using SeisSol) of seismic, acoustic and surface gravity wave propagation in elastic (Earth) and acoustic (ocean) materials sourced by physics-based non-linear earthquake dynamic rupture [*Krenz et al., 2021*]. Our new simulation capabilities open the possibility to fundamentally improve our understanding of earthquake-tsunami interaction in its full complexity, instead of relying on approximate 3D-2D linked methods. Not only is it now possible to capture the entire dynamics of this process in a unified 3D model; it is also efficient. Lastly, I will summarize a recent comparison of four earthquake-tsunami modelling methods *[Abrahams et al., 2022]* and discuss which methods are appropriate for various applications such as interpretation of data from offshore instruments in the source region.

Unusually fast and large tsunami generated by the 2022 Hunga Tonga – Hunga Ha'apai volcano eruption

Gusman, A.[1], Roger, J.[1], Noble, C.[2], Wang, X.[1], Power, W. [1], and Burbidge, D.[1]

1. *GNS Science, Lower Hutt, New Zealand*
2. *Meteorological Service of New Zealand, Wellington, New Zealand*

The Hunga Tonga – Hunga Ha'apai volcano eruption on 15 January 2022 generated a tsunami that was unusually fast and large, particularly at large distances from the source. Here we use an observation-calibrated air-wave model to simulate the tsunami generation process in a numerical model. We used pressure data observed at 94 stations in Niue, the Cook Islands, and New Zealand's main and outer islands to obtain a simple air-wave model. The modelled air-wave travels at an approximated constant speed of 317 m/s with an amplitude that decays proportional to the inverse square root of the distance from the volcano. We then simulated the generation and propagation of the tsunami due to the propagating air-wave in the atmosphere above the ocean. The leading sea surface displacement excited by the pressure disturbances travels at the same speed as the air-wave. This leading wave is then followed by subsequent water waves that travel in the same direction as the leading wave but at the conventional tsunami propagation speed (Figure 1). We found that the air-wave was more effective at generating tsunami when it travelled over a deep bathymetric feature like the Kermadec-Tonga Trench. The tsunami amplitudes observed at gauges do not decay as rapidly with distance from the volcano as would be expected for a localized tsunami source. This is due to the continuous excitation of the tsunami as the air-wave propagates across the ocean. In shallow water, the leading water surface displacement can often be much smaller than the later waves that were most likely to have been generated in the deep ocean. A better understanding of the complexities of tsunami generation and propagation from sources of this type is important for improving tsunami disaster mitigation in future events.

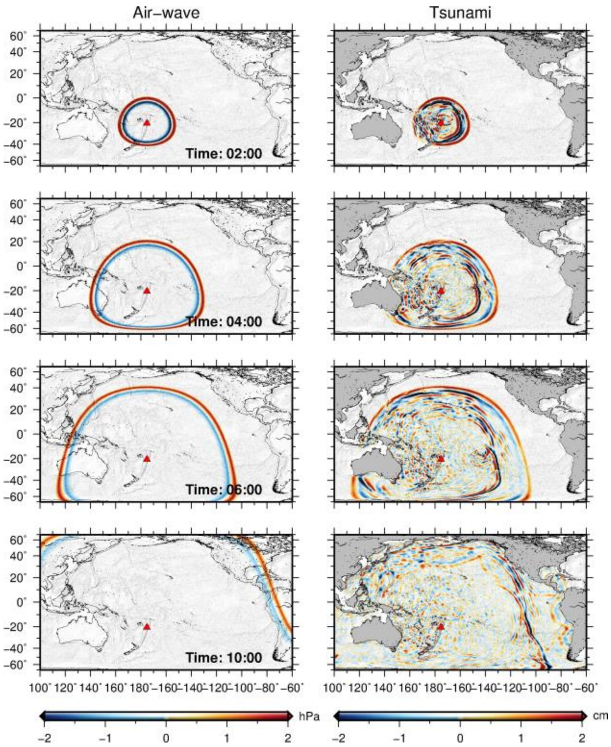

Figure 1. Snapshots of simulated air-wave (left panels) and tsunami (right panels). The indicated time is in hh:mm after the origin time that is estimated to be at 04:29 UTC.

Satellite altimetry and genesis of the 2022 Tonga volcanic tsunami

Y. Tony Song[1], Philip S. Callahan[1], Jean-Damien M. Desjonqueres[1], Severine Fournier[1] and Josh K. Willis[1]

[1]Jet Propulsion Laboratory, California Institute of Technology, Pasadena, CA, 91109

ABSTRACT

The 2022 Tonga volcanic eruption generated a surprisingly large air-pressure wave (lamb wave) and a locally damaging tsunami. The tsunami generation is still puzzling because both the air wave and submarine explosion drove changes in sea level. Here we have derived observational evidence from satellite altimetry (a rarity for a volcanic tsunami), assisted by a combined atmospheric and oceanic tsunami model, to shed light on its genesis. We found that three satellites had captured the sea level signal of the tsunami: the AltiKa satellite observed the near-field tsunami, 29 minutes after the eruption, while the Sentinel-6 Michael Freilich and Jason-3 satellites in tandem 30 seconds apart captured the tsunami through the volcano center and encountered the tsunami wave at about 54°S about 5 hours after the eruption. We proposed a mass-conserving tsunamigenic mechanism, which couples the volcanic ejecta to ocean waters filling in the erupted crater, to reconcile the satellite observations with other in-situ measurements. We concluded that the erupted air-waves had increased the tsunami's destructive power through the inverted barometer effect during their overlapping period in the near field, and orchestrated the far-field disturbance in the Pacific Ocean and beyond. Our study also demonstrated an altimetry procedure to isolate tsunamis from ocean dynamic features and a data-based approach to quantify volcanic tsunami source for early warnings.

Constraining Rupture Parameters of the 2010 M7.8 Mentawai Tsunami Earthquake Using Near-Field Simulated and Observational Data

Nye, T.[1], Sahakian, V. J.[1], and Melgar, D.[1]

1. *University of Oregon, Eugene, Oregon, USA*

We constrain values of key rupture parameters for the 2010 Mentawai tsunami earthquake (TsE). TsEs are rare, end-member earthquakes that generate tsunamis much larger than expected for their size and typically rupture the shallow megathrust. Currently, local tsunami early warning (TEW) systems have a difficult time identifying TsEs as threats because of their moderate magnitude (**M**~7-8) compared to typical hazardous tsunamigenic events (**M**~8.5-9). Methods involving energy-related ratios have previously been used to discriminate TsEs because these events radiate high frequency energy inefficiently [e.g., Newman and Okal, 1998; Newman et al., 2011]. However, such methods use teleseismic data and are inadequate for real-time discrimination. Thus, it is critical to use near-field data for timely warnings. Currently, near-field TsE data only exist for the 2010 **M**7.8 Mentawai TsE. We use a combination of near-field simulated and observational data for the Mentawai event to better understand the source physics of TsEs.

Using a set of semistochastic forward-modeling codes [Melgar, 2021], we generate synthetic rupture scenarios and waveforms patterned after the Han Yue et al. [2014] slip model. We modify the stress drop, rise time, and rupture velocity (V_{rupt}), as each of these rupture parameters is believed to be characteristically extreme for TsEs, to determine which combinations best reproduce the Mentawai TsE. We vary the stress drop between 0.01–5 MPa, the average rise time between 5–25 s, and the average V_{rupt} between 0.8–2.2 km/s. We compare characteristics of the synthetic waveforms with observed data by computing residuals (observed – synthetic) of time-to-reach peak ground displacement (tPGD), peak ground displacement (PGD), peak ground acceleration (PGA), peak ground velocity (PGV), and Fourier spectra bin averages. Figure 1 shows the expected residual trends using typical megathrust versus TsE parameters in our model.

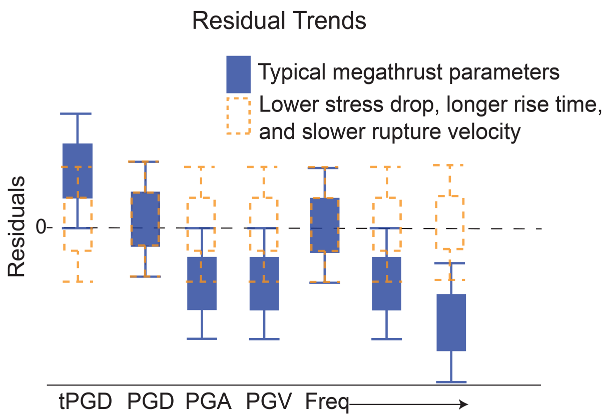

Figure 1. Expected residual trends for tPGD, PGD, PGA, PGV and Fourier amplitude spectra frequency bin averages.

We find stress drop and V_{rupt} to have the greatest influence on near-field observable intensity measures and thus are key rupture parameters in characterizing modeled TsE ground motion. We find rise time to have little influence on near-field observable intensity measures. Our final product is the expected mean and standard deviations for these rupture parameters, which can be used to generate synthetic TsE scenarios in other subduction zone environments. By characterizing TsE rupture parameters, we can improve TEW machine learning algorithms to be able to better identify these rare, but destructive events.

Probabilistic Assessment of Tsunami Hazards in New Zealand

Power, W.[1], Hughes, L.[2], Lane, E.[3], Savage, M.[2], Arnold, R.[2], Howell, A.[1,4], Shaw, B.[5], Fry, B.[1], Burbidge, D.[1], Gusman, A.[1], Nicol, A.[4]

1. *GNS Science, Lower Hutt, New Zealand*
2. *School of Geography, Environment and Earth Sciences, Victoria University of Wellington, New Zealand*
3. *National Institute of Water and Atmospheric Research (NIWA), Christchurch, New Zealand*
4. *University of Canterbury, Christchurch, New Zealand*
5. *Lamont Doherty Earth Observatory, Columbia University, Palisades NY, USA*

New Zealand is vulnerable to tsunami from a wide-variety of earthquakes and other sources, at distances which range from immediately adjacent to the coast to the other side of the Pacific Ocean. Among those close to New Zealand, earthquakes on the Kermadec, Hikurangi and Puysegur subduction zones all pose significant threats, as do many crustal faults as was demonstrated in the Kaikoura earthquake and tsunami in 2016. Appropriate mitigation of these hazards is greatly assisted by quantitative probabilistic assessment of the tsunami hazard. For this purpose a National Tsunami Hazard Model has been developed, and continues to evolve, along with procedures to convert estimates of tsunami hazard at the coast into probabilistic tsunami inundation maps. Currently, the hazard model processes tsunami heights using a synthetic catalogue of source events generated according to magnitude-frequency distributions assigned to each source. Here we present the development of an alternative approach to the estimation of tsunami hazard from local tsunami sources based on generating sythetic catalogues using a physics-based earthquake simulator (RSQSim - Rate and State Earthquake Simulator) that produces a set of complex rupture scenarios, allowing for interactions between faults, including multiple-fault ruptures, and generated in accord with physical constraints on slip rates. We demonstrate how this approach can be used to evaluate tsunami hazard at the coast from local sources (Figure 1), and how it may be used to evaluate inundation hazards, in both cases making use of COMCOT (the Cornell Multi-grid Coupled Tsunami model).

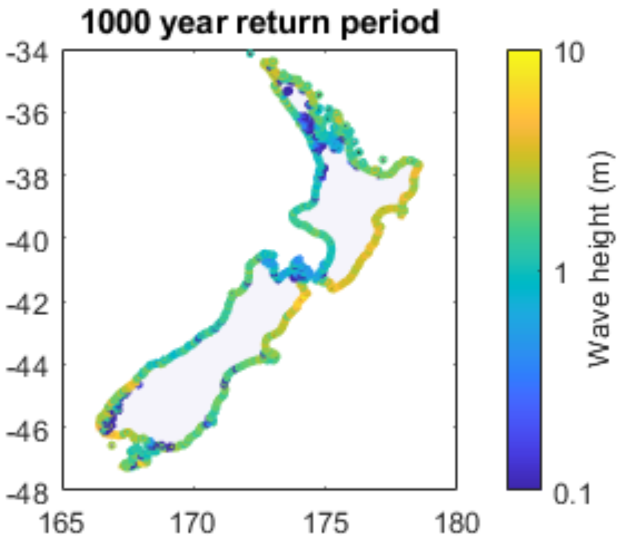

Figure 1. Estimated local-source tsunami hazard posed to New Zealand coastlines at a 1,000 year return period using an RSQSim-generated synthetic catalogue.

Lake Tsunami in Alpine Fault Earthquake Events – Numerical Studies in Lake Tekapo

Wang, X.[1], Holden, C.[2], Mountjoy, J.J.[3], Power, W.L.[1], and Liu, Y.[4]

1. *GNS Science, Lower Hutt, New Zealand*
2. *SeismoCity Ltd., Wellington, New Zealand*
3. *NIWA, Wellington, New Zealand*
4. *University of Tsinghua University, Beijing, China*

Recent research indicates that there is a 75% probability of a rupture on the central section of the Alpine Fault in New Zealand over the next 50 years, with an 82% probability that it will be a magnitude 8+ event. It is highly likely that such an earthquake would strongly shake Southern Lakes of New Zealand that are in close proximity to the fault, causing lake tsunami by the earthquake's ground motions and/or indirectly by seismically triggered landslides. Our two numerical studies in Lake Tekapo, one on seismic seiches and the other on landslide tsunami, provide insights into what might happen in these lakes.

To investigate seismic seiches in Lake Tekao, we applied 220-sec synthetic ground motions of an Mw8.2 Alpine Fault earthquake to the 3-D lake terrain (topography and lakebed) to drive lake water motions in a tsunami simulate model – COMCOT. Our modelling results reveal that lake water oscillations are mobilized immediately by the ground movement and further amplified by cross-lake seiches. Maximum amplitudes of the lake oscillations reach up to 4.0 m above normal lake level in the lake's narrow southern arm, up to 1.0 m along the shore of Lake Tekapo township, and about 1.5-2.5 m along many other parts of the lake shore (Figure 1). In contrast, vertical co-seismic displacements in the lake area, the conventional source mechanism used for tsunami generation, are too small to trigger tsunami waves of concern. In the other study, we numerically modelled landslide tsunami generated by individual subaerial, marginal, and subaqueaus mass failures, reconstructed from identified mass transport deposits, as well as by multiple mass failures. The numerial simulations show that landslide tsunami could push lake water up to over 5m above normal lake level at the shore of Tekapo township, overtop the lake Control Structure located 400-500 m downstream of the lake outlet, and flood further downstream.

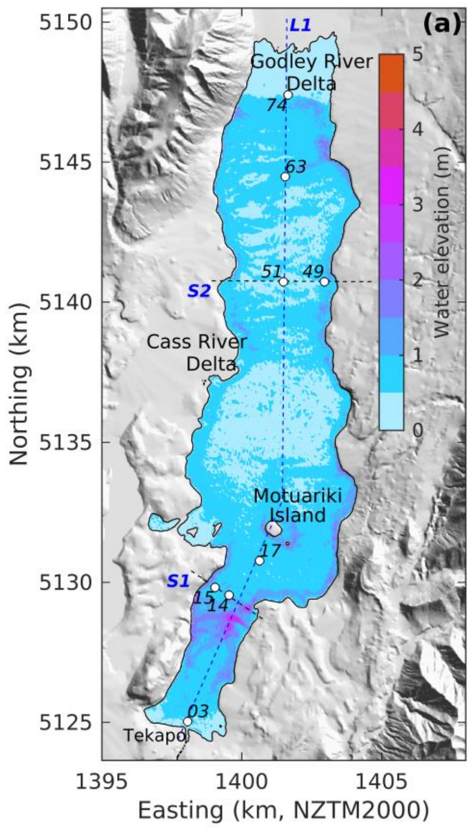

Figure 1. Maximum water elevations in Lake Tekapo caused by ground motions of an Mw8.2 Alpine Fault earthquake.

We conclude that in an magnitude 8+ Alpine Fault earthquake both seismic seiches and landslide tsunami could pose a significant threat to people and infrastructure in the water of Lake Tekapo, on the lake shorelines, and possibly at locations further downstream of the lake outlet.

A comparison of four subduction zones: The geodetic signatures of interseismic coupling and viscous mantle flow

Johnson, K.M.[1], Sherrill, E. [1], Burton, E.[1]

1. *Department of Earth and Atmospheric Sciences, Indiana University, Bloomington, IN, USA*

Elastic halfspace backslip models are widely used to model geodetic data at subduction zones because the models provide reasonable first-order descriptions of the interseismic coupling distribution on the subduction interface. Inversions of geodetic data with these models require regularization which usually implements some form of spatial smoothing. While these first order models are useful, they provide low-resolution images of interseismic coupling and often neglect time-dependent creep processes and viscous mantle flow. To further explore these limitations on resolution and time-dependent processes, we develop subduction zone coupling models that incorporate simple physical constraints on the distribution of creeping and locked regions on plate interfaces and distributed mantle flow and analyze data from four subduction zones: Northern Japan, Nankai, Cascadia and Hikurangi. In Northern Japan we find that decadal time-scale changes in coupling before the 2011 M9 Tohoku-oki earthquake can be explained with a simple physical model for shrinking asperities. Reduction in coupling over 10-15 years is explained with acceleration in creep surrounding locked asperities that reduce in size over time, following an analytical expression derived by Cattania and Segall using fracture mechanics. We find that an additional contribution to interseismic deformation must also come from relaxing interseismic flow in the mantle in order to explain both horizontal and vertical geodetic motions. At Nankai trough and Cascadia subduction zones we develop forward models that incorporate forward models with distinct boundaries delineating fully locked areas of the interface and regions that creep without stress accumulation (Figure 1). We further implement an analytical approximation for creep due to upward propagation of the lower locked zone. We conduct MCMC inversions and identify well-resolved spatial distributions of the boundaries surrounding fully locked regions on the interface. We further show that some features of the vertical geodetic signature in these regions are likely attributed to relaxing interseismic mantle flow. At the Hikurangi subduction zone we show that similar physically-constrained coupling models resolve a level of heterogeneity in interseismic coupling that is not fully revealed in kinematic backslip inversions.

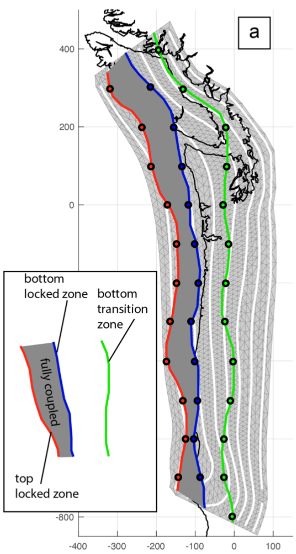

Figure 1. Delineation of subduction interface into locked and creeping zones. We conduct MCMC inversions for to the positions of the boundary nodes (small circles).

An Adjoint-based Optimization Method for Jointly Inverting Heterogeneous Material Properties and Fault Slip From Earthquake Surface Deformation Data

Puel, S.[1,2], Becker, T.W.[1,2,3], Villa, U.[3], Ghattas, O.[1,3,4], and Liu, D.[2]

1. *Department of Geological Sciences, The University of Texas at Austin, Austin, TX, USA*
2. *Institute for Geophysics, The University of Texas at Austin, Austin, TX, USA*
3. *Oden Institute for Computational Engineering and Sciences, The University of Texas at Austin, Austin, TX, USA*
4. *Walker Department of Mechanical Engineering, The University of Texas at Austin, Austin, TX, USA*

Analysis of coseismic and postseismic surface displacements can help constrain Earth structure and the physics of deformation mechanisms occurring at depth. Here, we propose a novel technique, based on an open-source finite-element modeling framework, to invert surface deformation data for inferring heterogeneous material properties, such as the Poisson's ratio or shear modulus in the crust and mantle wedge.

These inversions can be realized by using adjoint-based optimization methods, which efficiently reduce the misfit between the calculated and observed displacements. To quantify the associated model uncertainties, we extend the inverse approach to a Bayesian inference problem. Since the data are usually informative only in a few directions in parameter space, we use a low-rank Laplace approximation of the posterior distribution to make the inverse problem computationally tractable. The mean and the posterior covariance are approximated by the solution of the inverse problem (MAP point) and the inverse of the Hessian of the negative log posterior evaluated at the MAP point, respectively. We show how smoothly varying parameter fields can be reconstructed satisfactorily from noisy data.

To improve the spatial resolution of the inverse solution we solve a Bayesian optimal experimental design problem to find the best station configuration by maximizing the expected information gain, defined as the Kullback-Leibler divergence between posterior and prior distributions. We show how and why the optimal network improves the material property inference than evenly spaced stations.

Based on our previous work on inverting for fault slip without Green's function computations, we combine the two inversion schemes to jointly infer both model parameters, the coseismic slip and material properties distribution. The result demonstrates the potential of our computational framework for inferring both parameter fields with significant spatial resolution.

Lastly, we test this numerical forward/inverse framework with an application, the 2011 M9 Tohoku-oki earthquake in Japan. Both continuous land-based and six offshore acoustic GNSS stations located around the earthquake epicenter are inverted to jointly estimate the shear modulus and the fault slip during the megathrust event.

Detection of Plastic Strain Using GNSS Data of Pre- and Post-Seismic Deformation of the 2011 Tohoku-oki Earthquake

Fukahata, Y.[1], Meneses-Gutierrez, A.[2,3], and Sagiya, T.[3,4]

1. *Disaster Prevention Research Institute, Kyoto University, Japan*
2. *Institute for Advanced Research, Nagoya University, Japan*
3. *Disaster Mitigation Research Center, Nagoya University, Japan*
4. *Graduate School of Environmental Studies, Nagoya University, Japan*

In this study, we succeed in separating plastic deformation as well as viscous deformation in the northern Niigata-Kobe tectonic zone (NKTZ), central Japan, using GNSS data before and after the 2011 Tohoku-oki earthquake, under the assumptions that elastic deformation is principally caused by the plate coupling along the Japan trench and that plastic deformation ceased after the Tohoku-oki earthquake due to the stress drop caused by the earthquake. The cease of plastic deformation can be understood with the concept of stress shadow used in the field of seismic activity. The separated strain rates are about 30 nanostrain/yr both for the plastic deformation in the preseismic period and for the viscous deformation in both the pre- and post-seismic periods, which means that the inelastic strain rate in the northern NKTZ is about 60 and 30 nanostrain/yr in the pre- and post-seismic periods, respectively. This result requires the revision of the strain rate paradox in Japan (Figure 1). The strain rate was exceptionally faster before the Tohoku-oki earthquake due to the effect of plastic strain, and the discrepancy between the geodetic and geologic strain rates is much smaller in usual time, when the plastic strain is off. In oder to understand the onset timing of plastic deformation, the information on stress history is essentially important. This study is published by Fukahata et al. (2020, EPS).

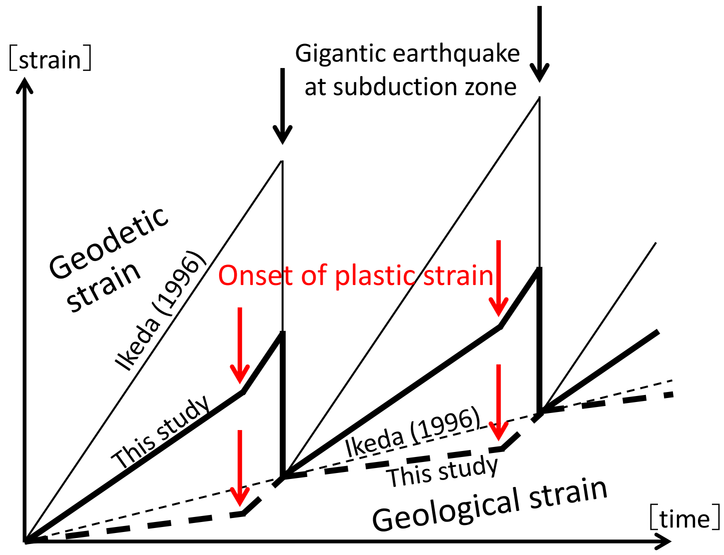

Figure 1. Revision of the strain rate paradox in Japan, advocated by Ikeda (1996). Ikeda's idea is shown by thin lines, while the revision by this study is by thick lines, which reflected a faster strain rate before a gigantic earthquake at subduction zone due to plastic deformation. Solid and broken lines represent geodetic and geological (inelastic) strain, respectively.

Evidence for Serpentinization in the Upper Mantle of SW North Island: Implications for Slow Slip and Gravity Anomalies

Stern, T. [1] and Dimech, J.[1,2]

1. *Victoria University, Wellington*
2. *Geoscience Australia, Canberra*

Deep seismic profiling (Fig.1) across South West North Island (SWNI) has provided evidence for serpentinization for parts of the upper mantle. This includes a reflection zone at a depth of ~ 50 km where both P-P and S-S reflections are generated. For the incidence angles of interest (10-20 degrees) this requires a drop in both P and S-wave speeds across the reflection interface. For another part of the profile we use the spectral decay method on reflection amplitudes to show that, rocks below the Moho require a large drop in Q_p (attenuation, or rock-quality, factor), suggesting a weak soft rock in the upper mantle. Finally, a seismic receiver function profile that runs from National Park to Whanganui city shows a relatively flat Moho, yet Bouguer gravity drops nearly 80 mgal along this same profile. A density inversion in the upper mantle is required to explain such a large drop in the observed gravity anomaly. In summary, we see evidence for a broad zone in the upper mantle of rocks of the SWNI that have low P- and S-wave speeds, are highly attenuative and are of a bulk density well below that required for the upper mantle. The most likely rock condition to meet all these requirements is a partially serpentinized upper mantle. This is not surprising as the cold and wet conditions in the upper mantle here are ideal for the peridotite to serpentinite (antigorite) transformation.

If this is correct then the deep (~ -100 to -150 mgal) gravity low that traverses from Hawke Bay, across the axial ranges, and into the Whanganui basin is, at least in part, likely to be due to serpentinite in the upper mantle. Deep slow-slip events of the SW North Island and Manawatu also show a spatial link to the deepest part of the gravity anomaly. We therefore propose there is a case for serpentinization being a possible source, or at least a contributing factor to, the cause of the deep slow slip events. This is not a new idea as serpentine has been linked to slow slip elsewhere in the world. It is not clear if this same process can explain the shallow slip events in the northeastern portion of the Hikurangi Margin. We do note, however, that serpentine is known to escape to the surface up a subduction channel and produce serpentinite-mud volcanoes in the forearc of the Mariannas.

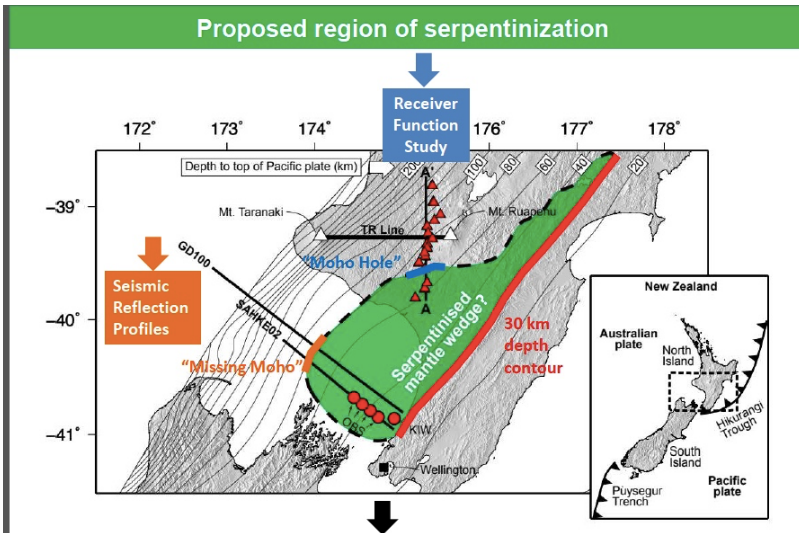

Generation and maintenance of low effective stress along faults by fluid flow in Laboratory and in Nature, and implications for Seismogenesis

Garagash, D.[1], Brantut, N.[2], Schubnel, A.[3], Bhat, H. [3], and Jolivet, R.[3]

1. *Dalhousie University, Halifax, Canada*
2. *University College London, UK*
3. *l'Ecole Normale Supérieure, Paris, France*

Near lithostatic pore fluid pressure and absolute weakness of continental transform faults at depth are suggested by observations of tidal triggering of slow slip at the base of San Andreas Fault (SAF) [Thomas et al 2009]. Mantle volatiles upwelling along deeply rooted faults at rates ~mm/year [Kennedy et al 1997] can lead to the elevated pore pressure [Rice 1992]. We show in a set of laboratory permeation experiments on micro-cracked rock samples that pore pressure does reach the level of imposed confining stress in ~ a half of the sample from the upstream end. Performed theoretical modeling of upwelling fluid flow in the lab and in nature settings shows, that the near-lithostatic pore pressure regime over the down-dip part of a fault can be explained by the effective-stress-hysteresis of the fault permeability (Fig. 1a).

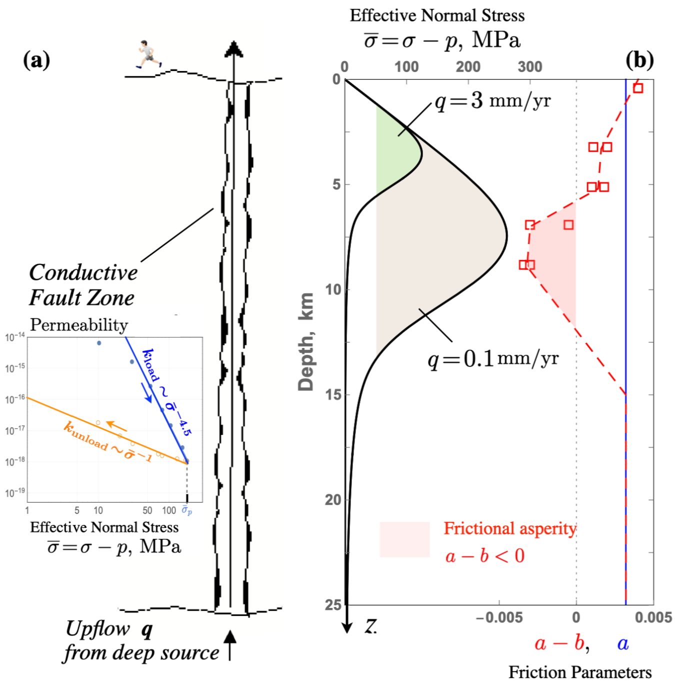

Fig. (a) Fault zone with deep fluid source *q* [Rice 1992] and hysteretic permeability [Wibberley 2002]. (b) Asperity-like distributions of effective stress: higher *q* leads to shallower and weaker stress-asperity. Friction parameter *a-b* for SAF [Moore et al, 2016].

We predict an asperity-like distribution of the effective-stress with depth in nature: increasing along the lithostatic-hydrostatic gradient in a shallower part and then rapidly decreasing to near-zero values along a deeper part of the fault (Fig 1b). The depth at the peak stress and its magnitude are decreasing functions of the upwelling fluid rate. For parameters representative of SAF fault rocks, varying fluid flow rate from low ~ 0.1 mm/yr to high ~ 3mm/yr results in upward migration of the diminishing stress asperity from about 7.5 km to 3 km depth.
Fault seismogenesis is linked to unstable, e.g. rate-weakening (*a*-*b*<0), friction rheology over a range of depth, i.e. a "frictional asperity". However, since the size of earthquake nucleation region is inversely dependent on effective stress [Rice 1993], an earthquake can nucleate within the frictional asperity only if it overlaps with the stress-asperity (Fig 1b). We show in 1D fault slip cycle simulations that seimogenic and aseismic/creeping segments of a fault such as SAF may stem from the *along-strike variability of the fluids supply* into the fault roots, which governs the overlap of the stress and frictional asperities, and not from differences in frictional rheology.

Spinning Up Earthquake Cycle Models

Allison, Kali[1]

1. *University of California Davis, California, USA*

One advantage of earthquake cycle simulations is that the behaviour of the system, once it's spun up, does not depend upon the choice of initial condition. In this talk, spin up is first defined in the context of a spring-slider model (a 1D earthquake cycle model). This is then generalized to 2D elasticity. Finally, the model is extended with the addition of several interseismic processes whose characteristic timescales can be comparable to, or longer than, the typical life-span of a strike-slip fault: power-law viscoelastic deformation, shear heating, and grain size evolution. The spin up time for cycle simulations with these processes scales with their characteristic timescales. As a result, spinning up the system can be quite computationally challenging. Thus, it is important to start these simulations with meaningful initial conditions, because the timescales involved are long enough that it is not feasible to brute force beyond memory of the initial conditions. Additionally, these very long timescales imply that the stresses, viscous strain rates, and grain size in the vicinity of a fault may not be well-represented by the assumption of steady-state. Going forward, we may want to relax the assumption of steady-state, and to instead consider the evolution of the fault and shear zone system.

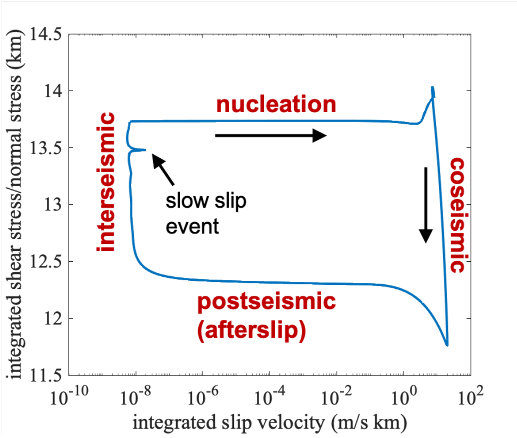

Figure 1. Phase diagram for a viscoelastic earthquake cycle simulation, showing the four phases of the earthquake cycle.

The role of frictional heterogeneities in the earthquake cycle, Blenheim, New Zealand, 28 February – 3 March, 2023

Liao, Y.-W. M..[1,2], Fry, B.[1], Howell, A.[1,2], Nicol, A.[2], Williams C.[1], and Rollins C.[1]

1. *GNS Science, Lower Hutt, New Zealand*
2. *University of Canterbury, Christchurch, New Zealand*

The determination of earthquake source models for seismic hazard assessments can be difficult and highly uncertain. Information such as recurrence interval of earthquakes for a given magnitude, earthquake origin and probability of multiple-segment rupture is often poorly constrained, especially for large earthquakes (M>7.0). Physics-based earthquake simulators offer a means of assessing uncertainties of hazard-related input parameters. Importantly, they also provide a pathway for future generations of seismic hazard models in which ground motions are calculated by modelling the seismic wave field, including the effects of variability in the earthquake source process. Earthquake simulators such as RSQSim, an earthquake simulator generating earthquakes basing on rate-and-state friction law, can generate long-term synthetic earthquake catalogs on a system of known faults, and help us have more understanding of the reccurence intervals of large earthquakes. However, the frictional stresses being inputted to RSQSim are simlified as a uniform number in the previous studies. This could produce characteristic earthquakes in the simulated catalogue. Thus, we introduce heterogeneity to the distribution of the frictional stresses to obtain more realistic and less characteristic catalogues for hazard assessment. We focus on a model of the Hikurangi-Kermadec subduction zone New Zealand is located at the southern end of this subduction zone, which has the potential to generate large (Mw>9.0) subduction earthquakes and is therefore very important to consider in seismic and tsunami hazard assessments. The state coefficient with fixed rate coefficient (b and a in rate-and-state equation) are also tested for reasonable coseismic slip values. The results are compared with the magnitude-frequency distribution (MFD) of the instrumental earthquake catalogue and the empirical scaling laws from global earthquakes. Considering the trade-off between the fitness to MFDs (Figure 1) and empirical scaling laws (Figure 2), the models with heterogeneous stresses and state coefficients of 0.002 and 0.003 can be the preferred stress settings for synthetic

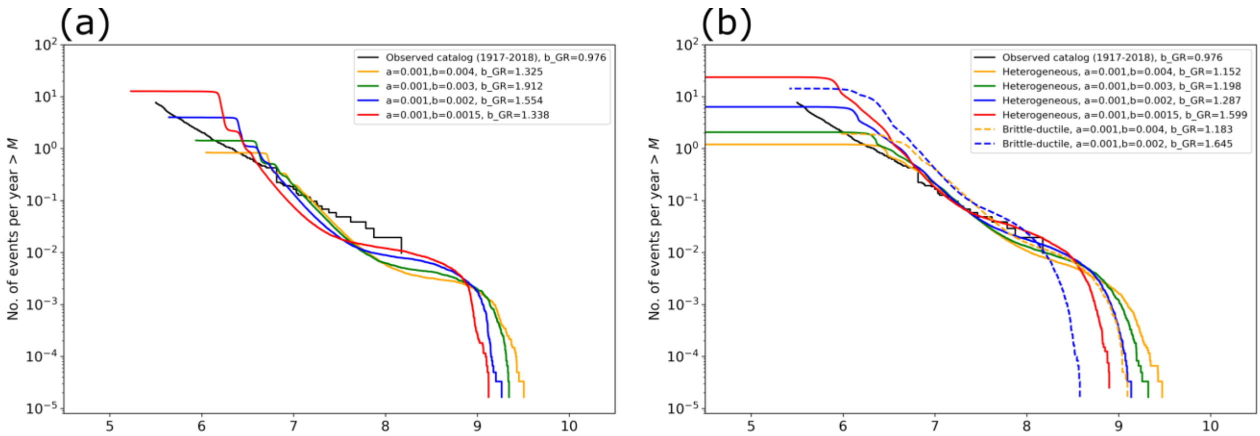

Figure 1. Magnitude-frequency distribution (MFD) of the models compared to the observed historical catalogue.

catalogue modeling of Hikurangi-Kermadec subduction interface. Heterogeneity of other stress-related parameters could also be applied to the RSQSim inputs as the next steps to improve the applicability of the synthetic earthquake catalogs to fundamental and applied seismic hazard problems.

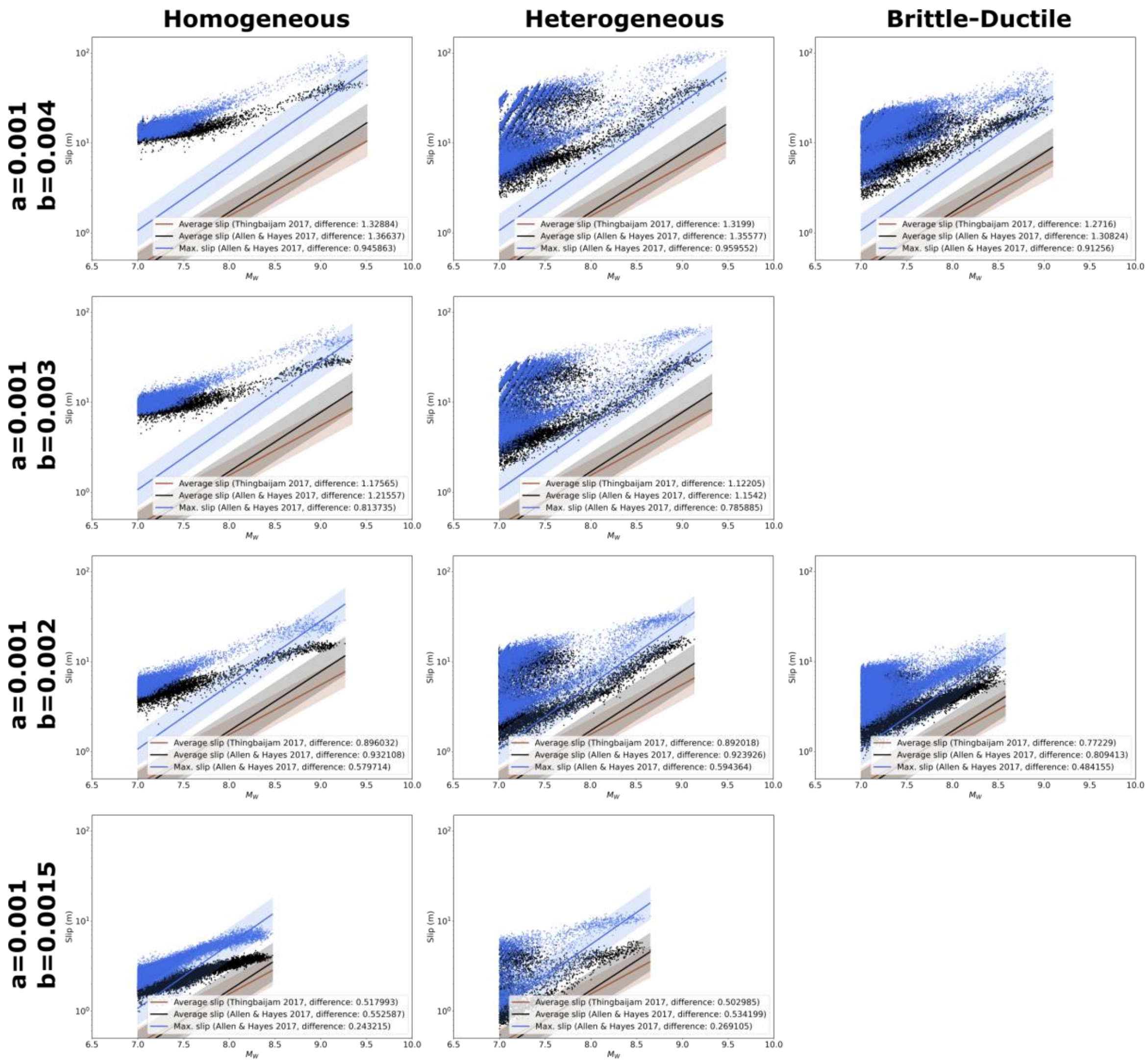

Figure 2. Scaling of maximum and average coseismic slip with earthquake magnitude. Columns from left to right are homogeneous, heterogeneous and brittle-ductile stress models respectively; rows from top to bottom are models with state coefficients of 0.004, 0.003, 0.002, and 0.0015 respectively. The maximum and average coseismic slip are presented as blue and black dots for earthquakes from the synthetic catalogues. Empirical scaling laws of maximum (blue lines) and average (black and brown lines) slips (Allen & Hayes, 2017; Thingbaijam et al., 2017) are also plotted as references for understanding how reasonable the synthetic slips are. The uncertainty of the empirical of the empirical scaling laws is represented by light blue (max slip), grey (average slip Allen and Hayes, 2017) and light brown (average slip Thingbaijam 2017).

Influence of Creep Compaction and Dilatancy on Earthquake Sequences and Slow Slip

Yang, Y.[1,2], Dunham, E.M.[2]

1. *The Chinese University of Hong Kong, Hong Kong*
2. *Stanford University, California, USA*

Fluids influence fault zone strength and the occurrence of earthquakes, slow slip events, and aseismic slip. We introduce an earthquake sequence model with fault zone fluid transport, accounting for elastic, viscous, and plastic porosity evolution, with permeability having a power-law dependence on porosity. Fluids, sourced at a constant rate below the seismogenic zone, ascend along the fault. While the modeling is done for a vertical strike-slip fault with 2D antiplane shear deformation, the general behavior and processes are anticipated to apply also to subduction zones. The model produces large earthquakes in the seismogenic zone, whose recurrence interval is controlled in part by compaction-driven pressurization and weakening. The model also produces a complex sequence of slow slip events (SSEs) beneath the seismogenic zone. The SSEs are initiated by compaction-driven pressurization and weakening and stalled by dilatant suctions. Modeled SSE sequences include long-term events lasting from a few months to years and very rapid short-term events lasting for only a few days; slip is ~1-10 cm. Despite ~1-10 MPa pore pressure changes, porosity and permeability changes are small and hence fluid flux is relatively constant except in the immediate vicinity of slip fronts. This contrasts with alternative fault valving models that feature much larger changes in permeability from the evolution of pore connectivity. Our model demonstrates the important role that compaction and dilatancy have on fluid pressure and fault slip, with possible relevance to slow slip events in subduction zones and elsewhere.

Seismicity of Regular and Slow Earthquakes in Relation to Seamount Subduction

Mochizuki, K.[1]

1. *Earthquake Research Institute, University of Tokyo, Tokyo, Japan*

The role of a subducted seamount at subduction zones has been one of the major subjects of studies about earthquake generation mechanisms (e.g. Wang and Bilek [2011]). Owing to recent establishments of offshore seismic networks and a growing number of offshore seismic observations, subsurface profiles of subducted seamounts and seismicity around them are becoming better resolved, especially in the following three regions: Southern Japan Trench, western Nankai Trough, and northern Hikurangi subduction zones.

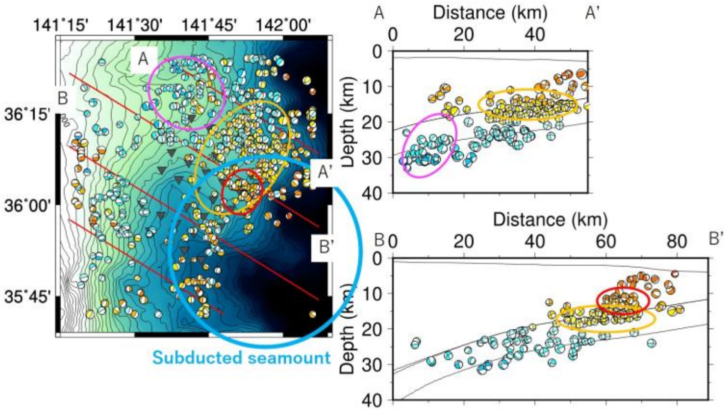

Figure 1. Hypocenters and CMT solutions of the aftershocks of the 2011 Tohoku-oki earthquake. Orange, red, and pink ovals outline the regions of reverse (yellow bolls), normal-fault (orage bolls) and deep strike-slip fault (light blue balls) type earthquakes, respectively.

The 2011 off the Pacific Coast of Tohoku Earthquake (Tohoku-oki earthquake) activated intensive aftershock activity including the largest aftershock to the south of the main shock focal region. The existence of a subducted seamount was revealed by an active-source seismic survey at a depth of ~10 km along the plate interface (Mochizuki et al. [2008]). The aftershock activity was recorded by an ocean bottom seismometer (OBS) array in the region. We determined the hypocenters and CMT solutions of relatively large aftershocks (Figure 1). Most of the aftershocks are of the thrust type. However, just above them without a large spatial interval, we found those of the normal fault type near the down-dip edge of the subducted seamount (Yamaya et al. [2022]). Such a distribution appears consistent with numerical modeling of seamount subduction (Sun et al. [2020]). In addition to the regular seismicity, tectonic tremors have been observed up-dip of the seamount. A similar pattern of regular and slow earthquake distribution has been identified in the northern Hikurangi subduction margin (Shaddox et al. [2020]).

In the Hyuda-nada subduction zone at the western end of the Nankai Trough, the Kyushu-Palau Ridge (KPR) subducts beneath the southwestern part of Japan. Frequent activities of tectonic tremors have been observed around the subducted KPR by OBS networks (Yamashita et al. [2022]). A seismic reflection profile over the tremor activities shows a step-wise change in the depth of the oceanic crust top while the decollement appears to be relatively flat. As a result, the thickness of the subducted sedimentary layers becomes thinner toward the subducted KPR. The thickness appears to be correlated with the tectonic tremor density; more tremor activity within the range of thicker sedimentary layers (Ma et al. [2021]). Such a thickness change may cause a variation in fluid abundance, and tectonic tremors may be prone to occur within a range of the fluid-abundant sedimentary layers.

Transient Fluctuations in Stress and Slip Caused by Geometric Irregularities in Shear Zones: Numerical Modelling of an Outcrop Analogue for Active Subduction Interface Deformation

Ellis, S.[1], Smith, S.A.F.[2], Tarling, M.S.[3], Negrini, M.[2], Allan, S.J.[2], Palmer, M.[2], and Viti, C.[4]

1. *GNS Science, Lower Hutt, New Zealand*
2. *University of Otago, New Zealand*
3. *McGill University, Canada*
4. *University of Siena, Italy*

We use 2-D numerical models to explore the development of incremental crack-seal textures in a fault-bound dilational jog (Figure 1). The models are based on a field example within a metre-scale phacoid embedded in a wide “block-in-matrix”-type (melange) serpentinite shear zone at the base of the Dun Mountain ophiolite (Miner River, Nelson, New Zealand). Slip on two overlapping fault surfaces cutting through the phacoid results from kinematic loading due to creep in the surrounding serpentinite matrix, and the dilational stepover between the two faults evolves in to an incrementally-developed serpentine vein.

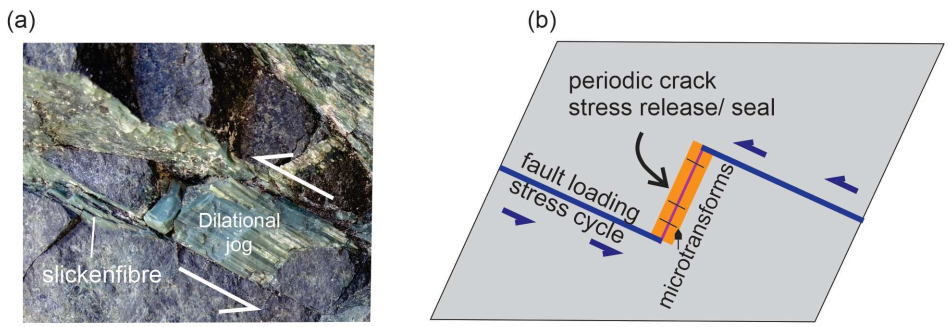

Figure 1. (a) Field example of a fault-bounded dilational jog in massive serpentinite. (b) Numerical model representation with fault stress cycling and transient crack opening accompanied by stress release.

We show how periodic exceedance of the tensile strength at the contact between the sealed vein and host rock leads to episodic opening and deposition of a new crack-seal band, where the band thickness (opening amount) for each opening event is limited by the release of localised stress concentrations built up around the tips of the stepover-bounding faults. The numerical models produce a repeated cycle of rapid cracking followed by precipitation of new material at both crack margins, until the crack is sealed. The dilational jog stress release depends on the tensile strength of the host material, but the overall static stress drop of the fault/jog system scales with crack length in the jog. The stress to drive the system cycles up and down by the stress drop, with its base level controlled by the static driving stress that would be needed to drive a single planar fault. Geometric irregularities leading to the formation of dilational jogs can prevent an otherwise stable or conditionally stable fault or shear zone from displacing at a steady rate, and cause local transient stress and slip pulses, analogous to episodic tremor and slip observed along active subduction interfaces.

Reconciling geologic and geodetic shortening rates with active folding in the Himalayan orogenic wedge

Sathiakumar, S.[1,2], Barbot, S.[1], and Hubbard, J.[2,3]

1. *Department of Earth Science, University of Southern California, LA, USA*
2. *Earth Observatory of Singapore, NTU, Singapore*
3. *Asian School of Environment, NTU, Singapore*

Geologic and geodetic estimates of fault slip motion provide key observational constraints on the mechanics of crustal deformation, but are often incompatible. This conundrum is well illustrated along the collision zone between India and Eurasia: the geodetic slip rates are 20-30% smaller than geologic slip rates in Central Nepal. Here, we show that these different observations can be reconciled by accounting for active folding and duplexing, key mountain building processes. Our kinematic structural models show that frontal thrusts can accumulate slip at a rate slower or faster than the long-term convergence rate during different phases of structural evolution depending on the architectural layout of the thrust sheet. Along-strike segments at different phases of structural evolution are likely, and the corresponding geomorphic rates from frontal thrusts at these locations may reflect the internal dynamics of the orogenic wedge. The along-arc geodetic rates, therefore, constitute a better estimate of the deep loading rate between the Indian plate and the Tibetan plateau. The spatial variability in thrust sheet evolution causes spatial and temporal variability of the long-term slip rate both along-strike and down-dip. This variability can induce earthquake segmentation patterns that are expected to shift every ~0.3-1.3 Myrs as the hanging wall evolves, with implications for seismic hazards.

Alpine Fault Seismogenesis and its Implications for Rupture Modelling and Ground-Shaking

Townend, J.[1], Holden, C.[1,2], Chamberlain, C.J.[1], Warren-Smith, E.[3], Juarez-Garfias, I.C.[1], Pita-Sllim, O.[1], Michailos, K.[4], Denolle, M.[5], van Wijk, K.[6], Curtis, A.[7], Miyake, H.[8], Lozos, J.[9], Boulton, C.J.[1], and Howarth, J.[1]

1. *School of Geog., Env., and Earth Sciences, Victoria University of Wellington, Wellington, New Zealand*
2. *SeismoCity Ltd., Wellington, New Zealand*
3. *GNS Science, Lower Hutt, New Zealand*
4. *Institute of Earth Sciences, University of Lausanne, Lausanne, Switzerland*
5. *Earth and Planetary Sciences, University of Washington, Seattle, Washington, USA*
6. *Department of Physics, University of Auckland, Auckland, New Zealand*
7. *School of Geosciences, University of Edinburgh, Edinburgh, UK*
8. *Earthquake Research Institute, University of Tokyo, Tokyo, Japan*
9. *California State University, Northridge, California, US*

Ground motions of societal concern are controlled by a combination of near-source conditions—the distribution, direction, and speed of rupture—and by the effects of three-dimensional variations in elastic and anelastic structures further afield. A key component, and challenge, of seismic hazard forecasting is to construct a comprehensive suite of geologically- and geophysically-plausible but as-yet unobserved rupture scenarios, and to evaluate the shaking from each one.

Much is known from detailed on- and off-fault studies about the paleoseismic chronology and coseismic segmentation of the Alpine Fault, and from field experiments and scientific drilling about the contemporary state of the fault with respect to temperature, fluid pressure, stress, and rheology. The paleoseismic results reveal the Alpine Fault to produce large or great earthquakes with remarkably consistent timing but of different magnitudes depending on which of the three principal sections of the fault rupture at any one time. What geometric or environmental factors enable the section boundaries to sometimes act as barriers to coseismic slip and at other times to allow ruptures to propagate unimpeded is the subject of active interdisciplinary research.

Here, we present results from field and dynamic modelling studies of the Alpine Fault and discuss how they can be incorporated in assessments of large-earthquake ground motions via "virtual earthquake" methods. Using data from the Southern Alps Long Skinny Array (SALSA), consisting of broadband sensors spaced 10–12 km apart along a ~450 km length of the Alpine Fault, and from seismometers and high-rate geodetic sensors throughout southern New Zealand, we can synthesize seismograms ("Green's functions") representing the farfield response to incremental slip anywhere on the fault surface. By convolving these Green's functions with kinematic rupture models incorporating observational constraints on along-strike and down-dip heterogeneity, present-day seismicity, and fault zone properties, we can compute ground motions at locations of interest in response to large numbers (millions) of plausible ruptures. This will enable us to comprehensively explore how the Alpine Fault's structure, heterogeneity, and present-day state will affect earthquake slip and ground-shaking in future large earthquakes.

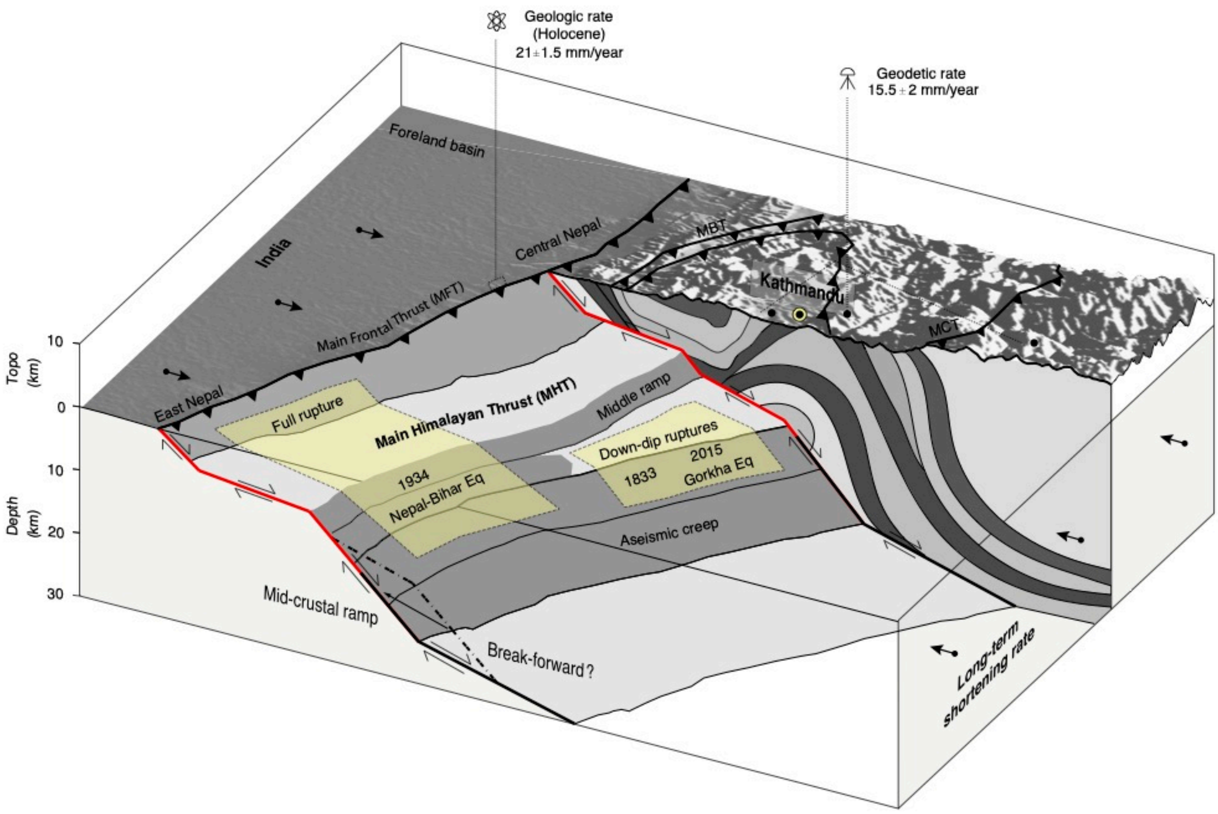

Figure 1: Perspective view of the Himalayan subsurface and observational constraints on the shortening-rate in Nepal. The three-dimensional fault geometry and the cross-sectional surface across Central Nepal are based on Hubbard et al. [2016]. The fault geometry at two representative cross-sections in Central and East Nepal (CN and EN, respectively) is highlighted with the frictionally unstable seismogenic zone in red and the creeping region in blue. The contours for the last known earthquakes in these segments, the M*w* 8.2 1934 Nepal-Bihar earthquake (EN) and the M*w* 7.8 2015 Gorkha earthquake (CN), are represented in yellow. Central Nepal features a middle ramp that is absent in East Nepal. Fault system evolution allows break-forward episodes of one or more ramps allowing accretion of Indian lithosphere onto the upper plate. The local long-term slip on individual fault segments, which may vary down-dip due to internal deformation of the orogenic wedge, is represented by double arrows.

A Kinematic Model of Quaternary Fault Slip Rates and Distributed Deformation at the New Zealand Plate Boundary

Hirschberg, H.[1], Sutherland, R.[1]

1. *Victoria University of Wellington, Wellington, New Zealand*

We construct a kinematic model of Quaternary long-term deformation at the New Zealand plate boundary that includes slip rates on major faults and strain rates between faults. We use an iterative method based on both statistical and physical principles to find a velocity field that fits fault slip rate observations, has consistent off-fault strain rate style, and is constrained by known plate motion. The kinematic model balances on-fault and off-fault deformation. It provides improved estimates of fault slip rates and uncertainties in a statistically rigorous manner appropriate for further use e.g., dynamical or seismic hazard modelling. The model includes estimates on faults with previously unknown or poorly constrained slip rates and it highlights locations where previous fault slip rate estimates may be inconsistent with slip rate estimates on nearby faults.

We predict shortening rates of 44±4 mm/yr, 33±3 mm/yr, and 10±2 mm/yr across the northern, central, and southern portions of the Hikurangi subduction margin respectively; these rates are smaller and better constrained by regional kinematics than previous estimates. The model predicts large strains adjacent to the Alpine Fault, indicating ~9 mm/yr of plate motion in central South Island on faults with currently unknown slip rates. Differences between our long-term velocity field and a contemporary velocity field arise mainly through interseismic locking on major faults. However, we suggest that differences with contemporary deformation in northeastern North Island are due to uncertainty in Havre Trough extension parameters.

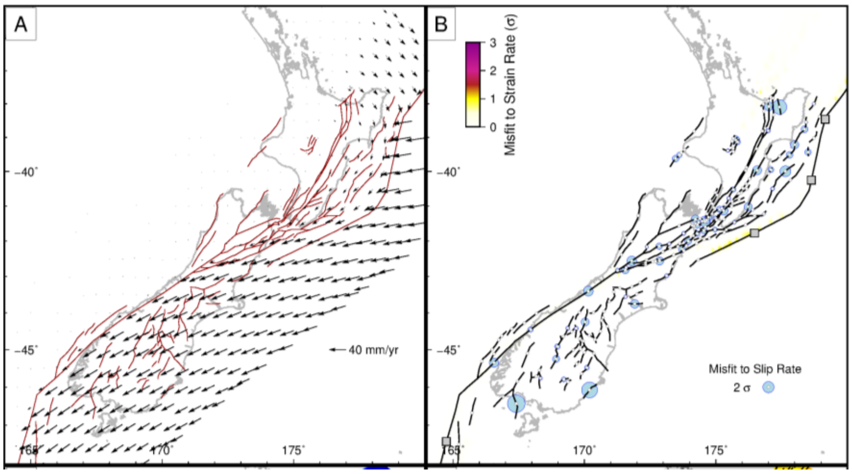

Figure 1. (a) Kinematic velocities modelled from fault slip rates relative to the Australian Plate. Red lines indicate faults used in the model. (b) Misfit to fault slip rate observations. Small, white circles indicate locations where misfit is calculated. The diameter of the blue circles is proportional to misfit.

Continuum Deformation Models of the Long-term Geodetic Displacement Field in the South Island of New Zealand

Houseman, G.A.[1], England, P.C.[2], and Evans, L.A.[3]

1. *School of Earth and Environment, University of Leeds, Leeds, UK*
2. *Department of Earth Sciences, Oxford University, Oxford, UK*
3. *School of Earth Atmosphere and Environment, Monash University, Clayton VIC, Australia*

The geodetic strain-rate field in New Zealand is now well characterized by an extensive array of GNSS measurements [Beavan et al., 2016]. While deformation is focused on the Australia-Pacific plate boundary, part of which is identified by the Alpine Fault, the adjoining continental regions are subject to significant rates of strain that are well represented by a continuous field of deformation. Using a thin viscous shell model, we calculate the velocity everywhere within the model domain, using the finite element method. The boundary conditions are based on the Australia-Pacific plate rotation vector, except for the Hikurangi margin and a cut through the North Island, where we apply tractions, which we determine by optimization of the model velocity field.

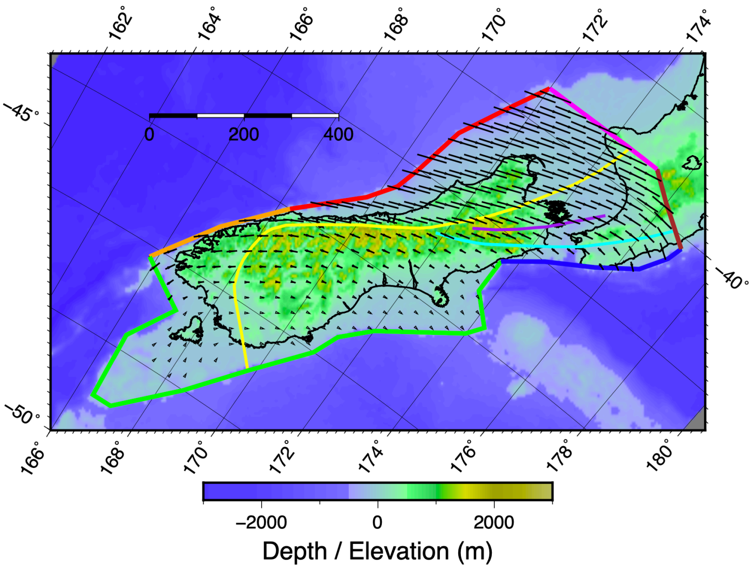

Figure 1. Model velocity field relative to the Pacific plate, constrained by GPS data. An oblique Mercator projection aligned with the Alpine Fault shows components of motion parallel and perpendicular to the fault. Allowing localized displacements on the structures indicated by yellow, purple and cyan lines improves the fit to data.

We consider a depth-averaged rheology for the lithosphere in which strain rate is proportional to the n^{th} power of deviatoric stress using a frame-invariant formulation. Scaling of internal buoyancy forces relative to depth-averaged viscous stress is determined by the Argand number. We also allow locally discontinuous motion associated with major structural features like the Alpine Fault, envisaged as sub-vertical ductile shear zones below the associated surface faults. The depth-averaged local shear stress acting on these structures is assumed proportional to the slip rate, with a proportionality constant *f*, referred to as the fault resistance coefficient.

The fit to the velocity field obtained from GPS measurements is described by the RMS misfit of model and GPS velocity vectors. For a stress strain-rate index $n = 3$ and Argand number = 2, optimization of the solution based on minimization of the model misfit achieves an RMS misfit of < 3 mm/yr for a set of 510 GPS measurements distributed across the region outlined in Figure 1. The strike-parallel model shear force acting on the Alpine Fault is 1.2 x 10^{13} N/m and the local slip rate is about 15 mm/yr of the total strike-parallel displacement rate of about 38 mm/yr.

Late Holocene earthquakes on the Papatea Fault and insights into its paleoseismic history from landscape change observations, Marlborough, New Zealand

Langridge, R.M.[1], Clark, K.J.[1], Almond, P.C.[2], S. Baize[3], and Howell, A.[1]

1. *GNS Science, Lower Hutt, New Zealand*
2. *Lincoln University, Lincoln, New Zealand*
3. *Institut Radioprotection Sûreté Nucléaire, Paris, France.*

The north-striking sinistral reverse Papatea Fault ruptured with a very large (up to 12 m) oblique slip as part of the 2016 M_W 7.8 Kaikōura earthquake in the northeastern South Island. Paleoseismic studies were undertaken at three sites along the Papatea Fault, named Murray's roadcut, Jacqui's Gully (both on the main strand), and Wharekiri trench (western strand). These sites provide evidence for up to three Late Holocene paleoearthquakes prior to 2016 (=E0) on this previously unmapped active fault, with preferred OxCal-modelled timings of 98–149 (E1), 546–645 cal yr BP (E2), and >738 cal yr BP (E3). Event correlations between the sites are generally consistent across these past events, implying that the two strands of the Papatea Fault link at depth and rupture together co-seismically as in 2016. Comparisons of its paleoseismic record with the Kekerengu Fault and uplift data from Waipapa Bay and Kaikōura, suggest that the Papatea Fault may have three distinct rupture modes: (i) Kaikōura-type multi-fault ruptures with multi-metre, anelastic block displacements and associated major landscape change; (ii) multi-fault earthquake ruptures with other regional fault combinations; and (iii) single-fault Papatea ruptures with metre-scale displacement. OxCal models offer the possibility that the E1 fault rupture occurred in 1855 CE.

Figure 1. The Papatea Fault rangefront (at back) in the Clarence valley from Observation Bend, circa 1864. Waipapa Station in foreground.

This presentation will also introduce unpublished datasets from uplifted and eroded other sites such as Priams Flat fan and the Wharekiri Stream that illuminate the Late Holocene record of landscape change. Preliminary dates indicate at least 1000 years and up to 4000 years since the last time the Clarence River avulsed across the Papatea Fault, and in contrast that major aggradation in the Wharekiri Stream valley may have taken place as recently as the 19th century.

Next-generation approaches to seismic hazard: challenges and current practices in Taiwan

Kuo-Fong Ma[1, 2], TEM team, and MiDAS team

1. Institute of Earth Sciences, Academia Sinica, Taiwan
2. Department of Earth Sciences, National Central University, Taiwan

(TEM, Taiwan Earthquake Model; MiDAS, Milun fault Drilling and All-inclusive Sensing)

The official publication of generalized Taiwan National Seismic Hazard Map (NSHM) was relatively young, compared to other earthquake prone countries, e.g. Japan, US, and New Zealand. Under the organization of Taiwan Earthquake Model (TEM), we published the first version of the Taiwan probabilistic seismic hazard assessment (named TEM PSHA2015) in 2015, and updating to the TEM PSHA2020 in 2020, which we considered an updated seismogenic structure with newly identified 3D fault geometry, and the earthquakes from multiple fault structures. For an active collision tectonic environment with high collision and erosion rate, the mapping of the multiple fault structures had been very challenging, especially for the blind faults in this fold-and-thrust belt tectonic setting with subduction zones. To characterize the mechanisms of damaging earthquakes, we studied significant historical earthquakes, and applied the dynamic modelling to decipher the involvement of the fault system associated with the historical earthquakes. For a rapid recurrence interval of Milun fault (~ 70 years), which involved in 1951 for a series of M7+ earthquakes, and the 2018 Hualien earthquake, we carried out a "Milun fault Drilling and All-inclusive Sensing (MiDAS)" by drilling a vertical hole into a recent ruptured active fault, and setup a cross-fault zone observatory using various state-of-the-art sensors, including the downhole optical fiber. We build up a long-term monitoring observatory to have the close-in data for the direct observation of understanding earthquake dynamics from subsurface and fault zone structure. This high-resolution emerging technique from Distributed Acoustic Sensing (DAS) demonstrates the capability in identifying the buried fault structure, and visualizing the effect of shallow velocity structure to ground shakings. Although the application of these results, and new developed technology into TEM PSHA practice are still not yet clear, however, we believe these approaches should be helpful in addressing the driving mechanism of the fault system in Taiwan, and the development in our ground motion model, especially for the near-fault long-period ground motion.

Strain rates in the Anatolia-Caucasus region from Sentinel-I InSAR and GNSS, and integration with earthquake catalogues

Rollins, C.[1,2], Wright, T.J.[2,3], Maghsoudi, Y.[2,3], Ou, Q.[2,3], Lazecky, M.[2,3], and Weiss, J.R.[4]

1. *GNS Science, Lower Hutt, New Zealand*

2. *Centre for the Observation and Modeling of Earthquakes, Volcanoes and Tectonics (COMET), UK*

3. *University of Leeds, UK*

4. *NOAA, Honolulu, Hawaii*

Geodetic measurements of surface deformation can provide crucial constraints on a region's tectonics and seismic hazard. To do so effectively, they need to be spatially dense (enough to highlight individual faults), spatially extensive (enough to capture the entirety of strain signals), temporally dense (enough that noise and nuisances can be understood), temporally extensive (enough to bring out gradual interseismic deformation), and accurate. A combination of InSAR and GNSS data is arguably the first data form that can be all five of these. In the Anatolia-Caucasus region, we are using Sentinel-IA InSAR frame velocities from the COMET LiCS system and pairing them with a high-quality GNSS velocity field to generate high-resolution maps of crustal deformation and strain rate. We find that the North Anatolian Fault is the dominant feature in the strain accumulation field, but also resolve deformation coinciding with other tectonic structures in western and southern Anatolia and throughout the Caucasus. To compare these strain rates with earthquake occurrence rates, we assemble an integrated earthquake catalogue for the region that covers many hundred years, and assess whether the moment release in earthquakes has kept up with the moment accumulation rates implied by our strain maps.

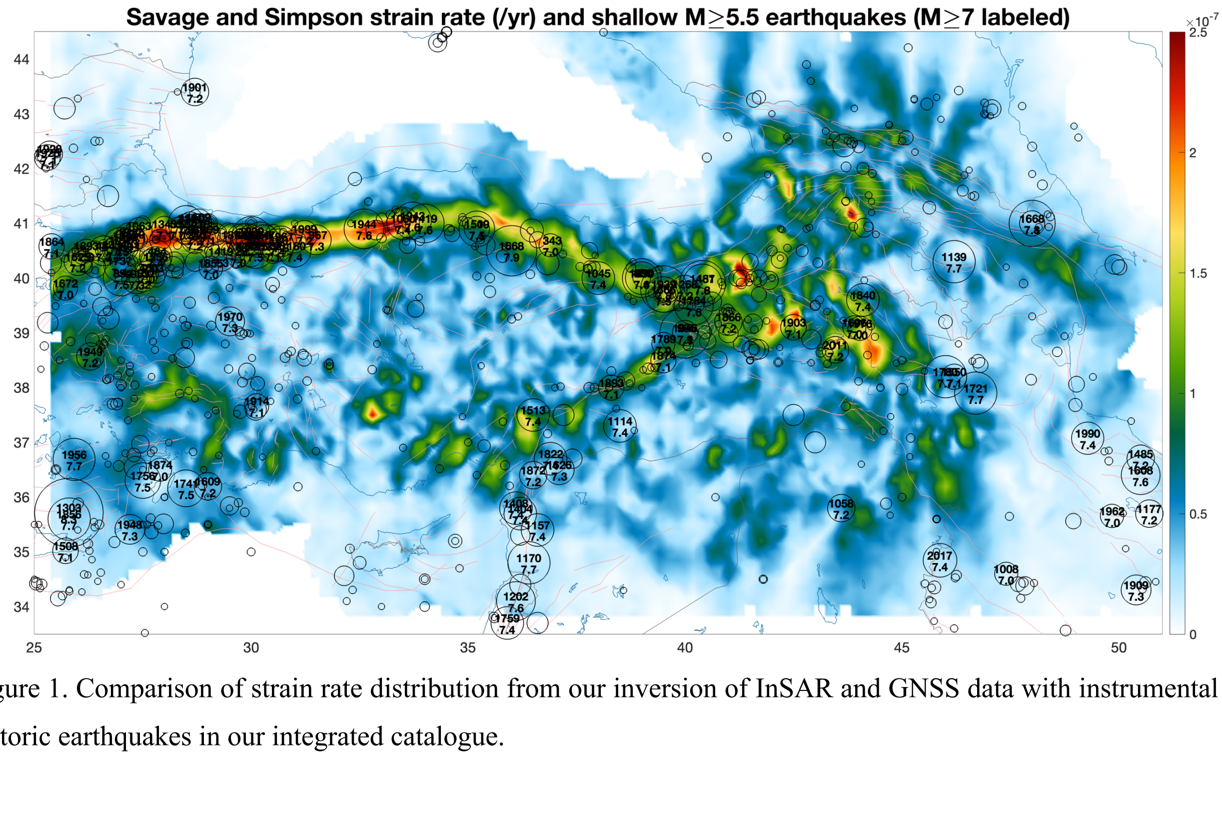

Figure 1. Comparison of strain rate distribution from our inversion of InSAR and GNSS data with instrumental and historic earthquakes in our integrated catalogue.

Anthropogenic influences on cascading earthquake hazards

Hill, E. M.[1,2], McCaughey, J. W.[3], Lallemant, D. [1,3], Wang, Y. [4], Sathiakumar, S.[1] and Switzer, A. D.[1,3]

1. *Earth Observatory of Singapore, Nanyang Technological University, Singapore*
2. *Asian School of the Environment, Nanyang Technological University, Singapore*
3. *ETH Zurich, Switzerland*
4. *Department of Geoscience, National Taiwan University, Taiwan*

Human modification of landscape and climate, at both a local and global scale, can change natural systems and modify equilibria such that the secondary hazards of earthquakes are amplified. Secondary hazards from earthquakes -- which can occur in addition to damage from surface rupture and shaking -- include tsunami, land height change (and thus relative sea-level change), earthquake-triggered landslides, and liquefaction. Locally, key human contributions to the impact of these secondary hazards include removal of coastal vegetation, land subsidence from groundwater withdrawal, removal of vegetation from slopes, modification of topography, and modification of hydrological systems (e.g., through irrigation). More globally, climate change is resulting in rising sea levels, stronger storms and increased risk of fires (the latter two of which can remove vegetation and destabilize slopes); we should expect more serious impacts of earthquake hazards as a result. Relations between human activities and secondary earthquake hazards are complex and can be hard to disentangle, especially when the causes and effects may span many generations of human history, but attempting to do so is key to better estimating risk. In this presentation we will review the connections and interrelations between human activity and secondary earthquake hazards, and examine relevant case studies that can help us determine recommendations for mitigation of future hazards.

Figure 1. Much of the destruction from the M_w 7.0 2010 and M_w 7.2 2021 Haiti earthquakes occurred on steep slopes where forests had been replaced with homes (photo by D. Lallemant).

High-frequency Ground-shaking Simulations for Alpine Fault Earthquake Scenarios

Holden, C.[1,2], Townend, J.[2], Chamberlain, C.J.[2], Warren-Smith, E.[3], Juarez-Garfias, I.C.[2], and Pita-Sllim, O.[2]

1. *SeismoCity Ltd., Wellington, New Zealand*
2. *School of Geog., Env., and Earth Sciences, Victoria University of Wellington, Wellington, New Zealand*
3. *GNS Science, Lower Hutt, New Zealand*

As part of the Southern Alps Long Skinny Array (SALSA) project, ~35+ seismometers have been deployed with 10–12 km spacing along a 450 km-long section of the Alpine Fault (Figure1). SALSA is focused on determining the ground motions likely to be produced by a future Alpine Fault earthquake. This project is addressing three principal objectives: 1. Determine the Alpine Fault's subsurface geometry, present-day slip rates, and spatial variations in how tectonic stresses are currently accumulating on the fault; 2. Estimate the ground shaking that would be recorded at seismometers throughout central and southern New Zealand by localised slip at different points on the Alpine Fault; and 3. Calculate the ground shaking hazard from geologically-informed earthquake rupture scenarios. Objective 2 is focused on the synthesis of long-period Green's functions representing accurate path effects between sources distributed along the fault and population centers throughout the South Island. To achieve objective 3, the synthesis of high-frequency ground motion still needs to be addressed, however, and this will rely on better characterization of stress drops (Objective1) and attenuation models. As shown in Figure 2, stress drop affects synthetic spectra markedly. In this presentation we will address the influence of stress drop variation and of the attenuation function on high-frequency ground-shaking for Alpine Fault earthquakes.

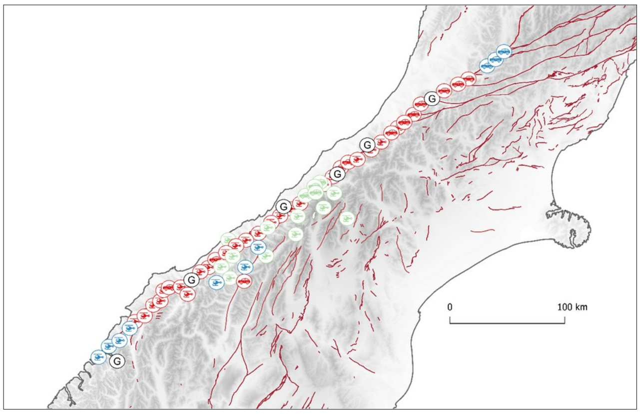

Figure 1. Map showing the locations of each of the seismometers being operated in the Southern Alps as part of the Southern Alps Long Skinny Array (SALSA) and nearby networks. Sites accessed by helicopter and car and are marked with the corresponding symbols. "G" denotes a GeoNet sensor.

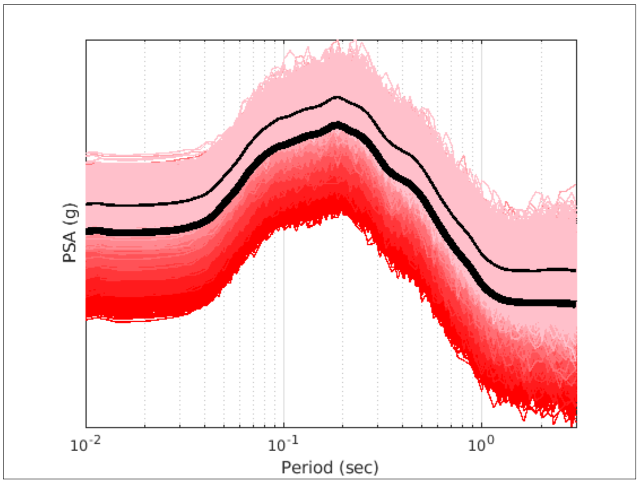

Figure 2. Synthetic response spectra (PSA(g)) for a specific location calculated for a M8.2 Alpine Fault earthquake and stress drop values ranging from 5 to 20 MPa. The thick line represents the median value and the thin line the 84th percentile.

The damaging November 2022 Mw 5.6 earthquake in West Java, Indonesia

Yun, S.[1,2,3], Salman, R.[1], Gunawan, H.[4], Widiwijayanti, C. [1], Way, L.[1], Hidayat, D. [1], Lythgoe, K. [1], Yukuan, C.[1], Susilo, S.[5], Feng, L.[1], Wei, S.[1,2], Taisne, B.[1,2], Ainscoe, E.[1], Chin, S.[1]

1. *Earth Observatory of Singapore, Nanyang Technological University, Singapore*
2. *Asian School of the Environment, Nanyang Technological University, Singapore*
3. *School of Electrical and Electronic Engineering, Nanyang Technological University, Singapore*
4. *Center for Volcanology and Geological Hazard Mitigation, Bandung, Indonesia*
5. *National Agency for Research and Innovation (BRIN), Indonesia*

On 21 November 2022, a M_W 5.6. earthquake hit Cianjur area in West Java, Indonesia. The moderate magnitude earthquake claimed 329 people's lives, and about 114,414 people were taking shelter in refugee camps as of 1 December 2022 according to the National Disaster Mitigation Agency (BNPB) of Indonesia. We produced maps of coseismic deformation and surface disturbance (a.k.a. Damage Proxy Map, DPM) using Synthetic Aperture Radar (InSAR) data acquired by the ALOS-2 satellite about 11 hours after the earthquake. The earthquake occurred on a previously unknown/unmapped fault. We combine and analyze ground observations, coseismic deformation and surface disturbance maps derived from ALOS-2 and Sentinel-1 SAR data, seismic waveforms of the mainshock and aftershocks, high-rate GNSS data, and tiltmeter data to characterize the source parameters of the earthquake and damage caused by the strong ground motion, landslides, and liquefaction, and study the potential impact of the event on the geohazards of the area.

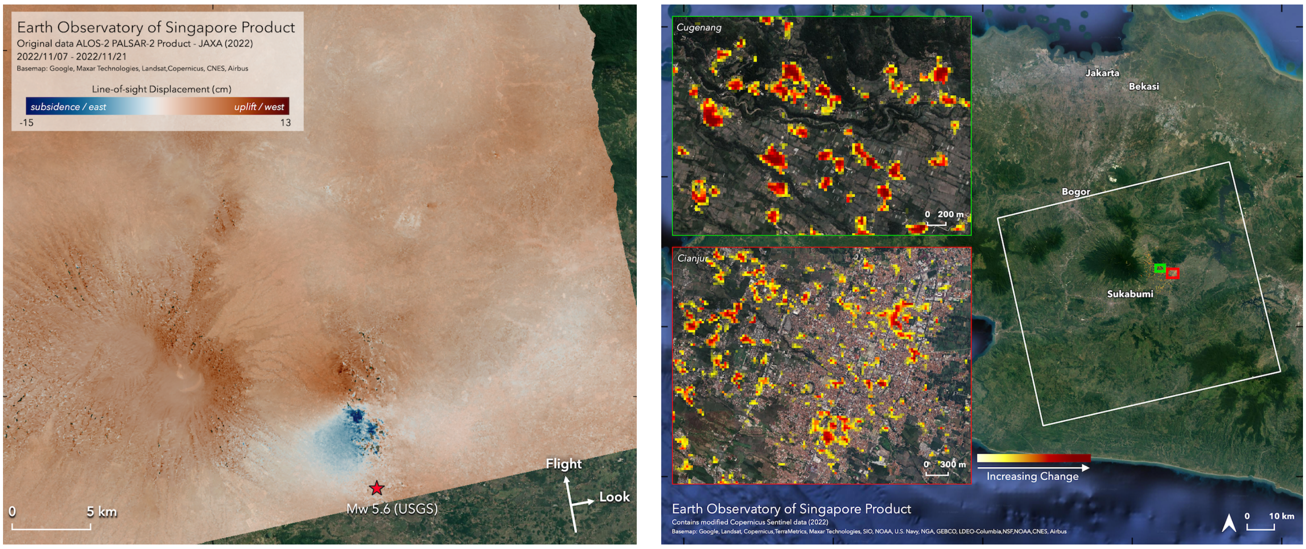

Left panel: Coseismic line-of-sight displacements measured by the ALOS-2 SAR satellite operated by JAXA. Right panel: Damage proxy map derived from Copernicus Sentinel-1 SAR observations with multi-temporal interferometric coherence analysis.

Multi-fault Earthquakes: Ground Rupture Displacements and Hazard Implications

Quigley, M.[1,2]

1. *School of Geography, Earth & Atmospheric Sciences, University of Melbourne*
2. *School of Earth and Environment, University of Canterbury*

Many crustal earthquakes involve the rupture of multiple faults with distinct geometries and kinematics [Quigley et al., 2017]. The geometric configuration of fault systems relative to pre-and co-seismic stress fields can affect their propensity for cascading multi-fault earthquakes [Quigley et al., 2019]. Whether fault systems are probabilistically favoured to rupture in multi-fault mode or independently as distinct faults affects earthquake frequency-magnitude statistics and seismic hazard [Quigley et al., 2019]. Where fault junctions are aligned with slip vectors, slip maxima may occur and be manifested at the ground surface as large ground surface rupture displacements [Yang et al., 2021]. Conversely, some fault junctions may terminate or disperse ruptures and be manifested at the surface by steep displacement tapers and complex fracture meshes [Vermeer et al., 2022; Yang et al., 2021]. Rupture complexity and short wavelength amplitudes of ground surface rupture displacement variability increase in fault junction zones [Duffy et al. 2012; Yang et al., 2021]. Rupture complexity does not appear to impart a first-order control on co-seismic stress drop. Foci of seismic hazard analyses could include geophysical-structural characterisation of fault junction zones to evaulate their kinematic compatibility and forecast their tendency for enabling multi-fault rupture cascades and enchancing ground surface rupture displacements and displacement variability.

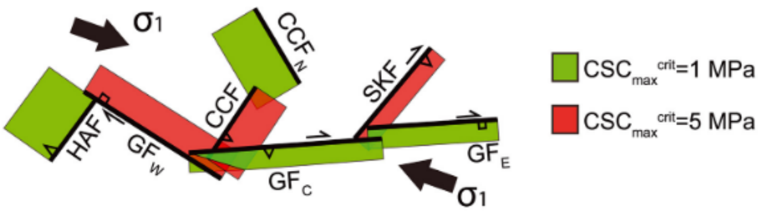

Hypocentral fault	CCF	GF_C	GF_W	SKF	GF_E	HAF	CCF_N
Source Mw	6.4	6.8	6.6	6.5	6.5	6.3	6.3
Total Mw	7.1	7.1	7.1	7.1	7.1	6.3	6.3

Figure 1. Rupture scenarios for the 2010 Mw 7.1 Darfield earthquake source faults, using slip tendency analysis to set Coulomb stress change rupture triggering thresholds and modelling rupture cascade propensity for different hypocentral faults. Rupture initiation on 5 of 7 faults favours a multi-fault rupture cascade across the entire network in a Mw 7.1 earthquake (Quigley et al., 2019).

The 2022 New Zealand National Seismic Hazard Model: Overview and Seismicity Rate Model

Gerstenberger, M.C.[1], Bora, S.[1], Bradley, B.[2], Kaiser, A.[1], Van Dissen, R.[1], Nicol, A.[2], Stirling, M.[3], Thingbaijam, K.[1], and The NSHM Team

1. *GNS Science, Lower Hutt, New Zealand*
2. *University of Texas Institute for Geophysics, Austin, Texas, USA*
3. *University of Otago, Dunedin, New Zealand*

Recently, an approximately three year project to revise the New Zealand National Seismic Hazard Model (NSHM) was completed. This was the most significant revision of the NSHM in more than 20 years and included fundamental changes to all components of the model. An underlying philosophy of the model development was that to best represent what we know about earthquake occurrence and, hence, make the best forecast, we need to represent a wide range of datasets, hypotheses and models in all components of the NSHM.

The Seismicity Rate Model (SRM) is the collection of component models that each forecast the magnitude, location and rate of earthquakes for the next 100 years. The Ground Motion Characterisation Model (GMCM) is the collection of models that forecast the range of shaking for each of the ruptures in the SRM. Broadly, the SRM is broken into two components: 1) ruptures on known faults, and 2) ruptures on faults that are not yet known about. For the known faults we have implemented the UCERF inversion recipe which allows for jointly fitting multiple datasets and models to provide rates on ruptures. Some key inputs are: the Community Fault Model; Deformation models, which provide slip rates on all faults; Rupture sets, which provide geometric constraints on potential ruptures; Models of timings of past earthquakes on known faults; and, Magnitude-frequency distributions of earthquake occurrence. For unknown faults, we have developed a hybrid model that represents a significant departure from smoothed seismicity models which are typically used in seismic hazard. Similar to the inversion model, the hybrid model also combines, geological and geodetic data with the earthquake catalogue to provide a more complete forecast than smoothed seismicity alone. Models have also been developed for lower-seismicity regions which incorporate geodetic strain and the low-bias seen in the NZ earthquake catalogue in lower rate regions. Finally, the SRM accounts for the much greater variability in rate observed in New Zealand than is modelled by standard Poisson assumptions.

The 2022 NZ NSHM forecasts larger shaking across New Zealand when compared to past NSHMs. What controls this difference is region and parameter specific; the largest contributions come from the GMCM with the SRM contributing significant forecast changes primarily in lower-seismicity regions but also providing important changes across the country.

Upper Plate and Subduction Interface Deformation Models of the NZ NSHM 2022

Van Dissen, R.[1], Johnson, K.[2], Seebeck, H.[1], Wallace, L.[1,3], Rollins, C.[1], Mauer, J.[4], Gerstenberger, M.[1], Williams, C.[1], Hamling, I.[1], Howell, A.[1,5], DiCaprio, C.[1]

1. *GNS Science, Lower Hutt, New Zealand*
2. *Indiana University, Bloomington, Indiana, USA*
3. *University of Texas Institute for Geophysics, Austin, Texas, USA*
4. *University of Missouri Science and Technology, Rolla, Missouri, USA*
5. *University of Canterbury, Christchurch, New Zealand*

Following the UCERF3 workflow [Field et al. 2014], deformation models provide the locations, geometries and slip rates of the earthquake-producing faults explicitly modelled within the NZ NSHM 2022. Within that model, the two main deformation model classes are upper plate, and subduction interface. For the upper plate, two types of models are developed – one using geologic-based slip rates and the other using geodetic strain-rate based slip deficit rates. For the two subduction interfaces relevant to ground shaking hazard in New Zealand, two deformation models are developed for the Hikurangi-Kermadec interface, and a single model for the Puysegur interface.

With only slight amendments, the upper plate geologic deformation model is derived directly from the fault geometries and slip rates characterized in the NZ Community Fault Model version 1.0 [Seebeck et al. 2022]. The upper plate geodetic deformation model utilises the same fault geometry model as the geologic model but with fault slip deficit rates derived by inverting geodetic strain rate [Johnson et al. 2022]. The geodetically-derived strain rates were developed using four different methods (VDoHS, body-force method, VELMAP, geostatistical) based on the published interseismic GNSS-derived velocity field of Beavan et al. [2016].

The geometry and slip deficit rates for the Hikurangi–Kermadec subduction interface deformation model are blends of a variety of data, constraints and interpretations. The geometry of the Hikurangi–Kermadec deformation model is a linear blend of the Hikurangi interface geometry of Williams et al. [2013] and the Slab 2.0 Kermadec interface geometry of Hayes et al. [2018]. Derivation of slip deficit rates on the Hikurangi portion of the deformation model are founded on the well-established block modelling methods described in Wallace et al. [2004, 2012] with "locked to trench" and "creeping at trench" slip deficit rate renditions defined. Slip deficit rate for the Kermadec portion of the Hikurangi–Kermadec subduction interface deformation model is based on convergence rate [Power et al. 2012] and locking (coupling coefficient) considerations. The two Hikurangi slip deficit rate renditions ('locked to trench' and 'creeping at trench') are smoothly combined with the single Kermadec slip deficit portrayal to yield two alternative slip deficit rate characterisations for the Hikurangi–Kermadec interface.

The geometry of the Puysegur subduction interface is taken directly from the NZ Community Fault Model v1.0. adopting a "cut by the Alpine Fault" rendition, and the slip deficit rate is derived from plate convergence rate [Wallace et al. 2007] and interface coupling [Berryman et al. 2015] considerations.

Capturing epistemic uncertainty in ground-motion prediction: the New Zealand national seismic hazard model (NSHM)-2022 and the challenges ahead

Bora, S.[1], Bradley, B.[2], Gerstenberger, M.[1], Manea, E[1]., Lee, R.[2], Stafford, P.[3], Atkinson, G[4]., Kaiser, A.[1] and Di Caprio, C.[1]

1. *GNS Science, Lower Hutt, New Zealand*
2. *University of Canterbury, Christchurch, New Zealand*
3. *Imperial College London, UK*
4. *Western University Ontario, Canada*

In the first part of my presentation, I will talk about the ground-motion characterization modeling (GMCM) framework adopted for the 2022 revision of the national seismic hazard model (NSHM-2022). It adopts a hybrid approach (to capture epistemic uncertainty) that involves using a multi-model and backbone ground-motion modeling framework. For active shallow crustal sources seven ground-motion models (GMMs) were considered that include four global, one New Zealand specific GMM and two New Zealand specific backbone GMMs developed within the purview of NSHM-2022. Similarly, the candidate models for subduction (interface/intraslab) sources include three recently developed global GMMs (NGA-Sub) and one New Zealand specific backbone model.

In the second part, I provide an outlook for future research efforts within NSHM. The major challenge in the context of New Zealand is the large epistemic uncertainty in ground-motion prediction for large rupture scenarios that dominate hazard at major urban centers. Moreover, the possibility of joint-ruptures (connectivity of interface and crustal faults) along with multiple ruptures poses a significant challenge for ground-motion modeling. In that context, variability of observed ground-motion in terms of source properties and in regional path attenuation needs to be explored further in New Zealand. For that purpose, ground-motion observations from other parts of the world will also be explored in addition to the New Zealand specific datasets. Furthermore, numerical simulations are expected to provide additional insights and hence constraints on the epistemic uncertainty.

How Characteristic are the Magnitude Frequency Distributions in the New Zealand National Seismic Hazard Model?

K.K.S. Thingbaijam[1] , M.C .Gerstenberger[1] , C. Rollins[1] , R.J. Van Dissen[1]

1. *GNS Science, Lower Hutt, New Zealand*

Probabilistic seismic hazard analysis requires a consistent seismicity rate model, in other words, a forecast of long-term earthquake rates over a range of magnitudes. The New Zealand National Seismic Hazard Model 2022 constructed the seismicity rate model by combining the independent forecasts of on-fault and off-fault event rates. The on-fault earthquake rates were derived by inverting slip rates while off-fault rates were based on the smoothed-seismicity distributions. Both forecasts were constrained by regional magnitude frequency distributions (MFDs) defined by the Gutenberg-Richter *b*-value and *N*-value (annual number of events for magnitude M_W 5.0). It is generally accepted that regional MFDs follow a Gutenberg-Richter (or negative exponential) law. However, the MFDs vary locally from one fault zone to another, reflecting the spatial variations in fault-slip rates and in recorded seismicity. Here, we investigate the patterns of the local MFDs and in particular, the characteristic behavior thereof, across individual fault zones. In the analyses, we consider both participation and nucleation rates, to understand the possible impacts that fault slip rate and time-dependent *versus* time-independent rate forecasts have on fault-zone-specific MFD shapes.

A Method for Handling Large Logic Trees in Seismic Hazard Computation: Application to the NZ NSHM 2022

DiCaprio, C.[1], Chamberlain, C.[1], Bora, S.[1], Bradley, B.[2], Gerstenberger, M.[1], Hulsey, A.[3], Pagani, M.[4], Simionato, M.[5]

1. GNS Science, Lower Hutt, New Zealand

2. University of Canterbury, Christchurch, New Zealand

3. University of Auckland, Auckland, New Zealand

4. GEM Foundation, Pavia, Italy and Adjunct Professor, ICRM-NTU, Singapore

5. GEM Foundation, Pavia, Italy

The 2022 New Zealand National Seismic Hazard Model (NZ NSHM) represents a massive revision of the NZ NSHM across both seismicity rate model (SRM) and ground-motion characterization model (GMCM) components. A primary goal of this model is to capture a large range of epistemic uncertainty in both source and ground motion. As a result, the final SRM logic tree comprises 324 branches and the GMCM) logic tree comprises 3024 branches. The final logic tree contains nearly 1 million branches, posing a significant computational challenge.

Our approach to the problem is to break the logic tree into several parts, dividing it by source components (active shallow crust, Hikurangi-Kermadec subduction interface, Puysegur subduction interface, and subduction slab) which are considered independent. Hazard curves can be practically calculated for individual source components. Weighted mean and quantile hazard curves are then calculated from the constituent parts in a post-processing phase. This approach has additional advantages as it allows us to easily reconstruct all hazard curve realizations for the purposes of exploring individual components of the hazard model, performing sensitivity tests, calculating new aggregate statistics, and performing disaggregations over the full logic tree.

The large number of source components of the NZ NSHM also poses a data management challenge. We've developed tools to make access to model components and metadata easy and ubiquitous. This facilitates sharing of results among the scientific team, tracking components of the large SRM logic tree, and providing model components to the public.

Towards an Automated Workflow for the Creation of Complex 3D Fault Models

Howell, A. [1,2], McLennan, T.[3], Penney, C.[1], Nicol, A.[1], Seebeck, H. [2] and Fry, B.[2]

1. Te Whare Wānanga o Waitaha — University of Canterbury, Christchurch, Aotearoa New Zealand

2. Te Pū Ao — GNS Science, Lower Hutt, Aotearoa New Zealand

3. Seequent Ltd, Christchurch, Aotearoa New Zealand

Fault geometry and the connectivity between faults at depth are both important controls on earthquake behaviour, so modelling these parameters accurately is essential to models of the earthquake cycle. However, the effects of uncertainties in fault geometry and connectivity are often not fully explored, partly because using current techniques building a fault model is difficult and time consuming. For example, the current 3D Community Fault Model — which results from several hundred person hours of work — represents only one of many hypothetical fault models that would be consistent with available constraints.

We present a preliminary automated workflow for the creation of 3D models of faults in Aotearoa New Zealand and worldwide, using python and the mesh-cutting capabilities of Leapfrog Software. This workflow creates a 3D fault model from: (1) GIS fault traces; (2) dip estimates; and (3) a text file containing information on which faults are thought to terminate against each other. Our approach is faster, more internally consistent and much less labour-intensive than previous (mainly manual) methods of fault model creation; it will allow a thorough exploration of the sensitivity of models to fault geometry and will therefore be of use in several diverse areas of earthquake science.

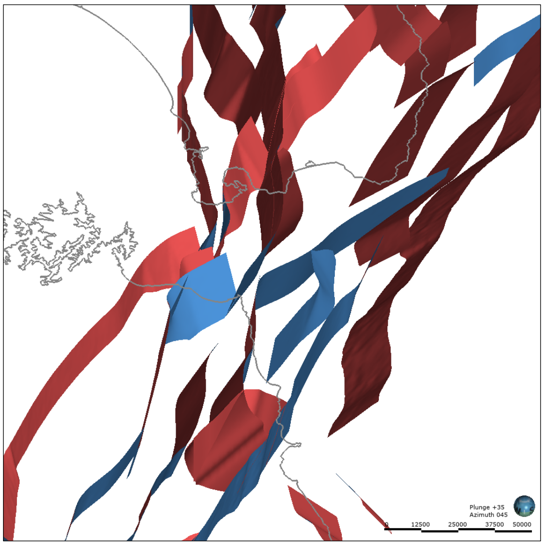

Figure 1. 3D model of faults in central Aotearoa-NZ created using our new method.

Study on the Predictability of Pattern Informatics Method Related to Selection of Study Region- A Case Study for the North-South Seismic Zone and Its Vicinity

Tian, W.X.[1], Zhang, Y.X.[1], Zhang, S.F.[1], Zhang, X.T.[2]

1. *Institute of Earthquake Science, China Earthquake Administration, Beijing 100036, China*
2. *China Earthquake Networks Center, Beijing 100045, China*

The Pattern Informatics (PI) method is a new approach for earthquake forecasting based on statistical physics which has been widely applied both at home and abroad due to its good performance in medium to long term earthquake forecasting. The algorithm of PI method includes the process of normalization of all grid parameters in the selected region, so the distribution of PI hot spots might be different with the selection of different study region theoretically. However, the predictability of PI due to the selection of study region has not been systematically studied in the past. In this study, we had the retrospective forecasting for 6 earthquakes above Ms6.0 in the North-South Seismic Zone in recent 5 years under different chosen regions. The earthquake catalogue since 1970 is taken from the China Earthquake Networks Center. Both the change interval and forecast interval are fixed as 5 years and the moving step is taken as 1 year in this study. The forecasting efficiency of PI is tested by R-value score and ROC (Receiver Operating Characteristic) test. The results showed that: 1) When other calculation parameters were the same, different region selection might lead to different forecasting results. 2) Under the R-value and ROC tests, the results showed that the selection of regions with lower different seismicity is better than those with higher different seismicity. In selected regions with higher different seismicity, target earthquakes in areas with higher seismicity tend to be predicted than those in area with lower seismicity, which is supposed to be caused by the fact that PI hotspots are more obvious in areas with higher seismicity and it will restrain the anomalous signal detected by PI algorithm in areas with lower seismicity, resulting in the missing prediction for the target earthquakes in areas with lower seismicity. 3) For the specific target earthquake, the imagine of PI hot spot around the epicenter will evolute with time, so the forward prediction using PI method should consider the combination of multiple forecasting windows. 4) Different from the hot spots evolution trend of other natural tectonic earthquakes, the hot spots appeared and disappeared repeatedly near the epicenter of Changning *M*s6.0 and Luxian Ms6.0 earthquakes. 5) The calculation results show that there are continuous PI hot spots at the boundary of South-West Yunnan, middle and eastern section of Haiyuan fault, the middle part of Xiaojiang fault, the southern part of the Longmen Shan fault and the northeastern part of the Xiaojiang Fault, which suggests that there will be seismic potentials with Ms 6 or above in these regions during the next 5 years.

Key words: Pattern Informatics (PI), North-South Seismic Zone, Earthquake Predictability, Strong Earthquake Forecasting, *R* score, ROC test

Magnitude and Slip Scaling Relations for Fault Based Seismic Hazard

Shaw, B.E..[1]

1. *Columbia University, New York, USA*

Scaling relations play an important role in fault-based seismic hazard estimates. Scaling relations impact estimates of the sizes and rate for a given fault area. Here we examine which relations are most useful for these estimates, and issues that arise. These include the depth of large event ruptures, transient deepening of seismicity following large events, difficulties in using classical continuum exponent fits, and the importance of large event asymptotics. A new analysis of land-based data calls into question non-specific exponent fitting, which is a standard practice. We show a dependence on the lower and upper cutoff magnitudes in the data in the best fitting slope parameter relating magnitude to log area with this approach. We show as well a dependence on assumed data uncertainties. These sensitivities make using this quite standard approach very problematic. Based on this evidence and other factors, we propose recommendations for minimal branch sets which preserve epistemic uncertainty for use in fault-based seismic hazard estimates. In addition to these observational and scaling discussions, we present as well earthquake simulator results which address these questions.

In good shape? The impacts of variable fault geometries on synthetic earthquake catalogues from physics-based earthquake simulators

Penney, C.[1], Howell, A.[1,2], McLennan, T.[3], Fry, B.[2] and Nicol, A.[1]

1. Te Whare Wānanga o Waitaha | University of Canterbury, Christchurch, Aotearoa New Zealand

2. Te Pū Ao | GNS Science, Lower Hutt, Aotearoa New Zealand

3. Seequent, a Bentley Systems, Incorporated company, 685 Stockton Drive, Exton, PA 19341, USA

A well-known problem in understanding seismic hazard is the short time period of the historical record relative to the time between large earthquakes. This short record means that not all possible earthquakes have been observed, and that the statistics of earthquake recurrence intervals are poorly constrained. These issues can be mitigated to an extent by paleoseismological investigations, but how these prehistoric data are interpreted is still limited by current understandings of which earthquakes are possible. In particular, recent multifault ruptures, such as the 2010 El Mayor-Cucapah and 2016 Kaikōura earthquakes, have demonstrated the potentially complex interactions of faults in single earthquakes, contrasting with the typical assumption of characteristic fault ruptures in seismic hazard assessment.

Physics-based earthquake simulators, such as RSQsim (Dieterich & Richards-Dinger, 2010; Richards-Dinger & Dieterich, 2012), offer one approach to expanding our understanding of potential multifault earthquakes. Here we investigate the effects of fault geometry on the outputs of such simulators. We use the Canterbury and North Marlborough regions of the South Island of Aotearoa New Zealand – the epicentral region of the 2016 Kaikōura earthquake – as a case study. Using recently developed fault modelling tools (Howell et al., ibid), we create 3D fault networks spanning the range of uncertainty of fault geometries in the region, including the potential for missing faults and variable geometries at fault intersections. The different networks we develop are motivated by key observations from the Kaikōura earthquake, such as the high proportion of previously unmapped faults in the rupture (Litchfield et al., 2018), and by explicit uncertainties in the New Zealand Community Fault Model (Seebeck et al., 2022). We generate synthetic earthquake catalogues on these different fault networks and investigate their similarities and differences, both statistically and in terms of the generated multifault ruptures. By doing so, we are able to better understand the effects of uncertainties in fault geometry on earthquake simulator outputs, which is critical before synthetic earthquakes can be used as a starting point for seismic hazard assessment or scenario planning.

The rates of large and moderate earthquakes in Aotearoa New Zealand

Rollins, C.[1], Christophersen, A.[1], Thingbaijam, K.K.[1], Hutchinson, J.[2], Rhoades, D.[1], Rastin, S.J.[1], Gerstenberger, M.[1], Eberhart-Phillips, D.[3], Van Dissen, R.[1], Graham, K.[1] and Fraser, J.[4]

[1] *GNS Science, Lower Hutt, New Zealand; c.rollins@gns.cri.nz*

[2] *Ocean Networks Canada, Victoria, British Columbia, Canada*

[3] *GNS Science, Dunedin, New Zealand*

[4] *WSP, Christchurch, New Zealand*

For use in the Seismicity Rate Model (SRM) component of the 2022 New Zealand National Seismic Hazard Model, we estimate the total magnitude-frequency distribution (MFD) of earthquakes in the greater New Zealand region and along the Hikurangi–Kermadec and Puysegur subduction zones. The former is a key input into multiple components of the SRM in the onshore and near-shore regions, while the latter is a key input into models of earthquake rupture rates on the subduction zones.

Recent work (Christophersen et al., 2022) has greatly improved and homogenized the earthquake magnitudes in the New Zealand earthquake catalogue for use in the NZ NSHM 2022. Other parameters in the catalogue remain of mixed quality, however, in particular earthquake depths. Therefore, we develop an augmented New Zealand earthquake catalogue in which we import higher-quality depths and depth uncertainties, focal mechanisms, and some locations and magnitudes from several relocated and global catalogues. Next, we use event depths, focal mechanisms, 3D models of the Hikurangi and Puysegur subduction interfaces, and relative plate motion directions to classify earthquakes as upper-plate, interface or intraslab.

Using this augmented catalogue and adapting an approach used previously in California, we estimate the MFD of earthquakes in the near-shore region incorporating data back to 1843, balanced with the better data in the more recent part of the instrumental catalogue. This method estimates both the mean earthquake rate and its uncertainty, and we supplement it with an alternative estimate of the rate uncertainty that is based on the rate variability in the catalogue over a range of shorter timespans. We estimate the MFDs on the Hikurangi–Kermadec and Puysegur subduction zones using a simplified version of the method used in the near-shore region, with more recent data. Finally, we describe a globally based method to estimate the potential earthquake rate uncertainty on the Hikurangi–Kermadec subduction zone.

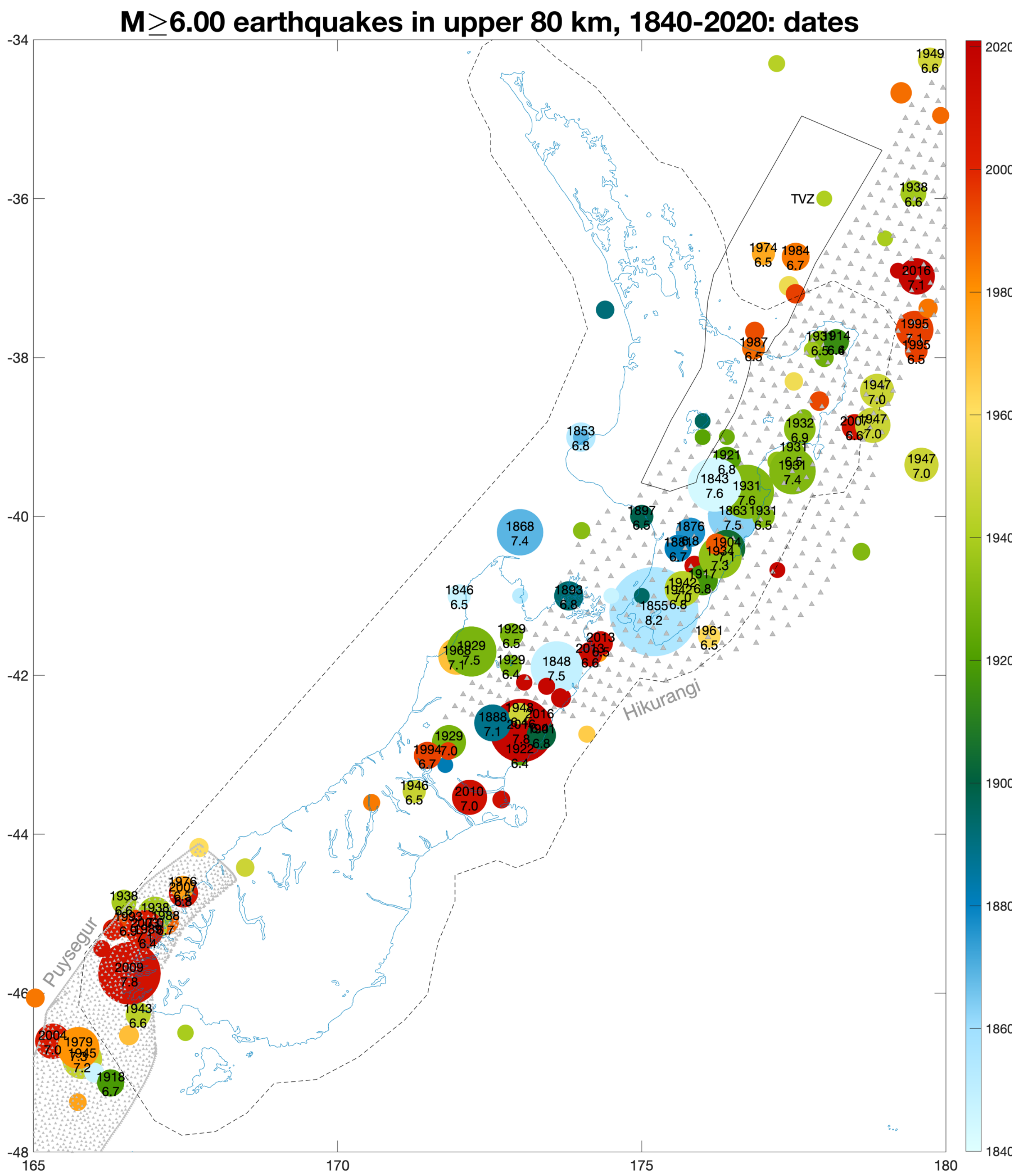

Figure 1. Shallow M≥6.0 earthquakes in Aotearoa New Zealand, 1840-2020, coloured by date of occurrence.

Towards Estimate Earthquake Hazard from Interseismic Locking Models

Yang, H. and Yao, S.

Earth and Environmental Sciences Programme, The Chinese University of Hong Kong, Hong Kong, China

Quantitative earthquake hazard assessment demands understanding of earthquake location, magnitude, and ground motions. The location of large earthquakes can be largely predicted based on historical earthquake records and modern observations of interseismic deformation. However, estimates of rupture extent and magnitude from those data bare large uncertainties due to the poor representation of rupture process that are dependent on a number of factors (Figure 1). Moreover, ground motion predictions in near-filed regions for large earthquakes usually suffer from inadequate data. Here, we conduct spontaneous rupture simulations to obtain plausible rupture process and ground motions in future earthquakes, in which interseismic locking models are adopted to constrain the stress accumulation patterns on faults.

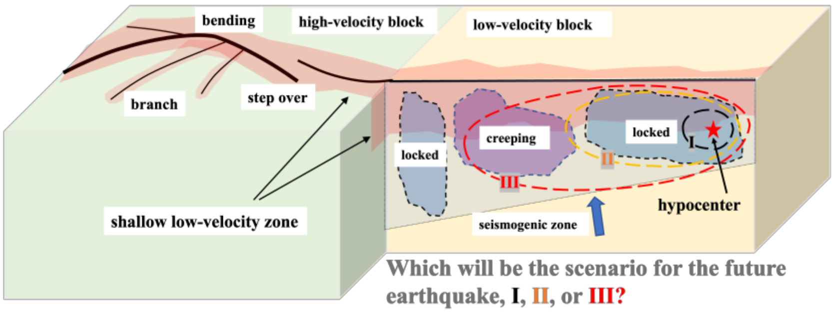

Figure 1. A map showing different factors that may affect rupture propagation, including fault geometry, near-fault material properties, along-strike variation of seismogenic zone and frictional properties. How can we predict future rupture scenarios?

Our study regions include the Nicoya megathrust in the central American subduction zone and the Anninghe fault in southwest China. Due to the lack of prior knowledge on future earthquake hypocenter locations, we test different nucleation sites. We find that the final slip distribution and final magnitude highly depend on the hypocenter locations. The moment magnitudes of scenarios for the Nicoya megathrust range from ~6 (self-arresting cases) to ~7.2 (segmented cases), and to ~7.5 (break the entire locked zone). We also find segmentation in scenarios along the Anninghe fault that are consistent with historical records. In addition, scenarios along the Anninghe fault can be buried or with significant surface slip (>3 m) in scenarios with different hypocenters, resulting in shallow slip deficit of 0 - 100%. Such hypocentral-dependent effects significantly influence ground motions mainly through different rupture directivities and shallow slip patterns.

We further quantify the standard deviations in predicted ground motions to be ~30% of mean predictions solely caused by the rupture indeterminism, as an important source of uncertainty from such an approach. To examine the reliability of predictions, we compare and validate them with traditional empirical ground motion equations (GMPEs) and observations during the 2012 Nicoya Mw 7.6 earthquake. Our results highlight the importance of rupture dynamics in predicting earthquake behaviors and the potential application of physics-based scenarios in future seismic hazard assessment.

An Integrated Project of Imaging, Monitoring and Simulating a Seismogenic Zone for Mitigation of Earthquake and Tsunami Hazards

Kodaira, S.[1], Fujie, G. [1], Araki E. [1], and Hori, T. [1]

1. *Japan Agency for Marine-Earth Science and Technology (JAMSTEC), Kanagawa, Japan*

Earthquakes and tsunamis in subduction zones have strongly impacted human society and the earth's environment. Looking at the subduction zones around Japan, it is clearly remembered the huge impact of the 2011 Tohoku-oki earthquake and earthquake activities after the Tohoku-oki earthquake. In addition, a high probability of occurrence of a large earthquake and huge damage of the Japanese society has been pointed out in the Nankai Trough and the southern part of the Kuril Islands Trench in the next thirty years. Toward mitigating hazards by subduction zone earthquakes and tsunamis, understanding subduction megathrust processes at present, and predicting a fault slip behavior in the future are central scientific themes and tasks that society expects a scientific community to address.

To challenge those scientific themes, we, JAMSTEC, have been conducting an integrated project in subduction zones which consists of imaging megathrust fault structures, monitoring a wide spectrum of fault slips, and simulating future fault behavior using the results of the imaging and monitoring studies (Fig. 1). The Nankai Trough megathrust seismogenic zone is one of the primally fields of the project. For imaging the Nankai megathrust zone, we have been mapping a precise 3D structure of the megathrust fault zone by densely deployed active-source seismic profiles covering the entire region of the Nankai Trough. From the 3D seismic image, we observe structural factors which are interpreted to control slips and coupling of the megathrust. We have been developing a real-time seafloor geodetic monitoring system to monitor activities of a wide spectrum of fault slips, including a regular earthquake, low-frequency tremors, very low-frequency earthquake, and short-term and long-term slow slip events. In this system, a tilt meter, pressure sensor, and fiberoptic strain meter are installed in a shallow or deep borehole. To continuously transfer the observed data to a land station in real-time, the geodetic sensors are connected to DONET, a cabled earthquake and tsunami monitoring system developed by JAMSTEC and operates by NIED. To simulate and forecast a megathrust slip behavior, we have been constructing a realistic 3D Nankai megathrust zone model and developing simulation techniques to estimate the temporal evolution of fault slip and coupling in the megathrust zone with consideration of uncertainties of the model and the data. Although the stage of a project is different, we apply the same approach in the Japan and the Kuril trenches.

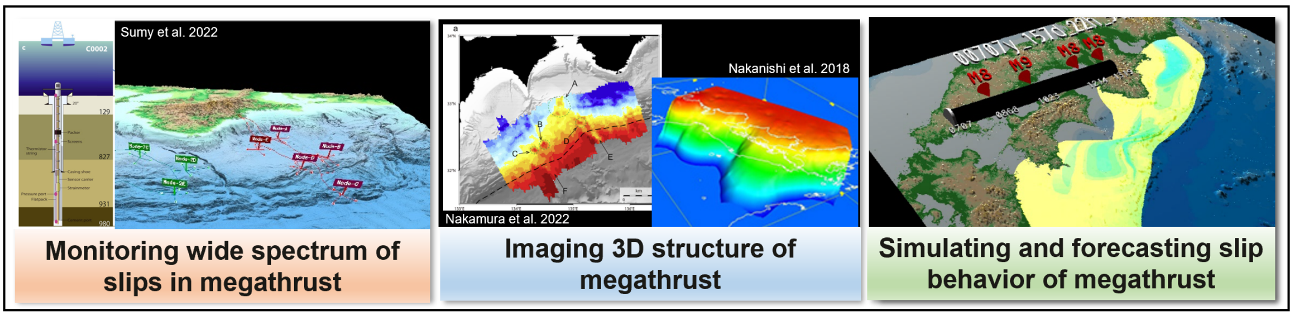

Fig.1 JAMSTEC's integrated project of imaging, monitoring and simulating a seismogenic zone

Integrated 3D P-wave Tomography Reveals Forearc Structure of the Central NE Japan Subduction Zone

Tozer, B.[1], Bassett, D.[1], Kodaira, S.[2], Arnulf, A.[3], Nakanishi, A.[2], Miura, S.[2], Fujie, G.[2] and Mochizuki, K.[4]

1. *GNS Science, Lower Hutt, New Zealand*
2. Japan Agency for Marine-Earth Science and Technology
3. *University of Texas Institute for Geophysics, Austin, Texas, USA*
4. *Earthquake Research Institute, the University of Tokyo*

Recent studies have shown that crustal structure of the overlying plate may play an important role in modulating the slip behaviour of megathrust faults. Here, we present an integrated active- and passive-source three-dimensional tomographic model of crustal structure in the central part of the NE Japan subduction zone – spanning the rupture area of the 2011 M9 Tōhoku earthquake. This model has been constructed using seismic travel-time data generated by over two decades of offshore seismic surveys undertaken by JAMSTEC, ERI and others, which were recorded passively by ~150 seismographs located both onshore (Hi-net, F-net, Tōhoku University and Japan Meteorological Agency (JMA) networks) and offshore (S-net and temporary deployed Ocean Bottom Seismometers). These data have been augmented by twenty years of earthquake travel-time arrivals recorded on ~350 seismographs from the same networks, as documented by the JMA and relocated in this study.

Notably, our model resolves a ~ 0.4 km s^{-1} reduction in P-wave velocity of the forearc crust from north to south across a pre-identified forearc segment boundary interpreted as the offshore extension of the Median Tectonic Line. This supports a previous interpretation of Bassett et al. [2016], whereby the differences in P-wave velocities can be attributed to lithologic heterogeneity in the forearc, with higher velocity volcanic rocks in the north and accretionary sediments in the south. It follows that upper-plate structure may have played a key role in modulating both the accumulation and release of elastic strain associated with the 2011 Tōhoku earthquake.

Striations of tectonic tremor and implication for fluid channels based on a dense seismic array in western Shikoku, Japan

Kato, A.[1], Takeo, A.[1], and Obara, K.[1]

1. *Earthquake Research Institute, the University of Tokyo, Tokyo, Japan*

Rapid tremor (a burst of low-frequency earthquakes) migration has been identified during slow long-distance migrations of a slow slip event by previous studies [Shelly et al., 2007; Kato and Nakagawa, 2020]. However, Rapid tremor migrations remain mysterious. What's the kind of structure to control rapid tremor migrations?

To reveal the detailed spatial-temporal evolution of tectonic tremors, we deployed a dense seismic array consisting of 100 portable seismometers at the western part of Shikoku, Japan, where clusters of tectonic tremors/low-frequency earthquakes have repetitively taken place over decades [Kato and Nakagawa, 2020]. We obtained continuous waveform data from the end of December in 2019 to the beginning of July 2020. During the deployment, an intensive activity of tremors happened beneath the seismic array around the end of February 2020. As shonw in Figure 1, the tremors occurred almost continusouly over 60 seconds during the intensive period. To detect and locate the tremor sources, the grid-points approach [Nakamoto et al., 2021] was applied to the continuous waveform. We assumed grid points (0.05 km interval) on the dipping plane that almost coincides with the plate interface model proposed by Hirose et al. [2008]. We then calculated a time series of semblance values over the seismic array by moving a 10s time window overlapping by 5s, based on the slowness vector of a seismic ray from each grid point to a reference station in the array. At each time step, we define a tremor as the grid point with the maximum semblance value within each time window greater than 0.3.

As an overall patten, the detected tremors initiated at deeper depth and moved to up-dip, then propagated slowly along strike-direction. We detected forward and backward migrations of rapid tremors along both dip- and strike-directions. The rapid tremor migrations with the speed of ~ 30 km/hr. The migration distance is small and the duration is short. Interestingly, we found out many striations with two different directions in the tremor distribution, namely WNW-ESE and NW-SE. The spatial interval of each striation is approximately1 km. These features imply that rapid tremor migrations might be controlled by fluid channels created by subduction of corrugated plate interface.

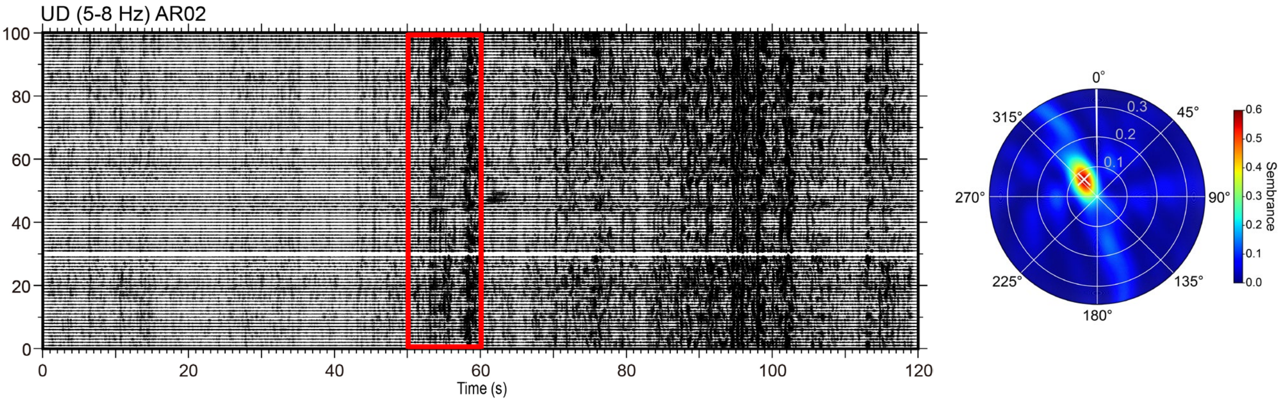

Figure 1. Left) Waveform traces during the initial stage of an intensive tremor activity (Vertical component). Right) Semblance at the time between 50 and 60 s (red rectangle in the left figure). The radius and angular of the polar coordinate indicate the slowness and the azimuth of arrival.

Estimation of the Locked and Transitional Creep Zones at Nankai and Cascadia Using Probabilistic Inversion Methods

Sherrill, E.M.[1], Johnson, K.M.[1], and Bartlow, N.M.[2]

1. *Indiana University, Bloomington, Indiana, USA*
2. *University of Kansas, Lawrence, Kansas, USA*

It is critical to understand the spatiotemporal distribution of the variety of slip behaviors (earthquakes, afterslip, slow slip events, and steady creep) observed at subduction zones in order to accurately assess seismic hazard. Growing evidence suggests that some large earthquakes at subduction zones begin with slow slip events (SSEs) near or within the fully coupled (or locked) zone and numerical models indicate that SSEs can load the locked zone and evolve into dynamic rupture. There is a gap, inferred by coupling inversions, between the locked zone and the slow slip zone at Cascadia. The presence or absence of this gap may greatly influence seismic hazard at subduction zones. It can be difficult to delineate the boundaries between locked, creeping, and slow slip regions using traditional least squares slip inversions because they often employ regularization techniques (such as smoothing) that smear the edges to avoid unrealistic slip distributions. We present here a Markov chain Monte Carlo inversion of interseismic velocities and baseline rate changes for the upper and lower boundaries of the locked zone at Nankai and Cascadia. This method allows us to obtain a posterior probability distribution of the boundaries to better assess the spatial relationship of the locked zone to slow slip and afterslip regions. We also invert for the boundaries of the upper and lower transition zones, defined as regions that are partially coupled above and below the locked zone. We assume creep at constant stress in the lower transition zone and allow upward propagation of creep following Bruhat and Segall [2017]. Our homogeneous elastic halfspace inversion infers that the regions of observed slow slip at both Nankai and Cascadia are within the lower transition zones. While there is minimal separation between the bottom of the locked zone and the top of the lower transition zone at Nankai, there appears to be a gap between the locked zone and lower transition zone at Cascadia (Figure 1). We will also explore the impact of elastic heterogeneity and viscoelastic cycle deformation on the coupling models. This work will provide insights into the spatial relationship of slow slip events to the seismogenic and transition zones at Nankai and Cascadia and inform seismic hazard assessment at both subduction zones.

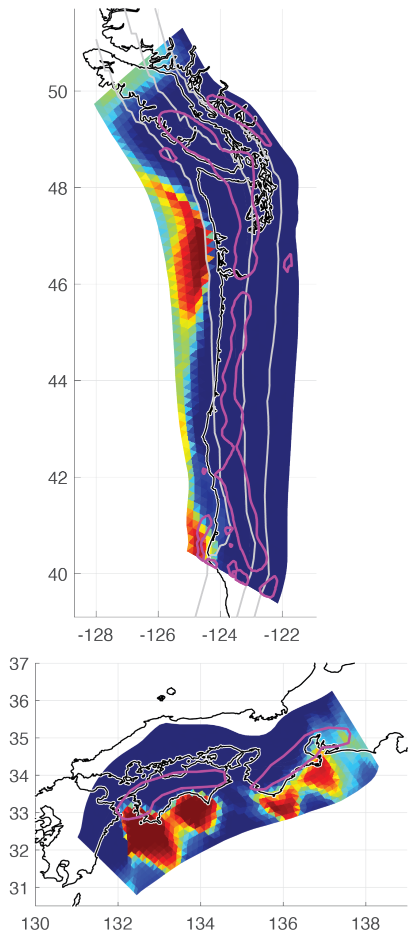

Figure 1. Probability that a patch is in the locked zone at Cascadia (top) and Nankai (bottom). Red is high probability and blue is low probability. The solid pink polygons are rough estimates of the slow slip zones.

Interseismic locking on megathrust controls long term strain partitioning in subduction zone

Lamb, S

School of Geography, Environment and Earth Sciences, Victoria University of Wellington, New Zealand

Along the Hikurangi Margin in New Zealand, the Pacific plate is obliquely (~45°) subducting beneath the Australian plate at ~40 mm/yr. The overlying deforming wedge has long term strain partitioning, with some trench-parallel plate motion focused on major dextral strike-slip faults in the back part of the deforming wedge. These faults pose a major seismic hazard, capable of rupturing as M6 to M8+ earthquakes.

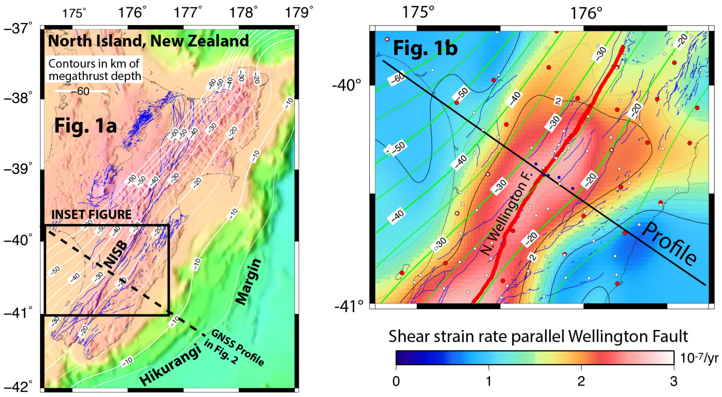

Here, I analyse GNSS measurements of the decadal interseismic strain rates in part of eastern North Island (Beavan et al. 2016), where the northern Wellington Fault is the only major active dextral strike-slip fault (Fig. 1a, b). The fault plane is subvertical, with an assumed slip rate over the Holocene of 5–10 mm/yr. The interseismic deformation is well modelled by a simple 2-D elastic dislocation model in which the underlying subduction megathrust is fully locked at depths between 30 and 8 km (Fig. 2a, b; note the enhanced microseismicity in the locked region). The creeping (or repeated slow slip SSE) deeper and shallower parts of the megathrust slip at the full relative plate velocity. Importantly, the model contains *no* information about the slip rate and geometry of the major faults in the overlying deforming wedge, and it *cannot* predict these slip rates; the pattern of interseismic strain rates appears to be dictated solely by the locking on the megathrust. However, the strike-slip fault is precisely located where the interseismic shear strain rate is at its maximum, directly above the deeper locking line, and so locking on the megathrust appears to determine the pattern of long-term strain partitioning too. During a large magnitude earthquake on the northern Wellington Fault, the entire thickness of the wedge must rupture. Inactive parallel faults adjacent to the active trace suggest there has been movement of the locking line over time.

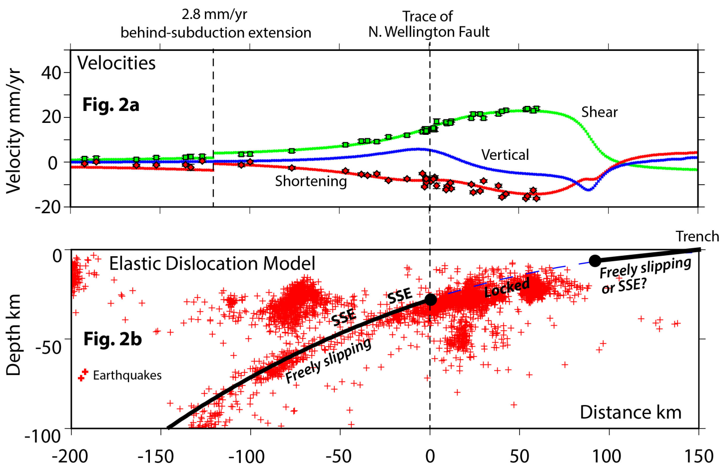

The degree of partitioning is a consequence of the relative frequency of large magnitude earthquakes on the megathrust compared to those in the overlying deforming wedge, assuming constant stress drops for individual earthquakes. The interseismic megathrust locking must be a key factor here, because this controls the stress field at the point where a large magnitude earthquake is most likely to nucleate, and thus which faults will rupture.

Repeated Rupture of Long-Lived Asperities at the Kermadec Subduction Zone

Lythgoe, K.H.[1], Bradley, K.[1], Zeng, H.[2], and Wei, S.[1,2]

1. *Earth Observatory of Singapore, Nanyang Technological University, Singapore*
2. *Asian School of the Environment, Nanyang Technological University, Singapore*

To what degree large earthquakes are 'characteristic' is a key question in understanding the fundamentals of the seismic cycle. Here we study the ruptures of the 2021 Mw8.1 earthquake sequence in the Kermadec subduction zone and compare them with the 1976 doublet that occurred at the same location (Figure 1). We find the 2021 mainshock likely re-ruptured the asperity of the 1976 Mw7.9 event, whereas the other ruptures differ in character and location. All earthquakes occur in an isolated area of the megathrust, bounded by changes in the lithospheric structure of the overriding plate, as indicated by residual bathymetric and gravity anomalies. The rupture areas are coincident with an isolated forearc sedimentary basin, which suggests that the sedimentary basin is formed by seismic slip, and that seismic slip has persisted here for several million years. We conclude that the stress heterogeneity within this bounded seismogenic zone is long-lived and has produced a rich spectrum of earthquake ruptures. Given the Kermadec margin is preferentially oriented to direct tsunami energy towards northern New Zealand, our results also have implications for seismic and tsunami hazards in the region.

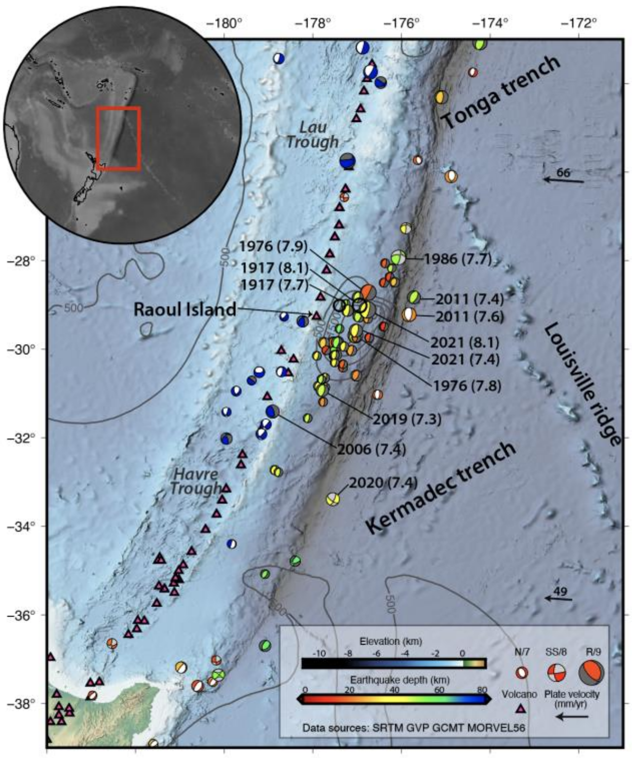

Figure 1 Tectonic overview of the Kermadec subduction zone. Moment tensors for earthquakes with magnitude > 6.5 are plotted with sedimentary thickness contours every 500 m.

Periodic Pore Fluid Pressure Perturbations on Rate-Strengthening Faults may Explain Characteristics of Slow Slip Events

Perez-Silva, A.[1], Kaneko, Y.[2], Savage, M.[1], and Wallace, L.[3,4]

1. Victoria University of Wellington, School of Geography, Environment and Earth Sciences, Wellington, New Zealand

2. Kyoto University, Department of Geophysics, Kyoto, Japan

3. GNS Science, Lower Hut, New Zealand

4. University of Texas, Institute for Geophysics, Austin, Texas, USA

Geophysical observations indicate that temporal pore fluid pressure changes correlate with slow slip events (SSEs) occurring along the shallow portion of the Hikurangi margin (Warren-Smith et al. [2019]) and in different subduction zones (Gosselin et al. [2020], Kita et al. [2021], Nakajima & Uchida [2018]). These fluctuations in pore fluid pressure are attributed to fluid migration before and during SSEs, which may modulate SSE occurrence. To examine the effect of pore fluid pressure changes on SSEs, we conduct numerical simulations in which we impose periodic pore-pressure perturbations on a rate-strengthening fault. We define two types of perturbations, assuming either a simplified (type I) or along-fault (type II) fluid migration. Both perturbations induce SSEs, whose properties depend mainly on the characteristics of the pore-pressure change (amplitude, characteristic length, and period). By varying the perturbation characteristics, we find models that reproduce shallow Hikurangi SSE properties (duration, magnitude, slip, recurrence) and SSE moments and durations from different subduction zones. Our results indicate that large permeability values of 10^{-14} to 10^{-10} m^2 are needed to reproduce the observed SSE properties. Such high values could be due to transient and localized increases in fault zone permeability in the shear zone where SSEs occur. Our model results suggest that a rate-strengthening fault subject to periodic pore-pressure perturbations may be a viable mechanism for SSE generation.

Near-Trench Slow Slip Events at the Osa Peninsula in Southern Costa Rica From GNSS Time Series

Perry, M.[1], Muller, C.[2], Protti, M.[2], Feng, L.[1], Hill, E.[1,3]

1. *Earth Observatory of Singapore, Nanynang Technological University, Singapore, Singapore*
2. *Observatorio Vulcanológico y Sismológico de Costa Rica (OVSICORI), Heredia, Costa Rica*
3. *Asian School of the Environment, Nanyang Technological University, Singapore, Singapore*

A challenge common to the identification and classification of shallow slow slip events (SSEs) is the lack of near-trench observations, and many of those that exist come in the form of ocean bottom data which is notoriously noisy and lacks spatial resolution. In southern Costa Rica, the Osa Peninsula and its surroundings provide a unique opportunity to use terrestrial methods to investigate subduction zone processes from stations as close to the trench as 20 km (often <40 km). Using continuous GNSS time series spanning from 2011 to 2022 from this region, we identify five distinct shallow SSEs that occurred beneath and immediately offshore the peninsula. While SSEs have been identified at Nicoya in northern Costa Rica, this is their first documentation in southern Costa Rica. The first event in June 2013 was registered at only one site, while the other four events were all recorded by several sites. The event in early 2018 occurred over a period of approximately 30 days, with a modeled slip accumulation of ~30 cm centered updip of a swarm of seismic activity that occurred at the same time. The second event occurred a few months later and was smaller in scale, with a modeled maximum slip of ~15 cm. Four years later, in 2022, we observe two additional SSEs, one in early 2022 and another in mid-2022. The early 2022 event occurred over about 30 days with an estimated slip accumulation of ~15 cm. The mid-2022 event occurred over approximately 15 days and modeling indicates ~10 cm of slip accumulation. The estimates spatial distribution of slip from all four events occurred roughly on the same updip patch of the Central American megathrust, near the region that ruptured during historical large earthquakes in 1904, 1941, and most recently in the 1983 M_w 7.4 Osa event, indicating that these slow slip events may modulate the magnitude and slip distribution of future large ruptures.

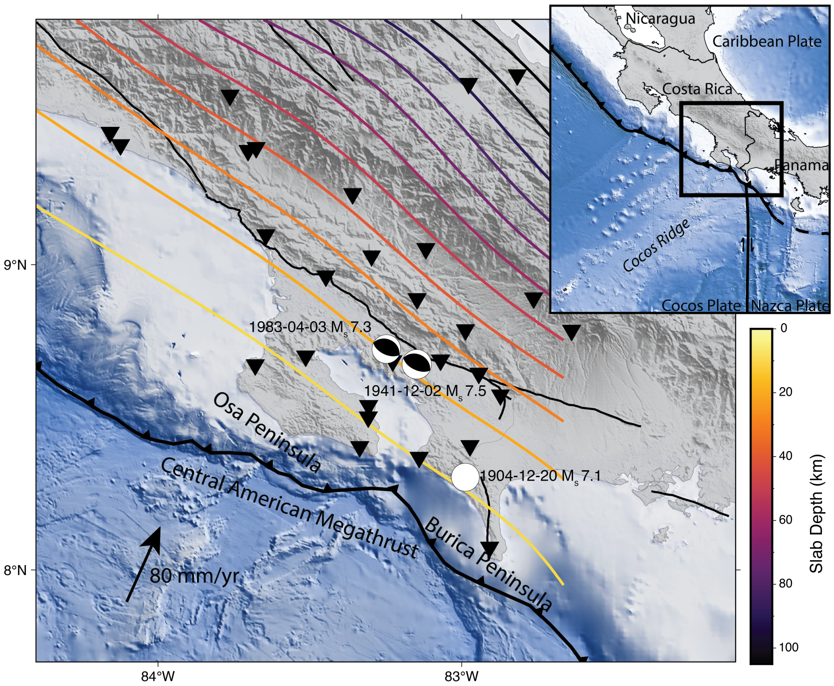

Figure 1: Overview of study area. Large historical earthquakes are plotted with locations and focal mechanisms (where available) from Amadek et al., (1987). GNSS stations in the region are plotted as black triangles. Slab depth is a shifted Slab2.0 geometry (Hayes et al., 2018) to better fit regional shallow seismicity.

Slow Slip Events at the Hikurangi Subduction Margin, New Zealand, from 2006 to 2017

Williams, C. A.[1], Wallace, L. M.[1,2], Bartlow, N. M.[3], and Haines, J.[1]

1. *GNS Science, Lower Hutt, New Zealand*
2. *University of Texas Institute for Geophysics, Austin, Texas, USA*
3. *University of Kansas, Lawrence, Kansas, USA*

Slow slip events (SSEs) are frequent along the Hikurangi Margin and understanding them is critical to our understanding of interseismic coupling, plate motion budgets, and the potential for damaging earthquakes. Deeper and less frequent SSEs are observed on the southern margin, while shallower and more frequent events are observed along the northern section. We are compiling a catalogue of Hikurangi SSEs covering the period from 2006 to 2017 to help us understand the spatial and temporal patterns of slip. Using this catalogue, we can begin the process of characterising the behaviour of Hikurangi SSEs, looking at properties such as depth, peak slip rate, total slip, and recurrence interval. It will also allow us to explore possible scaling relationships, such as that between moment release and event duration.

We use the Network Inversion Filter (NIF) [Segall and Matthews,1997; McGuire and Segall, 2003; Miyazaki et al., 2006] to perform our time-dependent slip inversions. We generate Green's functions using the PyLith finite element code [Aagaard et al., 2013] to include elastic property variations provided by the New Zealand-wide seismic velocity model [Eberhart-Phillips et al., 2010]. Previous results [Williams and Wallace, 2015; 2018] showed that SSE inversions that consider elastic heterogeneity provide significantly different results compared to elastic half-space solutions. Incorporating these effects significantly improves the accuracy and reliability of our time-dependent inversions. Our inversions also include recent absolute pressure gauge (APG) data to constrain offshore vertical movement during a recent SSE observed in 2014. Most recently, we have used the VDoHS technique [Haines et al., 2015] to provide much cleaner time series to use with the NIF. The catalogue represents the most comprehensive to date for the Hikurangi Margin, and the usage of APG data and consideration of elastic heterogeneity effects will provide the best possible constraints on the predicted slip distributions.

Wallace, L.M.[1,2], Ito, Y.[3], Saffer, D.[1], Woods, K.[4], Palmer, N.[2], Yamashita, Y.[3], Mochizuki, K.[5], Suzuki, S. [6], Hino, R.[6], Williams, C.[2], Davis, E.[7], Warren-Smith, E.[2], Jacobs, K.[2], and Savage, M.[4]

Insights into the occurrence and characteristics of near-trench slow slip events at the Hikurangi subduction zone from several years of seafloor geodetic experiments and IODP observatory data

1. *University of Texas Institute for Geophysics, Austin, Texas, USA*
2. *GNS Science, Lower Hutt, New Zealand*
3. *DPRI, Kyoto University, Japan*
4. *SGEES, Victoria University of Wellington, New Zealand*
5. *Earthquake Research Institute, University of Tokyo, Japan*
6. *Tohoku University*
7. *Pacific Geosciences Center, Natural Resources Canada*

Resolving the distribution of transient slow slip event (SSE) processes at offshore subduction zones is hampered by the difficulty of measuring offshore crustal deformation. Two methods are overcoming these challenges: (1) using ocean bottom pressure sensors to discern seafloor pressure changes due to vertical deformation, and (2) measuring pore pressure changes in subseafloor observatories as a proxy for formation volumetric strain. Both approaches have been employed (concurrently with deployment of ocean bottom seismometers) since 2014 in several experiments along the Hikurangi subduction zone offshore New Zealand, with the goal of capturing near-trench SSEs and their relationship to seismicity. We will overview results from several seafloor pressure sensor/OBS deployments undertaken over the last several years, to capture crustal deformation and seismicity during shallow, offshore slow slip events. In particular, we will highlight results from a May 2021 SSE offshore Pōrangahau at the central Hikurangi subduction zone, occupying the along-strike transition from deep interseismic coupling to aseismic creep, and from a large 2019 SSE spanning from the northern Hikurangi margin (offshore Gisborne) to the central Hikurangi margin (offshore Hawkes Bay).

We will also present new insights into offshore Hikurangi SSEs from two IODP borehole observatories installed in 2018 at northern Hikurangi, located within a few kilometres of the source of large, well-documented shallow SSEs. Formation pressure data reveal pressure changes equivalent to 0.1 to 0.3 microstrain during a large 2019 SSE. The subseafloor observatory data (together with onshore GNSS and seafloor pressure data) constrain the distribution and evolution of slip during the 2019 SSE, and require a maximum of 20 cm of slip at 6-7 km depth, with up to 10 cm of slip <10 km from the trench. The locus of early peak slip corresponds with peaks in expected dehydration of subducting volcaniclastic material, indicating possible influence from fluid overpressure. Our models also demonstrate that incorporating realistic near-surface elastic moduli (constrained by in-situ LWD measurements) is required to fit borehole strain and surface displacement data simultaneously.

Ambient Noise Tomography Above a Region of Slow-Slip, Hikurangi Margin, New Zealand

Jacobs, K.[1], Eberhart-Phillips, D.[1], Henrys, S.[1], Okaya, D.[2], Fry, B.[1], and Bell, B.[3]

1. *GNS Science, Lower Hutt, New Zealand*
2. *University of Southern California*
3. *Imperial College London*

The NZ3D-FWI project deployed a dense grid of broadband and short period instruments above a part of the Hikurangi subduction interface, North Island, New Zealand, that experiences slow slip events every 18 -24 months. The array was deployed to record air-gun shots from the R/V Marcus Langseth, which acquired a 3D multichannel seismic volume offshore in January 2018. Following the active source experiment, the broadband array of 49 CMG-6TD broadband seismometers from the NERC Geophysical Equipment Facility (SEIS-UK) were left in place for an additional 9 months for further passive studies.

We present results of ambient-noise tomography using station pairs from this dense broadband array, deployed with ~2 km spacing over a 20x10 km grid, into the surrounding permanent GeoNet network. The Gisborne region studied here also overlaps with the Seismogenesis at Hikurangi Integrated Research Experiment (SHIRE) which carried out a wide-angle, onshore-offshore, reflection-refraction active seismic survey together with a 4 month-long passive deployment.

To analyze the surface wave velocities, we first create daily cross-correlations. For each station-pair, daily cross-correlations are stacked for all available data during the 10-month deployment. Surface wave dispersion curves are then picked for all stacked station-pair cross-correlations. We focus on the period band between 5-10s (0.1-0.2 Hz) as it contains the most consistent energy across different pairs. We then invert the resulting Rayleigh wave group velocity maps for a 3D crustal structure.

Initial surface wave moveouts suggest very slow seismic velocity material (Rayleigh Wave Velocity < 1 km/s) over much of the region. These results will help define the extent of low velocity material inferred from previous waveform modelling (e.g. Kaneko et al. [2019]).

Coral Microatoll Paleogeodetic Records from Sumatra and Luzon

Meltzner, A.J.[1,2], Sarkawi, G.M.[1,2], Li, X.[1], Philibosian, B.[3], and Ramos, N.T.[4]

1. *Earth Observatory of Singapore, Nanyang Technological University, Singapore*
2. *Asian School of the Environment, Nanyang Technological University, Singapore*
3. *Earthquake Science Center, U.S. Geological Survey, Moffett Field, California, USA*
4. *National Institute of Geological Sciences, University of the Philippines, Diliman, Quezon City, Philippines*

Subduction megathrusts can produce the largest ruptures on Earth, but along many subduction zones, little is known of the seismic potential, owing to long recurrence intervals, short historical records, and insufficient geodetic monitoring. Geological proxy records of relative sea-level change allow us to inter past vertical land motion and hence tectonic deformation, but most proxies have large vertical and/or chronological uncertainties, limiting their utility. In some low-latitude coastal regions, coral microatolls (Figure 1) — coral colonies whose upward growth is limited by occasional exposure at extreme low tides — provide long, continuous, high-precision records of relative sea-level change over the coral's lifetime, yielding data to quantify abrupt and gradual vertical deformation.

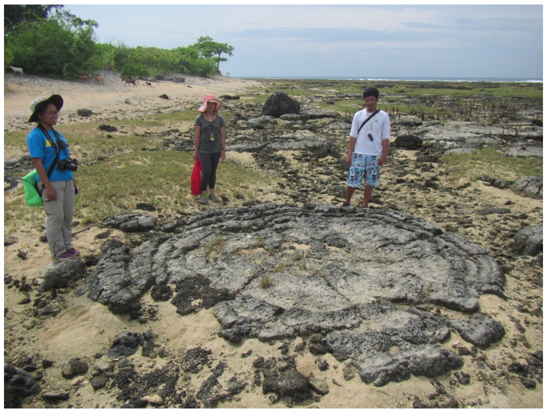

Figure 1. A fossil coral microatoll in Luzon that yielded an 85-yr record of subsidence and sea level, ~1000 yr ago.

In this presentation, we focus on corals along two subduction zones: the Sunda Megathrust off Sumatra and the Manila Trench off Luzon. The world was surprised in 2004 by a M_W 9.2 rupture of the northern Sunda Megathrust in the Indian Ocean, but subsequent work [e.g., Jankaew et al., 2008; Monecke et al., 2008; Meltzner et al., 2010] identified multiple prehistoric predecessors to this event that could have led us to anticipate the 2004 event. No earthquake along the Philippine portion of the Manila Trench has exceeded M_S 7.6 since at least 1589 CE [Repetti, 1946; Bautista and Oike, 2000], but coupling along this subduction zone is poorly constrained due to the limited geodetic data [Hsu et al., 2016]; as a result, the earthquake and tsunami hazard along this coastline is undetermined.

In Sumatra, outer-arc islands above the seismogenic zone host microatolls that allowed us to date and map the spatial extent of past $M \geq 8$ megathrust ruptures [Meltzner et al., 2010, 2012, 2015; Philibosian et al., 2012, 2014, 2017]; to characterize frequent to persistent barriers to rupture [Morgan et al., 2017; Philibosian and Meltzner, 2020]; to identify long-term slow-slip events lasting 15–32 years [Tsang et al., 2015a; Mallick et al., 2021]; and to quantify interseismic subsidence rates that vary spatially and over the seismic cycle, or from one seismic cycle to the next [Meltzner et al., 2010, 2012, 2015; Philibosian et al., 2014, 2017; Tsang et al., 2015b]. In northern Luzon, where the plate interface dips steeply, microatoll sites lie over portions of the megathrust downdip of the seismogenic zone. Although our analysis is preliminary, coral microatoll records from Luzon likely provide evidence for both megathrust and offshore splay-fault ruptures, manifesting as coseismic subsidence and coseismic uplift, respectively.

Past earthquakes on the southern Hikurangi Subduction Zone

Litchfield, N. [1], Clark, K.[1], Howell, A.[1,2], Pizer, C.[3]

1. *GNS Science, Lower Hutt, New Zealand*
2. *University of Canterbury, Christchurch, New Zealand*
3. *Victoria University of Wellington, Wellington, New Zealand*

The southern Hikurangi Zone is a complex transition zone where convergence is increasingly accommodated by upper-plate faults towards the southwest, making identification of past subduction earthquakes challenging. Historical, primarily upper-plate fault earthquakes, in 1855 (M8.1+ Wairarapa) and 2016 (M7.8 Kaikōura) also involved slip on the interface, demonstrating that combined interface-upper plate fault ruptures are also likely.

Paleoearthquake investigations have been undertaken at a number of coastal sites in the southern North Island and northeastern South Island over the last two decades. Subsidence and tsunami records from Holocene estuary core records (e.g, Figure 1a) and uplift records from Holocene marine terraces (e.g., Figure 1b) show past uplift and subsidence earthquakes in areas that match with the pattern of current interseismic locking. Subduction earthquakes have been identified through comparison of the locations and vertical land movements with dislocation models, tsunami models, and upper-plate fault records. These show four subduction earthquakes in the past 2000 years, resulting in a recurrence interval of ~500 years and a probability of a large subduction earthquake in the southern Hikurangi Subduction Zone of 26% in the next 50 years. Ongoing work in the southern Hikurangi Subduction Zone is hoping to extend the length of these records (to ~7500 years?) and to further investigate combined subduction interface – upper-plate fault earthquakes.

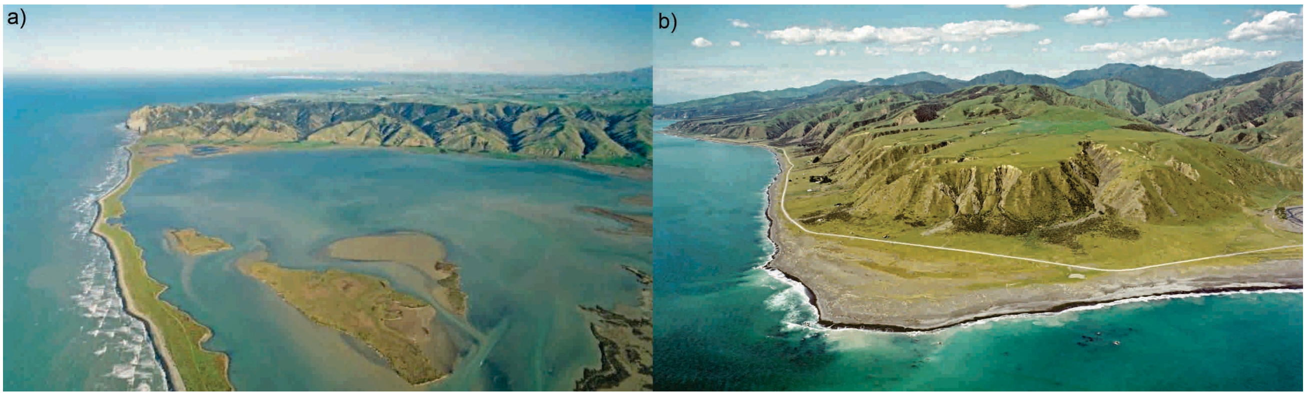

Figure 1. a) Mataora-Wairau Lagoon, eastern Marlborough, South Island. B) Te Humenga Point, southern Wairarapa, North Island.

Causes of permanent vertical deformation at subduction margins: evidence from elevated late Pleistocene marine terraces of the southern Hikurangi Margin, Aotearoa New Zealand.

Ninis, D.[1], Howell, A.[2,3], Little, T.[4], and Litchfield, N.[3]

1. *Seismology Research Centre, Richmond, Wurundjeri Woi Wurrung Country, Victoria, Australia*
2. *School of Earth and Environment, University of Canterbury – Te Whare Wānanga o Waitaha, Christchurch, Aotearoa New Zealand*
3. *GNS Science – Te Pū Ao, Lower Hutt, Aotearoa New Zealand*
4. *School of Geography, Environment and Earth Sciences, Victoria University of Wellington – Te Herenga Waka, Wellington, Aotearoa New Zealand*

Studies of the seismic cycle at convergent plate boundaries anticipate that most coseismic deformation is recovered, yet significant permanent vertical displacement of the overriding plate is observed at many subduction margins. To understand the mechanisms driving permanent vertical displacement, we investigate tectonic uplift across the southern Hikurangi subduction margin, Aotearoa New Zealand, in the last ~200 ka. Marine terraces preserved along the Wellington south coast have previously been dated as Marine Isotope Stages (MIS) 5a, 5c, 5e and 7a in age (Ninis et al. 2022). We use these ages, together with new reconstructions of shoreline angle elevations, to calculate uplift rates across the margin and to examine the processes responsible for their elevation. The highest uplift rate – 1.7 ± 0.2 mm/yr – and maximum tilting – 2.9º to the west – are observed near Cape Palliser, the closest site to (~40 km from) the Hikurangi trough. Uplift rates decrease monotonically westward along the Palliser Bay coast, to 0.2 ± 0.1 mm/yr at Wharekauhau (~70 km from the trough), defining a gently west-tilted subaerial forearc domain. Locally, active oblique-slip upper-plate faults cause obvious vertical offsets of the marine terraces in the axial ranges (>70 km from the trough). Uplift rates at Baring Head, on the upthrown side of the Wairarapa Fault, are ~0.7-1.6 mm/yr. At Tongue Point, uplift on the upthrown side of the Ōhāriu Fault is 0.6 ± 0.1 mm/yr. Dislocation modelling of faulting constrained by these uplift rates indicate that deep-seated processes – the earthquake cycle on the subduction interface, the buoyancy of the subducting Hikurangi Plateau, and sediment underplating – contribute ≤0.4 mm/yr, and potentially much less, to permanent vertical displacement across the margin. By contrast, slip on faults within the overriding Australian Plate dominates the ≳1 mm/yr of uplift at Cape Palliser and Baring Heads and are responsible for >20% (and probably >50%) of permanent uplift; depending on their geometry and slip rate, such faults could be responsible for ≥80% of Late Pleistocene uplift along the southern Hikurangi Margin. These results indicate a significant contribution of slip on upper-plate faults to permanent uplift and tilting across the subduction margin and suggest that in regions where upper-plate faults are prevalent, strong constraints on fault geometry and slip rate are necessary to determine contributions of deeper-seated processes to uplift.

Ground Motion Models for Subduction seismicity in New Zealand

Manea, E. F.[1,2], Bora, S.[1], Kaiser, A.[1], and Gerstenberger, M.[1]

1. *GNS Science, Lower Hutt, New Zealand*

2. *National Institute for Earth Physics, Măgurele, Romania*

The New Zealand National Seismic Hazard Model (NSHM; Gerstenberger et al., [2022]) has undergone its first significant revision in 10 years, and a newly compiled high - quality ground - shaking motion database was built and comprises all the seismic events with Mw≥4 recorded across NZ since 2000 (Hutchinson et al., [2021]). Beside this, significant improvements were also done on the evaluation of the local site parameters for stations within the national seismic network (Wotherspoon et al., [2022], Manea et al., [2022]).

By exploiting this database, a new ground motion model (GMM) for subduction seismicity was developed for various intensity measures such as, peak ground acceleration and 5% - damped pseudo - spectral acceleration up to 10 seconds. Beside common predictors (e.g. magnitude, depth, distances, Vs30), additional parameters were added to quantify the distinct attenuation patterns of the seismic waves observed along and behind the Havre Trough - Taupo Rift for the Hikurangi subduction zone trench. We observed different trends in the residuals in these regions based on the hypocentral-depth location on the slab and three distinct attenuation coefficients were added for each region in accordance with the observed 3D attenuation. This delineation with depth of the ground motion despairs after 1 second while the effect of the attenuation is still being present but reduced at longer periods.

To capture the local site amplification along the sedimentary structures, the local site variability was constrained based on multiple site parameters (e.g. fundamental frequency of resonance). Additionally, epistemic uncertainty in regional source, path and site properties was constrained using a partially non-ergodic methodology. We also derived a heteroscedastic aleatory uncertainty model that accounts for soil nonlinearity in addition to the magnitude and distance dependance of sigma.

The new GMMs have a robust performance compared to regional observations and their forecast capabilities of the different parameters are consistent with the ones computed using the selected GMMs. The subduction model is recommended for application to interface and inslab earthquakes with Mw ranging from 4 to 7.8, and rupture distance less than 500 km. Future works will be done on implementing the proposed GMMs in the NSHM evaluation to constrain the local variability and regional path effects.

References:

1. Hutchinson J, Bradley BA, Lee RL, Wotherspoon LM, Dupuis M,Schill C, Motha J, Kaiser AE, Manea EF. 2022. 2021 New Zealand Ground-Motion Database. Lower Hutt (NZ): GNS Science. 45 p. (GNS Science report; 2021/56). doi:10.21420/Z20E-5507.
2. Gerstenberger MC, Bora S, Bradley BA, DiCaprio C, Van Dissen RJ, Atkinson GM, Chamberlain C, Christophersen A, Clark KJ, Coffey GL, et al. 2022. New Zealand National Seismic Hazard Model 2022 revision: model, hazard and process overview. Lower Hutt (NZ): GNS Science. 106 p. (GNS Science report; 2022/57). doi:10.21420/TB83-7X19.
3. Manea, Elena, Anna Kaiser, Liam Wotherspoon, Andrew Stolte, and Matthew Hill (2022). Evaluation of site parameters to inform seismic site characterization in New Zealand. Australian Earthquake Engineering Society Proceeding.
4. Wotherspoon LM, Kaiser AE, Manea EF, Stolte AC. 2022. National Seismic Hazard Model: Site Characterisation Database summary report. Lower Hutt (NZ): GNS Science. 54 p. (GNS Science report; 2022/28). doi:10.21420/363X-CK83.

Deep Megathrust Rupture and Faulting Interaction during the 2021 M_W 8.1 Kermadec Earthquake Sequence

Lingling Ye[a], Yangmin Hu[a], Xiaofei Chen[a], Thorne Lay[b], Hiroo Kanamori[c], Fabrizio Romano[d], and Stefano Lorito[d]

[a] *Department of Earth and Space Sciences, Southern University of Science and Technology, Shenzhen, China*

[b] *Department of Earth and Planetary Sciences, University of California Santa Cruz, Santa Cruz, CA, USA*

[c] *Seismological Laboratory, California Institute of Technology, Pasadena, CA, USA*

[d] *Istituto Nazionale di Geofisica e Vulcanologia, Roma, Italy*

A sequence of large earthquakes with an M_W 7.4 event preceding an M_W 8.1 event by 1 hr 47 min struck the northern Kermadec megathrust with inferred interface locking from the occurrence of major near-trench deep compressional faulting and prior geodetically-measured slip deficit. Joint inversion of teleseismic body waves and static displacement at GNSS station RAUL for the two major events show that large slip, up to ~6 m, is concentrated from 30-50 km along the deeper part of the megathrust, with the M_W 7.4 foreshock nucleating near the down-dip edge of the M_W 8.1 mainshock. There is a significant overlap of the slip regions in the two events, and a moderate number of small events occurred in the time between them. Most aftershocks were concentrated up-dip of the mainshock with little coseismic slip. The mainshock model is validated by forward modeling of tsunami recordings, and the lack of shallow rupture reduced the corresponding tsunami excitation. The shallower portion of the megathrust has experienced substantial small to moderate earthquakes since the 1976 M_W 7.9 sequence that involved deep major thrust earthquakes spaning the 2021 rupture zone. Although this region of the plate boundary has hosted substantial earthquake activity, we demonstrate that the largest 1976 M_W 7.9 event differs in rupture from the 2021 mainshock, and that the 1917 M_W 8.1 event may have had a different (intraplate) mechanism, so no simple seismic cycle. Overall, there appear to be strong stress interactions between the stick-slip failure and strain accumulation of the deep megathrust where the major events occur, the weaker shallow megathrust where extensive background activity and aftershocks occur, and the trench-slope region where stresses in the bending plate are modulated by the interplate seismic cycle and, in turn, feedback on the shallow megathrust stress regime.

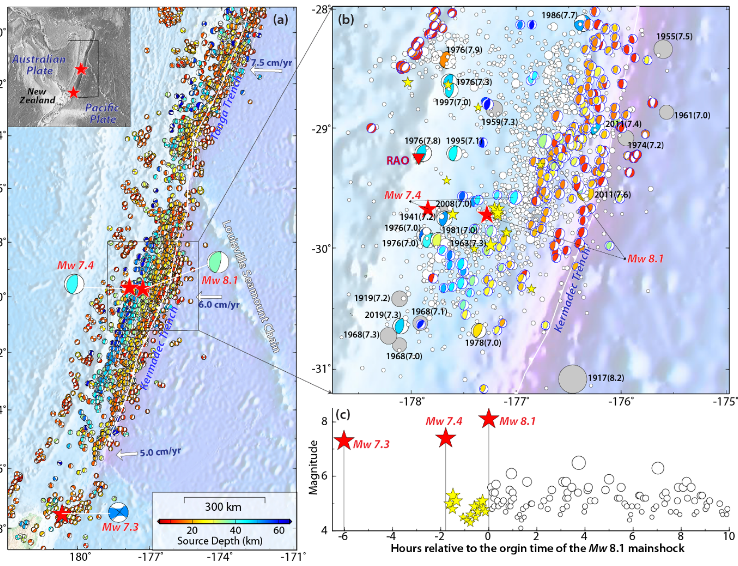

Figure 1. Focal mechanisms and seismicity around the 2021 M_W 8.1 Kermadec earthquake sequence.

Rapid Estimation of Single-Station Earthquake Magnitudes With Machine Learning on a Global Scale

Dybing, S. N.[1,2], Yeck, W. L.[2], Cole, H. M.[2], and Melgar, D.[1]

1. *University of Oregon, Eugene, Oregon, USA*
2. *USGS National Earthquake Information Center, Golden, Colorado, USA*

We present a method for rapid and automatic estimation of single-station earthquake magnitudes using raw three-component P waveforms observed at local to teleseismic distances. We use the MagNet regression model architecture (Mousavi and Beroza, 2020), which utilizes both convolutional and recurrent neural networks. Our model was trained using hundreds of thousands of waveforms approximately centered on the first P-phase arrival (P, Pn, or Pg) and labeled by U.S. Geological Survey (USGS) authoritative magnitude (principally Mw, ML, and mb). These waveforms and labels come from the Machine Learning Asset Aggregation of the Preliminary Determination of Epicenters (MLAAPDE), which is a dataset and query tool built from the Preliminary Determination of Epicenters (PDE) bulletin published by the USGS's National Earthquake Information Center (NEIC). MLAAPDE is designed to facilitate rapid prototyping of machine learning applications for global earthquake monitoring. We test a variety of input data parameters (e.g., window length) that can impact the effectiveness of our model in real-time monitoring applications. At the longest waveform window length of just less than two minutes, our model can estimate earthquake magnitudes in the range of M2.8-8, with magnitudes above ~M6 tending to be increasingly underpredicted to up to half a magnitude unit above M8 9. As the waveform windows are shortened to as little as a few seconds to determine how fast this process could work in real-time, the point at which higher magnitudes begin to be underpredicted moves toward lower magnitudes, and the degree of underprediction increases. This is suggestive of magnitude saturation effects. Importantly, this method can determine earthquake magnitudes with individual stations' waveforms without instrument response removal and without knowing the source-station distance of the event. This will enable the NEIC to more rapidly distinguish large, potentially tsunamigenic global earthquakes, which would allow for other automatic process (e.g., association, location, and moment tensor solution calculation) to be optimized. This would ensure that source characterization (e.g., location, magnitude, and style of faulting) is prompt and accurate for use in emergency response and hazard assessment activities.

Deep Learning with Uncertainties for the phase onset time prediction, Blenheim, New Zealand, 28 February – 3 March, 2023

Novoselov, A.[1], Pace, J.[2], Wiliams, J.[2], and Beroza, G.[1]

1. *Stanford University, Department of Geophysics, CA, USA*
2. *Global Technology Inc, Atlanta, GA, USA*

The Deep Learning has become an important tool for seismology and earthquake monitoring. We present a deep learning method that detects seismic phases and estimates the corresponding picking uncertainties.

Seismic phase picking is the process of identifying the onset time of a seismic phase in a seismogram. The arrival time of a seismic phase is one of the most important pieces of information in seismology and is used in a wide range of applications. These include locating earthquakes, determining earth structure, and identifying nuclear explosions. The detection and picking of seismic phases is a time-consuming and labor-intensive task when performed manually. The need for automation has driven the development of several algorithms and neural networks that attempt to solve this problem.

Deep Learning methods have been shown to be able to outperform conventional methods of phase picking. However, those methods usually lack an estimation of model's uncertainty. The knowledge of the uncertainty of the phase pick helps to improve the accuracy of the location. If the arrival time is overestimated, the distance between the seismic station and the earthquake is overestimated and the estimated location of the earthquake will be further away from the seismic station than it is. If the arrival time is underestimated, the distance between the seismic station and the earthquake is underestimated and the estimated location of the earthquake will be closer to the seismic station than it is.

In this work, we are demonstrating Deep Learning phase picker that can estimate the uncertainty of the pick.

Heterogeneity in Microseismicity and Stress Near Rupture-Limiting Section Boundaries Along the Late-Interseismic Alpine Fault

Warren-Smith, E.[1], Townend, J.[2], Chamberlain, C. J.[2], Boulton, C.[2], Michailos, K.[2,3], Lozos, J.[4]

1. *GNS Science, Lower Hutt, New Zealand*
2. *Victoria University of Wellington Te Herenga Waka, Wellington, New Zealand*
3. *University of Lausanne, Switzerland*
4. *California State University Northridge, USA*

Paleoseismic evidence from the late-interseismic Alpine Fault suggests key section boundaries (south of Haast and near Inchbonnie, Figure 1) conditionally inhibit rupture, but it remains unclear what physical processes control this segmentation. We use data from a two-part seismometer network (DWARFS) to characterise ~7500 earthquakes and ~800 focal mechanisms, producing high-resolution structural images of these boundaries to study the effects of material and structural heterogeneities on mode-switching rupture behaviour.

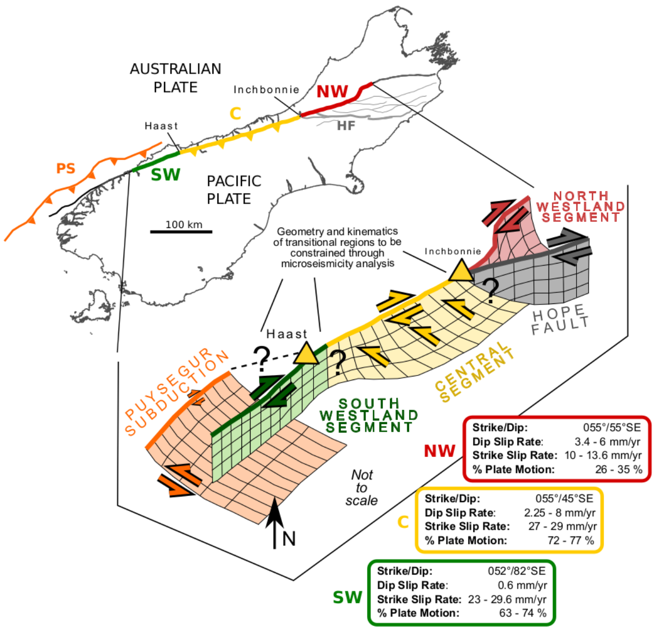

Figure 1. Schematic of major Alpine Fault Sections and boundary regions (yellow triangles) analysed using microseismicity.

We find that lithologically controlled frictional behaviour and crustal strength appear to influence lateral and vertical on-fault seismicity distributions. Specifically, ultramafic hanging-wall serpentinite and related fault core minerals along the South Westland (SW) boundary may result in abundant on-fault microseismicity and a localised 30-50% shallowing in seismogenic depths (to ~8km), reducing the fault width available for rupture. Furthermore, we show that a 40º dip change at the SW boundary may be accommodated by either a single through-going fault plane – a difficult geometry across which to obtain multi-segment earthquakes when considering rupture dynamics – or by a deeper vertical fault strand truncated by a shallower listric plane. Despite complex along-strike geometrical variations, we show that rotations in the maximum horizontal compressive stress near boundaries, coupled with spatially variable fault frictional properties are more important than geometry alone in controlling Sections' relative frictional stability. Whereas the SW and Central Sections are well-oriented for failure, the North Westland Section is severely misoriented compared with faults of the Marlborough Fault Zone, which are favourably oriented and possibly facilitate a preferred rupture route.

Finally, we discuss our rationale to use our high-resolution observations to inform and construct a range of plausible 3D fault geometries on which we perform fully dynamic single earthquake rupture simulations to ascertain the role geometrical complexities and stress distributions play in influencing rupture.

Dynamic Rupture Simulations on the Alpine Fault: Investigating the Role of Fault Geometry on Rupture Size and Behaviour

Lozos, J.[1], Warren-Smith, E.[2], and Townend, J.[3]

1. *California State University, Northridge, Los Angeles, California, USA*
2. *GNS Science, Lower Hutt, New Zealand*
3. *Victoria University of Wellington, Wellington, New Zealand*

The right-lateral transpressional Alpine Fault is the primary plate boundary fault on the South Island of New Zealand. At a broad scale, its onshore surface trace between Milford Sound in the southwest, and the branching Marlborough Fault System in the northeast consists of two planar sections connected by a major geometrical boundary at Martyr River. This boundary is characterised by both a dip change of as much as 40° over an along-strike length of only ~5 km (e.g., Warren-Smith et al. [2022]) and by two small (8–13 km) subparallel strands near a ~6° restraining bend. Several previous studies suggest that changes in dip along a strike-slip fault (e.g., Lozos [2021]) as well as smaller fault features can both affect rupture dynamics (e.g., Lozos et al. [2012]); we therefore hypothesise that these geometrical features affect conditional earthquake segmentation behaviour on the Alpine Fault, as documented by the extensive paleoseismic record (e.g., Howarth et al. [2001]).

We use the 3D finite element method to simulate dynamic ruptures on four idealised parameterizations of the onshore Alpine Fault geometry (Figure 1): 1. a single vertical plane, 2. a vertical plane with two smaller parallel vertical planes at the restraining bend, 3. a single dipping plane, and 4. a dipping plane with two smaller dipping planes at the bend. We embed the faults in a 1D velocity structure and impose heterogeneous initial tractions computed using seismologically estimated local principal stress orientations and magnitudes computed using a critically-stressed crust model. We compare the modelled rupture lengths and surface slip values to geologic and paleoseismic studies to ensure that we are producing physically-plausible simulations consistent with observations. These simulations may be helpful not only in assessing the hazard associated with the Alpine Fault, but also in constraining the geometry of the fault and implications for rupture directivity.

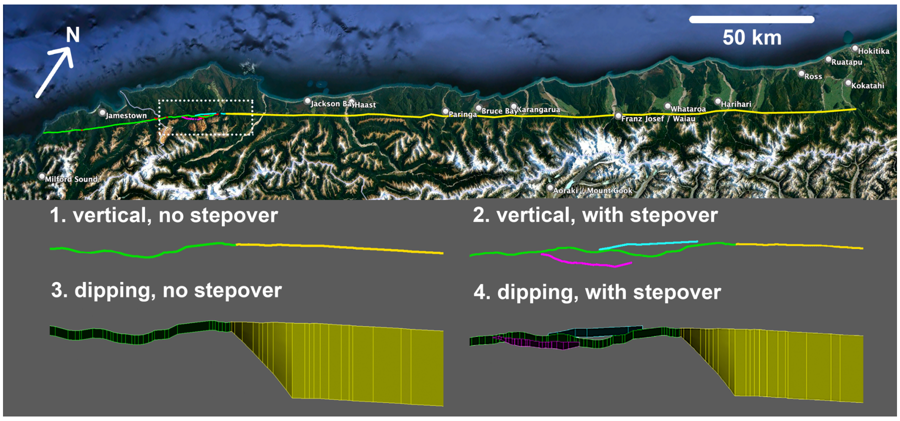

Figure 1. (Top) Surface trace geometry of the modelled portion of the Alpine Fault (top). The dotted white box highlights the stepover and dip change region. (Bottom) Top-down views of four geometric parameterisations.

Fault frictional heterogeneities can explain the inferences of slow earthquake transiting to fast rupture

Kaneko, Y.[1], Nealey, S.[2], Tape, C.[2], Ito, R.[1], Perez-Silva, A.[3]

1. *Kyoto University, Kyoto, Japan*
2. *University of Alaska – Fairbanks, Alaska, USA*
3. *Victoria University of Wellington, Wellington, New Zealand*

While most earthquakes start abruptly, with no evidence for a nucleation process, accelerating foreshock sequences within or in the vicinity of the eventual mainshock rupture zone for some moderate to large crustal earthquakes have been documented previously. In particular, Tape et al. [2018] reported unique observations of nucleation signals of crustal earthquakes in the Minto Flats fault zone in central Alaska, manifested by ~20 seconds of simultaneous high-frequency foreshocks and a very low-frequency earthquake. One potential explanation for such observations is a slow slip front propagating over the fault and triggering these foreshocks as it transitions into the mainshock rupture [e.g., Tape et al., 2018]. Another explanation may be that accelerating foreshocks represent cascading sequences of fault ruptures due to static and/or dynamic stress changes, without underlying slow slip, as known as a cascading hypothesis [e.g., Ellsworth and Bulut, 2018]. Here we show that a numerical fault model incorporating full inertial dynamics and rate-and-state friction laws with frictional heterogeneities reproduces ~20 seconds long, accelerating foreshock sequence that led to a mainshock as observed in the Minto Flats fault zone (Figure 1). We find that the time scale of accelerating foreshock sequence depends on the degree and size of frictional heterogeneities and tectonic loading rate. In the models, a foreshock triggers another foreshock mainly via the propagation of afterslip in the neighboring rate-strengthening patches. Accelerating afterslip due to numerous foreshocks eventually triggers the nucleation of the mainshock, and hence slow deformation plays an important role in the generation of accelerating foreshocks. Furthermore, an accelerating foreshock sequence occurs in only a transitional regime between an earthquake swarm regime and the regime of mainshocks with no foreshocks. This may explain why the observations of accelerating foreshock sequences are relatively rare.

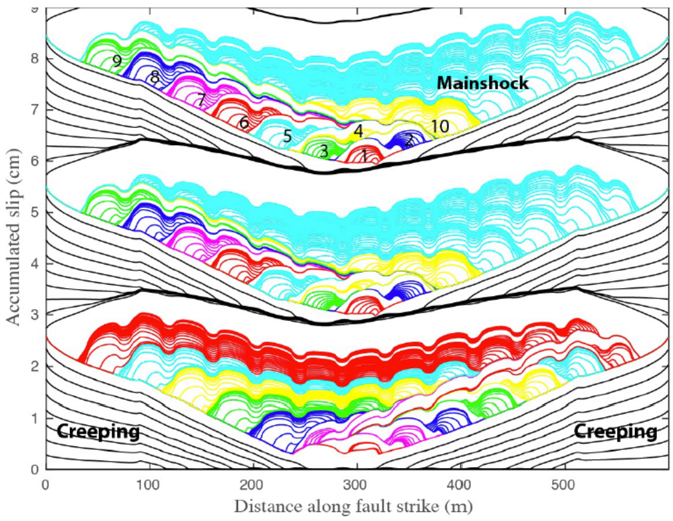

Figure 1. Earthquake cycle model with fault frictional heterogeneities that results in accelerating foreshock activity prior to the mainshock, as observed in central Alaska.

Estimation of Friction Parameters and Slip Distribution from the Strain Gauge Array beneath the Fault during the Large-scale Bi-axial Friction Experiments

Noda, K.[1] and Fukuyama, E. [1,2]

1. *Kyoto University, Kyoto, Japan*
2. *National Research Institute for Earth Science and Disaster Resilience*

It is generally considered difficult to measure directly the slip distribution on the fault. The only possible way was by the waveform inversion of seismic waves assuming appropriate Green's functions. Fukuyama et al. [2018, Tectonophys] measured the shear strain distribution beneath the sliding fault surface during stick slip events in the large-scale friction experiments, which could be one of the first near-fault observations during faulting. They reported that the measurements at the end of the rock specimens were not sufficient to capture the whole image of the slip distribution on the fault due to the 2-D nature of the rupture. We thus investigate the possibility to estimate the slip distribution and the distribution of friction parameters from the near-fault strain array data.

First, we conducted numerical experiments to examine the feasibility to reconstruct the slip distribution from the shear strain array data. Assuming the slip distribution and rupture velocity on the fault and the regularized Yoffe function [Tinti et al., 2005, BSSA] as the slip time function, we constructed spatiotemporal slip functions on the fault. This "true" slip distribution is estimated by the following numerical exercises. Using this slip distribution, we numerically constructed the shear stress distribution using the boundary integral equation [Hok and Fukuyama, 2011, GJI]. This spatiotemporal distribution of shear stress is considered to the virtual observation data for this exercise. We then extracted the initial shear stress distribution from the virtual observation data and used the initial condition of dynamic crack simulation of Hok and Fukuyama [2011] assuming a linear slip weakening friction. We search for the friction parameters of yielding stress, frictional stress and slip-weakening distance that fit the shear stress distribution (i.e., the virtual observation data). By this numerical exercise, we confirmed that the shear strain distribution on the fault enabled us to estimate the slip distribution as well as the friction parameters on the fault.

We then applied this method to the real observation data. Fukuyama et al. [2018] reported about 95 stick slip events with the rupture propagation types. We focused on the Type 2 events where the nucleation occurred inside the fault surface. We first constructed the initial stress distribution on the fault using the observed shear strain array data. To fit the observed shear stress distribution, dynamic rupture simulations were conducted to find the friction parameters that explain the observed shear strain data. We could successfully estimate the friction parameters as well as the slip distribution on the fault using the shear strain array data beneath the fault. We hope this approach will provide additional information on the earthquake rupture process that we could not see from the waveform inversion analysis.

3D Dynamic Rupture and Ground Motion Simulations for the Gulf of Aqaba Fault System

Li, B.[1], Mai, P.M.[1], Ulrich, T.[2], Gabriel, A.A.[2,3], Klinger, Y.[4], Jónsson, S.[1]

1. *King Abdullah University of Science and Technology (KAUST), Saudi Arabia*
2. *Ludwig-Maximilians Universität München (LMU), Germany*
3. *Scripps Institution of Oceanography, University of California (UCSD), USA*
4. *Institut de Physique du Globe de Paris – CNRS (IPGP), France*

The ~180 km long Gulf of Aqaba (GoA) is part of the Dead Sea Transform Fault (DSTF), a left-lateral strike-slip plate boundary separating the Arabian plate from the Sinai micro-plate. Over the past decades, the fault system in GoA has been the seismically most active portion of the DSTF which included the 1995 M_w 7.3 Nuweiba earthquake. With the potential to produce M_w 7.3 or larger earthquakes, the GoA fault system both poses a high seismic hazard in the area, leading to high seismic risk for the rapidly developing NEOM and nearby coastal communities. However, the offshore fault system and limited data availability make reliable seismic hazard assessments (SHA) challenging.

In this study, we use SeisSol (https://github.com/SeisSol/SeisSol/) to run 3-D spontaneous dynamic rupture simulations of the GoA fault system and investigate the resulting local ground motions. Using recently-mapped bathymetry and seismic data in the GoA region, we construct various fault geometries to represent alternative possibilities of the GoA fault system. Our simulations include high-resolution topography and bathymetry, off-fault plasticity and fault roughness. By varying the hypocenter location in different fault models, we explore the dynamics and fault interactions of a number of rupture scenarios in the GoA fault system, and identify variations in the resulting ground-shaking patterns. By adapting the mesh resolution to seismic velocities, we generate a ~42 million cell mesh to resolve ground motions above 1 Hz up to 50 km fault distance. Using a regional stress-tensor approach to set the initial fault loading from local observations, we can simulate the 1995 Nuweiba rupture (Figure 1).

Our results reveal that fault geometry, nucleation location, and initial stress condition affect how/if the rupture propagates across the multi-segment GoA fault system and thus lead to different slip patterns and magnitudes. A M_w 7.38 scenario occurs if the rupture breaks the entire GoA fault system shown in Figure 1. An alternative fault model with more off-shore and on-shore fault segments indicated by local seismicity shows the potential to host an even larger earthquake in the GoA region. Ground motions vary spatially both along and across the GoA fault system (Figure 1c), with strong shaking at geometric fault complexities and in the forward rupture direction. Topographic effects either amplify or diminish ground motion amplitudes. Our dynamic rupture scenarios, constrained by priori observations, and associated ground shaking results contribute to future SHA work in this currently data-scarce region, specifically in a probabilistic sense by guiding the selection of ground motion models (GMMs). Running a large suite of dynamic simulations of mechanically plausible scenarios allows to establish physics-based GMMs and to support probabilistic seismic hazard assessment in the region.

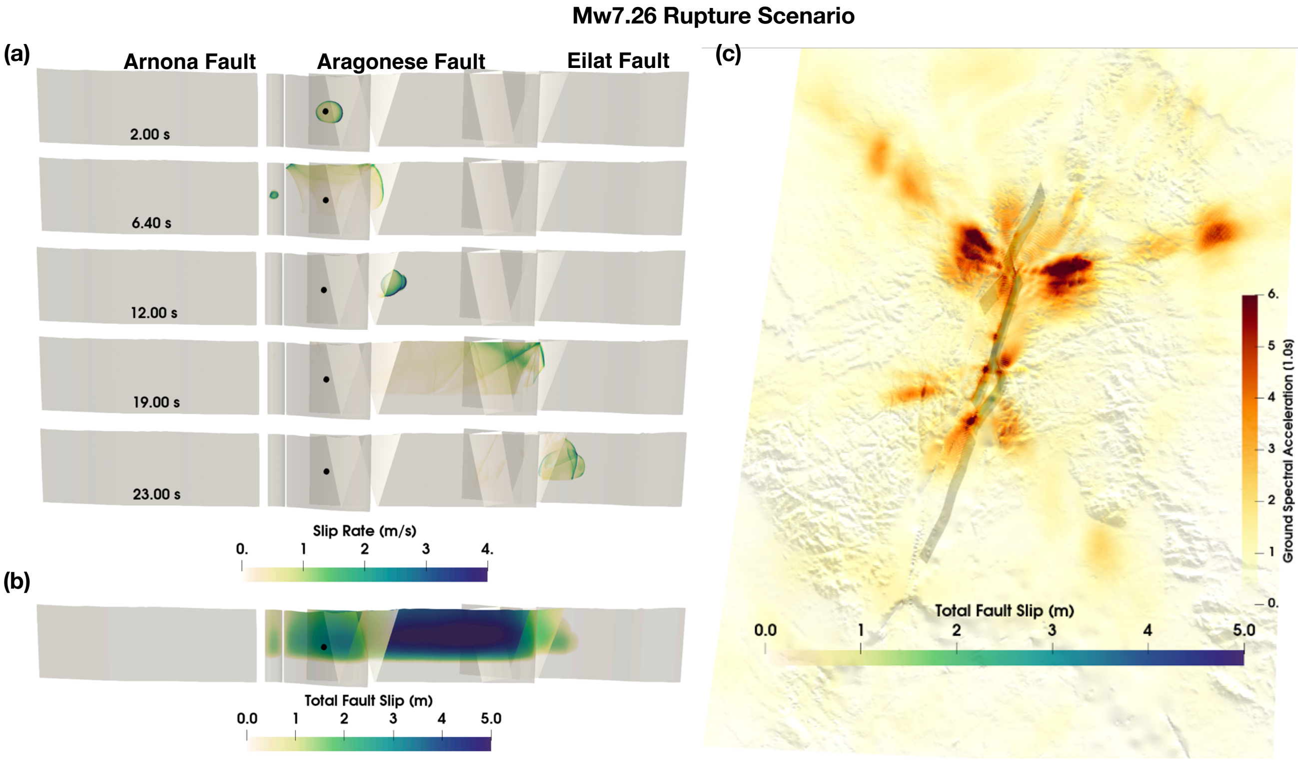

Figure 1. Overview of a M_w 7.26 rupture scenario. (a) Snapshots of the dynamic slip rate at different simulation time. Supershear rupture starts when rupture reaches the Aragonese fault. Black dots mark the nucleation location. (b) The resulting fault slip distribution and (c) the corresponding ground motion (spectral acceleration [1.0 s] in m/s^2) of the M_w7.26 scenario.

Coulomb Fault Stress Transfer Through the Hope-Kelly-Alpine Fault Intersection Zone

Vermeer, J.[1,2], Quigley, M.[2], Langridge, R.[3], Duffy, B.[2,4], Mildon, Z.[5], and Diercks, M.[5]

1. *U.S. Geological Survey, Moffett Field, California, USA*
2. *University of Melbourne, Melbourne, Australia*
3. *GNS Science, Lower Hutt, New Zealand*
4. *GHD Pty Ltd, Melbourne, Australia*
5. *University of Plymouth, Plymouth, United Kingdom*

The intersection of the Hope and Alpine Faults in the South Island of New Zealand is a geometrically and kinematically complex zone, but it may be favorable for earthquake ruptures to propagate between these two major plate boundary faults. Mapping of active fault traces based on their surface expression shows that the Hope Fault splays westward into multiple fault strands (Hope-Kelly Fault system), becoming a broad deformation zone abutting the Alpine Fault. The structure of the intersection zone is reconstructed based on strike and dip of faults inferred from mapped traces, fault kinematics determined from geomorphic offsets, and slip vector balancing. Using a simplified three-dimensional model of structurally and kinematically representative faults, we modelled static Coulomb fault stress (CFS) transfer to test the effects of several different earthquake scenarios, with ruptures reaching intersection from the south along the central Alpine Fault (Figure 1A), from the east along the Hope Fault and from the north along the northern Alpine Fault. The source ruptures were terminated at fault branching points within or at the edge of the intersection zone.

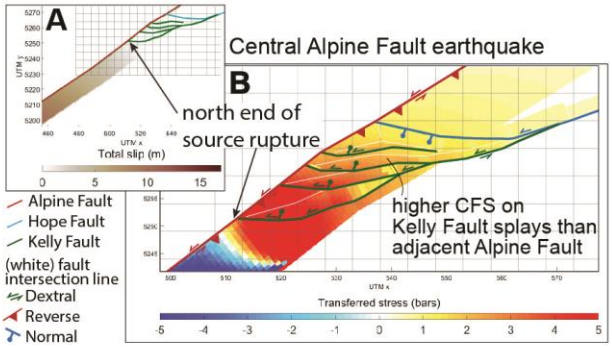

Figure 1. CFS results A) Source rupture of central Alpine Fault with total slip shown in meters. Model fault surface traces are shown in red, blue and green. B) Static CFS in bars. Fault plane intersection lines are shown in white. Kinematics are indicated by symbols. There is slightly greater static CFS on Kelly Fault splays than adjacent Alpine Fault.

The static CFS modeling results indicate that central Alpine Fault ruptures enhance static stresses on the Kelly Fault splays and northern Alpine Fault, with equal or greater positive stress change on the Kelly Fault splays compared to adjacent parts of the Alpine Fault (Figure 1B). Rupture of the Hope Fault from the east through the intersection zone causes increased CFS on the central Alpine Fault and decreased CFS on the northern Alpine Fault. An earthquake on the northern Alpine Fault that reaches the Hope-Alpine intersection causes negative CFS change (a stress shadow) on the Hope-Kelly Faults. While there are many factors that contribute to dynamic earthquake behavior, if static CFS is a controlling factor, these results suggest that rupture of the central Alpine Fault could propagate through the intersection zone or promote sequential large earthquakes on the Hope Fault, and vice versa. In contrast, the Hope-Kelly Faults and northern Alpine Fault are less likely to have rupture propagation between them and may suppress future large earthquakes due to the negative CFS change they exert on each other. These results highlight the potential for multi-fault earthquake hazards across this geometrically and kinematically complex fault intersection.

Can Tectonic Scale Analogue Modelling Provide Insight Into the Initiation and Complexity of the 2016 Kaikoura Earthquake Ruptures?

Withers, M.[1], Cruden, A.R.[1], and Quigley, M.C.[2]

1. *Monash University, Australia*
2. *University of Melbourne, Australia*

The dominantly strike-slip Marlborough Fault System (MFS), located in northeast South Island, New Zealand, has developed to accommodate strain across a plate boundary transition zone between the continental transform Alpine Fault and the congested Hikurangi subduction zone (Figure 1) (Bilich, Frohlich and Mann, 2004; Wilson *et al.*, 2004; Rattenbury, Townsend and Johnston, 2006; Wallace *et al.*, 2007, 2012). The 2016 Mw 7.8 Kaikoura earthquake is associated with the ongoing development of the Marlborough Fault System (MFS) (Hamling *et al.*, 2017; Berryman *et al.*, 2018). The extreme structural complexity of this earthquake highlights the importance of understanding how strain is accommodated across plate boundary transition zones. Here we recreate the tectonic strike-slip boundary conditions of plate boundary transition zones in scaled analogue (sandbox) experiments to test the development and evolution of fault networks, such as the Marlborough Fault System, through time. Results from our experiments show that fault networks in plate boundary transition zones, develop sequentially as crustal scale Riedel shears, to accommodate increasing strain distributed between the two plate boundary faults (Figure 1). Our results show how each Riedel shear develops from a zone of diffuse deformation that localises into a single, continuous fault. We present the similarities between our experiments with the present day Marlborough Fault System (Figure 1) and discuss how tectonic scale analogue modelling, combined with smaller scale structural mapping, could provide insights into the initiation and complexity of the Kaikoura Earthquake ruptures.

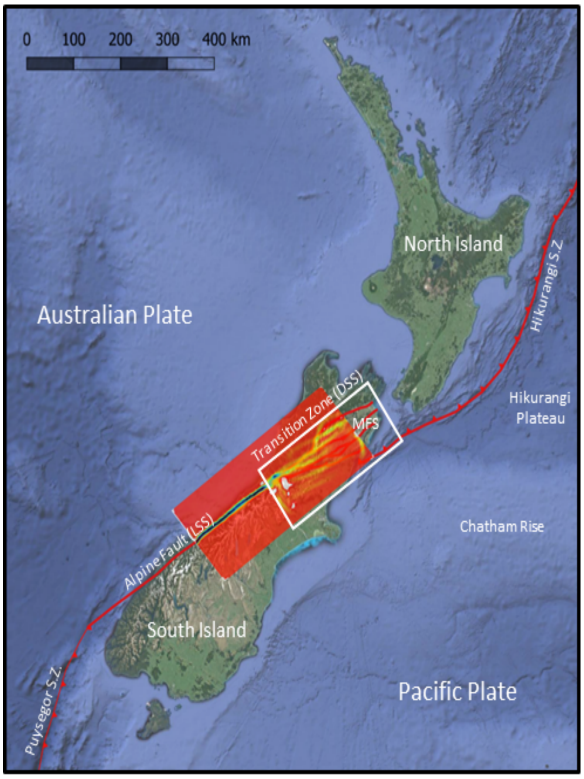

Figure 1. Map of New Zealand's major plate boundary faults overlain with a Digital Image Correlation map showing fault development in a plate boundary transition analogue experiment (red = no shear strain; yellow-blue = high shear strain). The transition zone, where the Marlborough Fault System (MFS) has developed, is highlighted by the white rectangle. The transition zone has developed because the Alpine Fault is 'misaligned' (i.e., does not directly connect) with the Hikurangi subduction zone, resulting in a transition from localised simple shear (LSS) along the Alpine Fault to distributed simple shear (DSS) across the transition zone in the MFS.

Rupture Path of the 2016 Kaikoura, NZ, Earthquake Inferred from Dynamic Rupture Simulation

Ando, R[1]

1. *University of Tokyo, Tokyo, Japan*

The complex muti-rapture is observed in the 2016 Kaikoura earthquake. Although the overall slip pattern, including the extent of the rupture propagation and the slip amount, was well explained by dynamic rupture simulations (i.e., Ando and Kaneko, 2018, GRL), its rupture path is still under debate. One of the questions remains on the reason why the dynamic rupture bypassed the Hope fault, which is the primary active upper plate fault. Another question is which paths of the landward (i.e., Ando and Kaneko, 2018) or the seaward (i.e., Chamberlain et al., 2021) were followed to bring the rupture from the southern to northern faults after nucleated at the southern end of the fault system (Figure 1).

In this study, we first test a hypothesis that the stress level of the Hope fault is lower than the surrounding faults reflecting the stress drop by the last event before 2016. A set of parameter studies shows that 70-80% lower stress level on the Hope fault leads to the passive partial slip resembling the observation of 2016. According to paleoseismological studies (Langridge et al., 2003; Hartem et al., 2019), the passage time normalized by the average recurrence interval is about 60-160 %. This value certainly has large error bars, but the range can bracket the inferred value by the simulation.

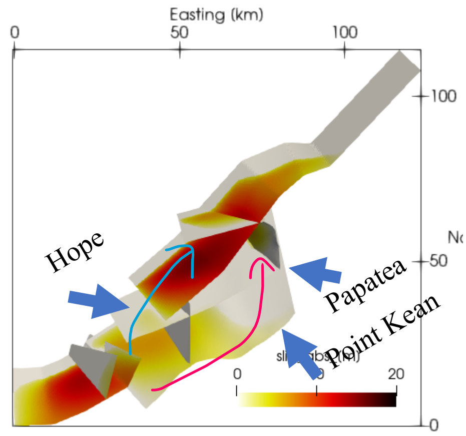

Figure 1. Map view of fault geometry of the Kaikoura earthquake. Blue and red arrows indicate the landward and seaward rupture paths.

We next explore the second question of whether the rupture can follow the seaward path within the uncertainty of the observational constraint of the stress field. We refer to the results of the stress tensor inversion based on the focal mechanisms. This method can have relatively larger uncertainty in the stress ratio v than in the principal stress orientation. Thus, we conduct the parameter study over v in the range $0.5 < v < 0.99$. Here $v = 0.66$ was determined by Townend et al. (2012) and used by Ando and Kaneko (2018), which obtained the landward path of the dynamic rupture propagation. As the results of the parameter study, we find that the larger value of v causes more slip on the Point Kean fault. However, the Papatea fault was unfavorably oriented so strongly, and it wasn't easy to be ruptured within the observationally admissible values of the parameter sets. Therefore, the dynamic rupture simulation favors the landward rupture path.

Acknowledgment: This work benefits from the discussions with Y. Kaneko. A. Howell, A. Nicol, R. Langridge and I. Hamling. The super-computer resource is provided by the "Joint Usage/Research Center for Interdisciplinary Large-scale Information Infrastructures" and "High Performance Computing Infrastructure" in Japan (Project ID: jh210023-NAH).

How a strike-slip earthquake caused the 2018 Indonesian Palu tsunami

Y. Tony Song[1], Kejie Chen[2&3], Gegar Prasetya[4]

[1]Jet Propulsion Laboratory, California Institute of Technology, Pasadena, CA, 91109

[2]Division of Geological and Planetary Sciences, California Institute of Technology, Pasadena, CA, 91125

[3]Now at Department of Earth and Space Sciences, Southern University of Science and Technology, Shenzhen, 518055, China

[4]Indonesian Tsunami Scientific Community (IATsI), The Tsunami Research Foundation Indonesia, Indonesia

ABSTRACT

The destructive power of the deadly 2018 Palu tsunami after a Mw7.5 strike-slip earthquake continues to puzzle the research community. Previous studies using either the vertically-forced or landslide-induced tsunami theory could not explain the tsunami's power and arrival times at the Mamuju tide-gauge. This study demonstrates that the horizontally-forced tsunami theory with purely strike-slip faulting can explain both observations within and outside Palu Bay. Three earthquake inversions from seismographs, satellite radar and optical imagery were used to replicate the strike-slip earthquake, showing to generate multiple tsunami sources due to the horizontal displacement of seafloor slopes. Sources from the deep waters formed a long-wave tsunami, matching the Pantoloan tide-gauge record with two distinguished peaks before striking the Palu City. A source outside Palu Bay resulted in the "early arrival" tsunami at Mamuju, which confused the local early warning system. Our findings suggest a different tsunami formation mechanism for considering strike-slip earthquakes.

Tsunamigenic Threats From the Manila Trench: Preliminary Assessment for Singapore and the Southeast Asian Countries

Tan, E.[1,2], Li, L.[3], Qiu, Q.[4], Chua, C.T.[1], Watanabe, M.[1] and Switzer, A.D.[1,2]

1. Earth Observatory of Singapore, Nanyang Technological University, Singapore

2. Asian School of Environment, Nanyang Technological University, Singapore

3. Department of Earth Sciences and Engineering, Sun Yat-Sen University, China

4. South China Sea Institute of Oceanology, Chinese Academy of Sciences, China

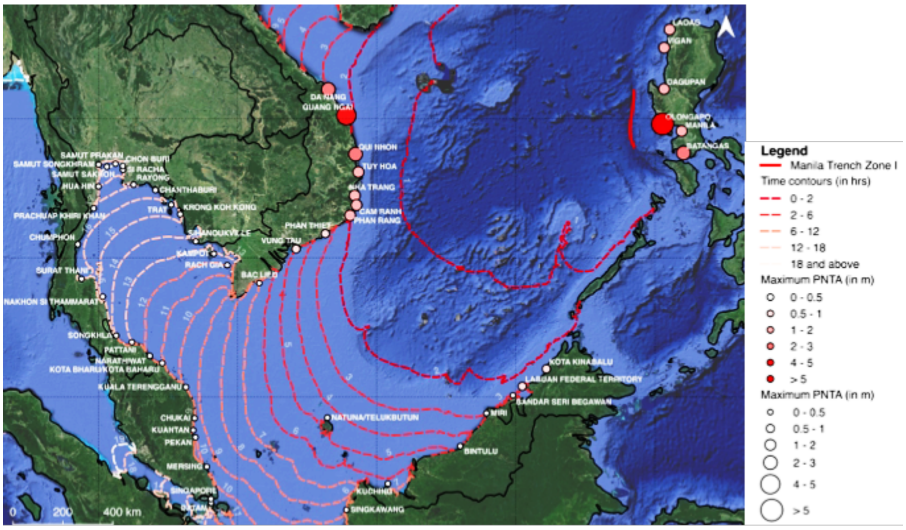

Figure 1. Maximum peak nearshore tsunami amplitudes (PNTA) for 52 synthetic wave gauges across the South China Sea and wave travel time in the form of time contours. These 52 sites are either towns, cities, ports, or areas that hold important infrastructure like oil and gas facilities. Only contours within the South China Sea and the Straits of Singapore are shown. The base map uses google map imagery [Google, n.d.].

The 2004 Indian Ocean, 2010 Chile, 2011 Tohoku-Oki, 2018 Palu tsunami events have demonstrated the destructiveness of tsunami to both near and far-field communities. Since these occurrences, many coastal cities have started to place more emphasis on preparing for tsunamis as rare but potentially catastrophic events. The distribution of tsunami research work is, however, uneven. In Southeast Asia, where these hazards are proximal and frequent, such studies are rare, even for developed countries like Singapore, whose maritime successes are vulnerable to extreme events. This study aims to bridge this knowledge gap and build coastal resilience through probabilistic tsunami hazard assessments. Previous work in the region has identified the Manila Trench to be a potential tsunami source within the South China Sea [e.g. Megawati et al., 2009; Li et al., 2016]. Using this knowledge, we model the wave propagations from heterogeneous fault slips, for magnitudes ranging from 7.4 to 8.4, along the southern segment of the Manila Trench, and develop hazard curves for 52 sites in equatorial Southeast Asia. Our results show that the hazard, based on wave heights and arrival times, is variable on both the regional and local scales (Figure 1). Amongst all the Southeast Asian countries, the Philippines and Vietnam are identified to be most at risk, with high mean peak nearshore amplitudes and short wave travel times. The least impacted countries include Singapore, western Malaysia, Indonesia (excluding the Natuna Islands), Thailand and Cambodia. Although the hazard for Singapore appears to be low, we acknowledge that tides and wave run-up are not yet accounted for in this regional study. Thus, we re-model the worst-case scenario for the highest astronomical tides and bottom friction. Our

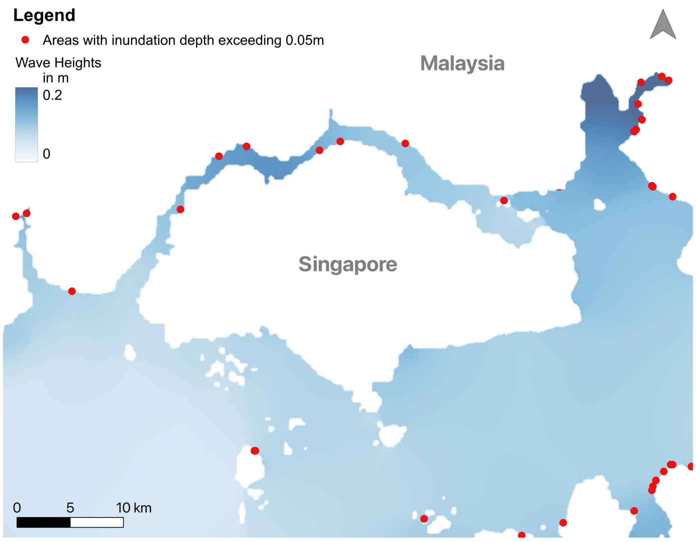

Figure 2. Wave heights distribution around Singapore waters. This is simulated with the same fault slip inputs that generated the highest PNTA for Singapore. Wave heights are referenced to the highest astronomical tide (averaged) in Singapore.

preliminary results show that Singapore can experience maximum wave heights and inundation depths, up to 0.15 m and 0.08 m respectively (Figure 2). The relatively low wave heights and inundation depth, coupled with associated low inundation distances, suggest that the tsunamigenic hazard in Singapore from the Manila Trench is low. The hazard from tsunami currents, however, remains undetermined at this stage.

The Spatiotemporal Distribution of Tectonic Tremor Activities Revealed by Multi-Year Offshore Seismic Observations at the Northern Hikurangi Subduction Margin, New Zealand

Aoyama, T.[1,2], Mochizuki, K.[1], Yamashita, Y.[3], Yamada, T.[1]
Jacobs, K.[4], Warren-Smith, E.[4], Savage, M. K.[5], Wallace, L.[4], and Shinohara, M.[1]
1. *Earthquake Research Institute of the Univ. Tokyo, Tokyo, Japan*
2. *Department of Earth and Planetary Science, The University of Tokyo, Tokyo, Japan*
3. *Miyazaki Observatory, Disaster Prevention Research Institute, Kyoto University, Miyazaki, Japan*
4. *GNS Science, Lower Hutt, New Zealand*
5. *Victoria University of Wellington, Wellington, New Zealand*

At the northern part of the Hikurangi subduction margin, off the east coast of the North Island, New Zealand, the Pacific plate subducts beneath the Australian Plate at a rate of ~45 mm/yr (Wallace et al. [2012]). The HOBITSS experiment was conducted from May 2014 through June 2015 using Ocean Bottom Seismometers (OBSs) in the northern margin where multiple subducted seamounts have been identified on seismic reflection sections. In October 2014, a large SSE occurred beneath our OBS network around one of the subducted seamounts (Wallace et al. [2016]). Todd et al. [2018] observed for the first time offshore tremors accompanying the SSE around the down-dip side of the seamount using an envelope correlation method (ECM). They put high constraints on the detection parameters, and determined epicenters of 120 tremors. Iwasaki et al. [2022] applied an S-wave splitting and polarization method to the HOBITSS data and revealed the continuous occurrence of tremors for about two weeks from near the end of the 2014 SSE.

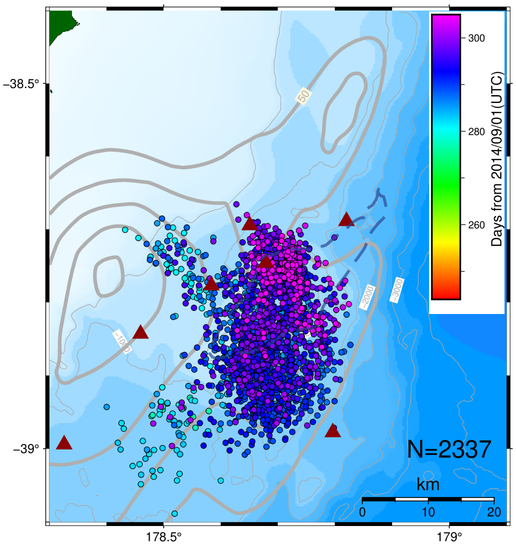

Figure 1. Tremor distribution around the large SSE in 2014. The dots, triangles, grey contours and blue dashed line show the tremors (this study), OBS stations for tremor detection, SSE slip contours and a subducted seamount, respectively.

Another one-year offshore seismic observation in the same area was conducted starting October 2018. A large SSE occurred in March 2019. Yamashita et al. [2020] applied an ECM with lower constraints on the detection parameters to reveal persistent tremor activities in the north of the OBS network as well as more than 2600 tremors accompanying the 2019 SSE. The tremor activities around the SSE migrated from north to south near the end of the SSE, and migrated back to north.We applied the same method as Yamashita et al. [2020] to elucidate the tremor activity accompanying the 2014 SSE in detail. We successfully detected more than 2000 tremors over the subducted seamount (Figure 1). The tremor distribution largely overlaps that of the 2018 activity. However, it appears to show a single south-to-north migration.

The same method was applied to another one-year OBS dataset that was acquired in the same region from October 2021. There was no major SSE during the period. We observe persistent tremor activity in the same patch in the north of the OBS network at the down-dip side of the subducted seamount.

Estimating the Rupture Extent and Depths of Creep Events on the San Andreas Fault Using Strainmeters.

Gittins, D B.[1], Hawthorne, J C[1]

1. University of Oxford, Oxford, UK

Surface creep on the San Andreas Fault was first identified in the 1960s (Steinbrugge et al., 1960). Following heavy instrumentation, this creep was observed to occur in bursts known as creep events, which are observed on strainmeters and creepmeters (Gladwin et al., 1994). Despite knowing about these creep events for 50+ years, there is still no consensus on the rupture extent of these events, with previous estimates suggesting one of three scenarios: short and shallow (Goulty and Gilman, 1978), long and shallow (Slater and Burford, 1979), or long and deep (Bilham et al., 2016). Here we use strainmeter and creepmeter data to constrain the rupture extent and depth of creep events.

Using the creep event catalogue of Gittins and Hawthorne (2022), we have isolated time windows around creep event onsets in which to look for a signal in the PBO strain records from strainmeters located at the northern end of the creeping section of the San Andreas Fault. We find short-lived (~1-2hr) steps in the strain record that occurs before the onset of the creep event as recorded on USGS creepmeters. We have then manually picked these strain steps to estimate their magnitude, which we find is typically on the order of 2-5 nanostrains. Following the identification of these strain signals, we model them as rectangles of slip (Okada, 1992, 1985) on a vertical planar fault, varying the width and length of the rectangular patch as well as its depth, location on the fault and the magnitude of the slip event. Here we present the results of our work on these strain steps, including examples related to creep events and modelling results for the three creep event scenarios. We also present slip probability distributions for events observed on both creepmeters and strainmeters at the northern end of the San Andreas Fault.

Extent and Rate of Fault Creep Along the Aceh Segment of the Sumatran Fault System Inferred from ALOS Observations

Salman, R.[1], Feng, L.[1], Sathiakumar, S.[1], Bradley, K.[1], Qiang, Q.[2], Liang, C.[3], Mallick, R.[4], Lindsey, E. O.[5], Hill, E. M[1,6], Yun, S-H.[1,6],

1. Earth Observatory of Singapore, Nanyang Technological University
2. South China Sea Institute of Oceanology, Chinese Academy of Sciences
3. Institute of Remote Sensing and Geographic Information System, Peking University
4. California Institute of Technology
5. University of New Mexico
6. Asian School of the Environment, Nanyang Technological University

We analyse ALOS-1 and ALOS-2 Interferometric Synthetic Aperture Radar (InSAR) observations to investigate the extent and rate of aseismic fault creep along the 200-km-long Aceh segment of the strike-slip Sumatran Fault System (Figure 1). Our results show that the along-strike extent of the fault creep (~110-km-long) coincides with the spatial distribution of serpentinite, an ultramafic hydrous mineral that plays an important role in subduction dynamics, suggesting that the fault creep is likely governed by the lithology of the rock. In addition, the estimated maximum creep rates show a temporal decrease from ~20 mm/year (2006–2010) to ~5 mm/year (2015–2021). One explanation for the decrease in the creep rates is the influence of stress changes in the downgoing oceanic lithosphere following the 2012 M_w >8 Wharton Basin earthquake sequence.

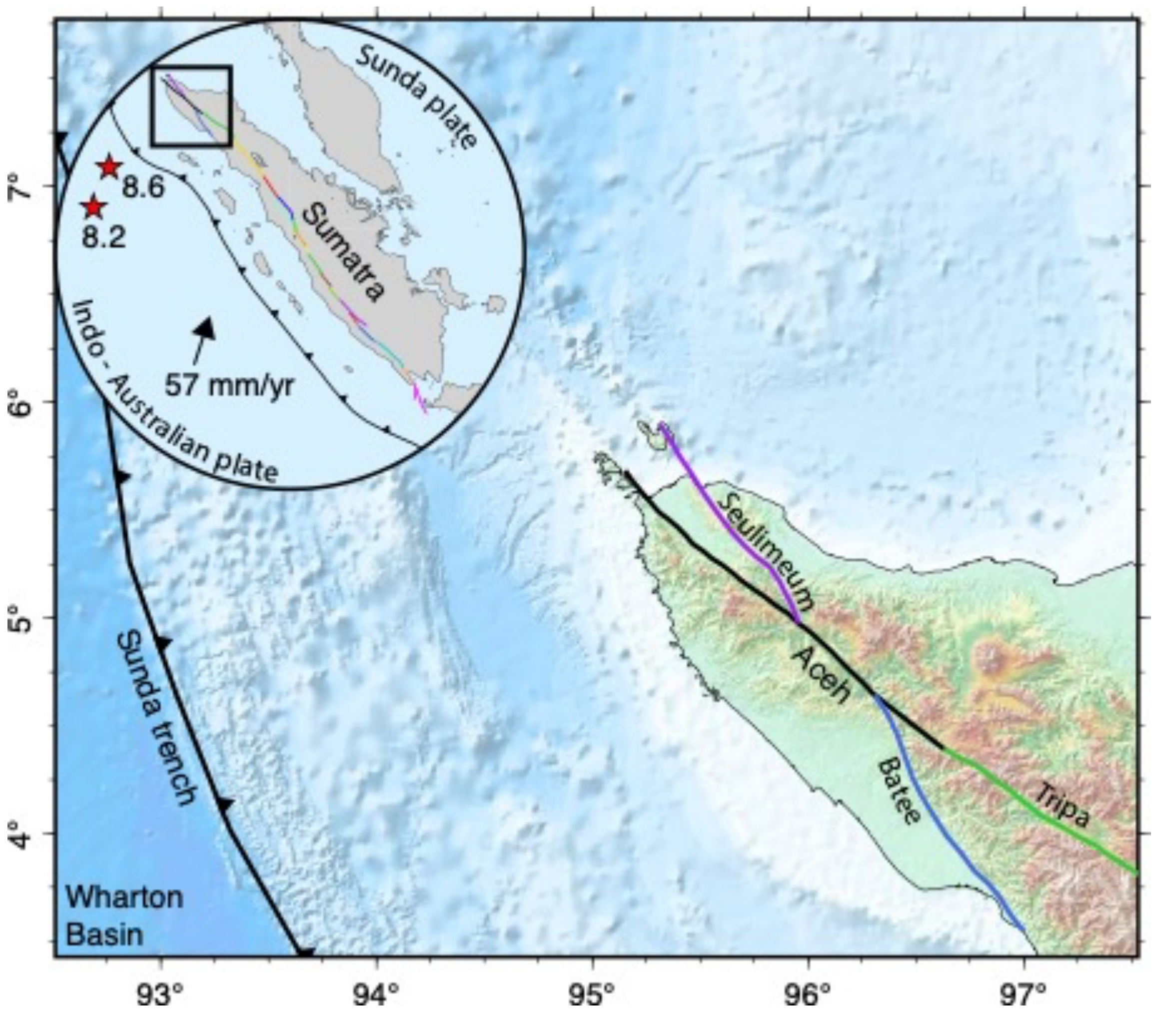

Figure 1. The Aceh segment is part of the Sumatran fault system that accommodates the strike-slip component of the oblique convergence between the Indian–Australian and Sunda plates.

Coastal Land Change due to Tectonic Processes and Implications for Relative Sea-Level Rise in the Samoan Islands

Sauber, J.[1], Huang, S.[1], Han, S.C.[2], Ray, R.[1], Luthcke, S.[1] and Fielding, E.[3]

1. *Geodesy and Geophysics Lab., NASA GSFC, Greenbelt, MD, USA*

2. *School of Engineering, University of Newcastle, Australia*

3. *Jet Propulsion Laboratory, Caltech, Pasadena, CA, USA*

Of the major coastal land change mechanisms responsible for relative sea-level change, tectonic subsidence is generally quoted as ranging from < mm/yr to 1 cm/yr. However, we documented coseismic and ongoing post-earthquake surface displacements from continuous GPS and tide gauge/altimetry data that indicated rapid subsidence on two of the major Samoan Islands of 12 - 20 cm during and following the September 29, 2009 Tonga-Samoa earthquake. Earlier results and our modeling of GRACE-derived gravimetric data provided a preliminary forecast of future relative sea-level rise through rapid land subsidence [*Han et al.,* 2019]. Of course, these numerical forecasts of time-dependent deformation are only as good as our input observations and our assumed rheological models.

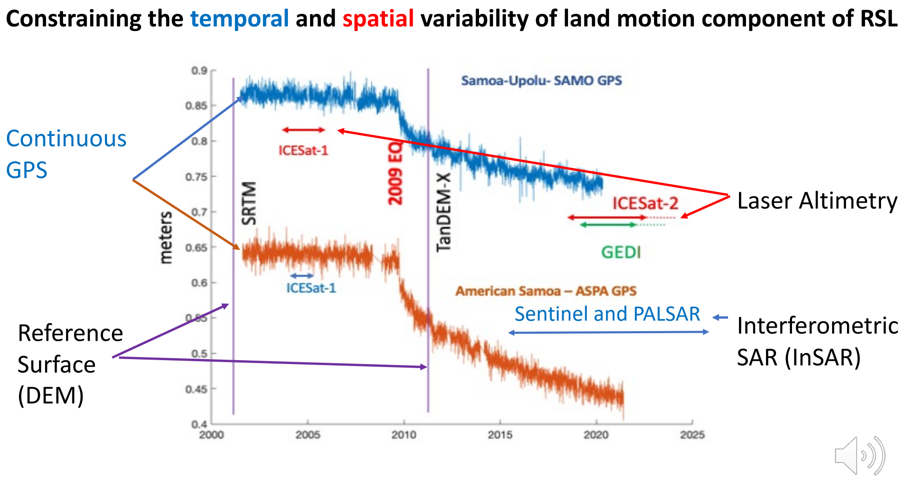

Figure 1. Data used to constrain the ongoing rate of vertical land motion on American Samoa and Upolu Island, Samoa.

As part of our current NASA study, we are obtaining a wider range of data (Figure 1) to constrain and test alternate models of ongoing postseismic deformation across American Samoa and Upolu, Samoa: (1) times series of altimetry plus tide gauge data processed to complement the cGPS data available to provide high-temporal resolution, point measurements of uplift/subsidence, (2) InSAR derived observations of surface deformation across the highly vegetated Samoan Islands, (3) evaluating and using NASA satellite lidar data (ICESat-I & ICESat-II, GEDI) for fusion with multi-source topographic data sets (NASADEM, TANDEM-X, aircraft Lidar) and for estimating topographic change on the decadal time scale. We are evaluating and using these new observations to better understand and separate out local, island-wide, and multi-island subsidence patterns and to constrain rheological models of post-seismic relaxation to estimate the subsidence rates into the next 10-20 years.

Earthquakes and Seismic Hazard in Southern New Caledonia, Southwest Pacific

Chin, S.[1], Sutherland, R.[1], Savage, M.[1], Townend, J.[1], Collot, J.[2], Pelletier, B.[3], Monge, O.[2], and Illsley-Kemp, F.[1]

1. *School of Geography, Environment and Earth Sciences, Victoria University of Wellington, Wellington, New Zealand*
2. *Service Géologique de Nouvelle-Calédonie, Nouméa, New Caledonia*
3. *Géoazur (UMR 6526), IRD, Nouméa, New Caledonia*

We use 12 temporary and 9 permanent broadband seismometers that were operating for ~400 days from October 2018 to November 2019 to generate the first published earthquake catalogue and local magnitude function for southern New Caledonia. Local earthquakes were mostly shallower than 20 km. Hypocentres in New Hebrides-Vanuatu subduction zone are < 30 km deep west of the trench and deepen to > 100 km eastward. Our local magnitude estimates M_L for 107 earthquakes in the subduction zone are consistently 1.1 units smaller than M_w and mb over a range of M_w from 4.5 to 7.5, as determined by the USGS. Our catalogue has 460 earthquakes with $M_w \geq 3.7$ in the subduction zone and the largest event in southern New Caledonia has M_L 3.8. Seismicity rates in southern New Caledonia are low, but $M_L > 5$ earthquakes are 2.7 times more frequent than elsewhere in the northern Australian plate. The probability of an $M_L > 5$ event in 50 years is 0.6 in southern New Caledonia. Seismic shaking hazard in southern New Caledonia is dominated by local moderate-magnitude earthquakes, rather than large-magnitude subduction events. The predicted peak ground acceleration (PGA) for Nouméa at 10% probability of exceedance in 50 years is 0.08 g. Residual analysis of ground accelerations demonstrates that the hazard for Nouméa from subduction earthquakes is currently overestimated and that new regionally-specific ground motion prediction equations are needed. Our results highlight the inadequacy of current ground motion prediction equations in subduction zone footwall settings and the need for additional studies of this type of setting.

Using a Multi-Disciplinary Approach to Investigate Destructive Earthquake Ground Motions in Continental Foreland Basin Settings

O'Kane, A.[1,3,4], Copley, A.[1], Mitra, S.[2], and Wimpenny, S.[1,5]

1. University of Cambridge, Cambridge, UK
2. Indian Institute of Science Education and Research Kolkata, West Bengal, India

Now at:

3. University of Canterbury, Christchurch, NZ | 4. GNS Science, Lower Hutt, NZ | 5. University of Leeds, Leeds, UK

For the first time in history, over half of the world's population lives in urban areas (Demographia, 2021), many of which are at risk of experiencing one of the most devastating natural hazards known to humankind: earthquakes. Many of the most destructive earthquakes of the past have been along the margins of mountain belts within the interiors of the continents (England and Jackson, 2011). However, the hazard associated with these earthquakes, and the effect that the regional structure of the Earth's crust plays on the intensity of the resultant ground shaking, is poorly understood and a topic of current research (Douglas and Edwards, 2016).

Previous estimates of earthquake-induced ground motions are lacking in much of the NW Himalayas, including in Jammu and Kashmir, where there have been few large earthquakes since the advent of instrumental recordings, despite the potential for M_W ~8 events (e.g. the neighbouring 1905 M_W 7.8 Kangra earthquake; Ambraseys and Bilham, 2000). In this study, seismological, structural, and geomorphological observations were used to constrain the present-day geometry of the buried Main Himalayan Thrust beneath the NW Himalayas. These results were then used to construct seismic-wavefield models (as seen in Figure 1), to determine earthquake ground motion estimates if the Main Himalayan Thrust in the region were to rupture. Simulations using the fault geometry representative of other Himalayan regions were also conducted to investigate how the evolution of deformation through space and time may influence the seismic hazard posed. The results show that the peak ground motions are very sensitive to minor variations in the fault geometry, so accurately mapping the shallow thrust geometry is extremely important for seismic hazard assessment. This work also demonstrates the effectiveness of combining observational and modelling approaches to establish the geometry of active faulting and quantify the resulting seismic hazard.

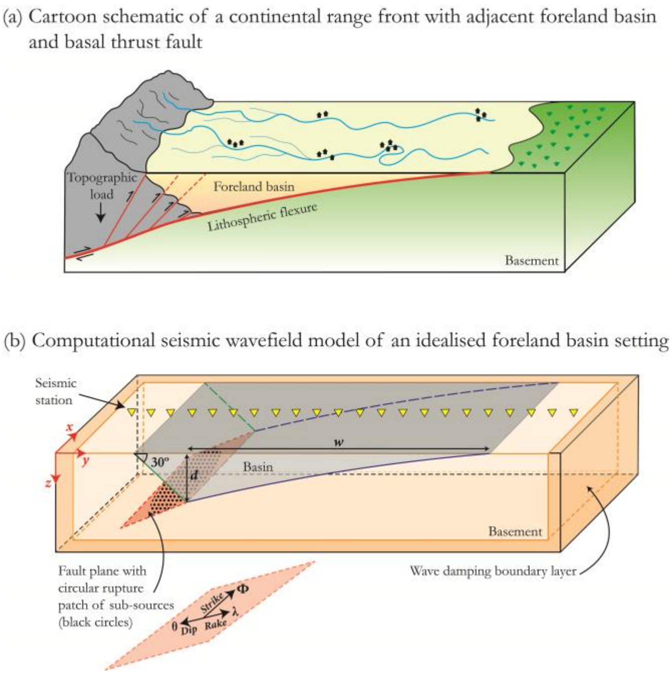

Fig 1: Real-world view and computational model setup used to simulate the seismic wavefield of range-front thrust faults.

A Hybrid method of earthquake mid-long term forecasting based on numerical simulation and seismic statistics: an application to China Seismic Experimental Site

Yao, Q.[1], Wang, H.[1] , Zhang, Y.[1] , and Wu, Z.[1]

1. *Institute of earthquake forecasting, CEA,China*

Displacement boundary is widely used in earthquake simulations. However, the error range and variations with the earthquake cycle bring gaps between the account step and the real-time. Normally, scientists tried to match the simulation with real-world hardly considering real-time, or match them over long time scales. It hinders the application of numerical simulation on earthquake mid-long-term forecasting.

We explored a hybrid method of earthquake mid-long-term forecasting based on numerical simulation and seismic statistics and applied it to China Seismic Experimental Site (CSES). Here earthquakes and related forecasting are divided into three levels by magnitude, forecasting methods, and seismogenic mechanism. First, a three-dimensional finite element simulation was applied to calculate the long-term stress variation based on the principle of active blocks controlling big earthquakes. Next, the co-seismic earthquake stress released by moderate earthquakes, which occurred after the last big earthquake for decades, was superimposed on local regions. Then, the annual scale's seismic statistic for small earthquakes was also overlaid by reclassification and weighted calculation. And last, all the results were nondimensionalized and hybrid together according to weight. We illustrated the graded seismic risk east of the Sichuan-Yunnan border from 2021 to 2030. Since the result brought to put on October 2020, 3 in 4 MS≥6 earthquakes occurred in the research region were exactly located in or near relatively high seismic damage risk region (Fig. 1). The 2022 Lushan M_S 6.1 earthquake, the 2021 Yangbi M_S 6.4 earthquake, and the 2021 Luzhou M_S 6.0 earthquake occurred in the high-risk area, but the 2022 Maerkang M_S6.0 earthquake occurred in the low-risk region.

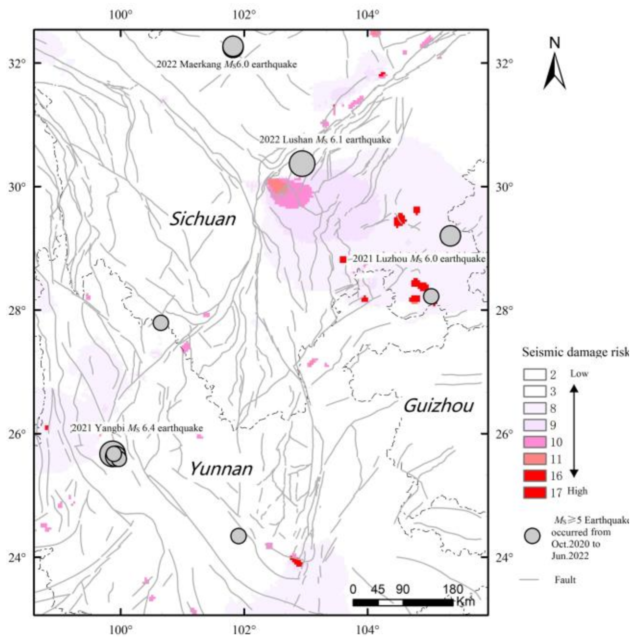

Figure 1. Simulated seismic damage risk using a hybrid method and earthquakes occurred since October 2020. The region with pink and red color refers to a relative high seismic damage risk region. The grey dots point out the location of M_S≥5 earthquakes from Oct.2020 to Jun.2022.

The hybrid method presented in this paper solves the lengthy calculation step in numerical simulation applied to earthquake forecasting. It includes both physics-based numerical simulation and statistical seismological analysis.

Automated Seismic Analysis Based on Deep Learning: a Case Study of the 29 October 2022 M 4.1 Goesan Earthquake, South Korea

Sheen, D.-H.[1], Seo, K. J.[1], Kim, S.[1], Byun, A.-H..[1], and Hong, Y.[1]

1. *Chonnam National University, Gwangju, South Korea*

This study presents an automated seismic analysis of a moderate earthquake (M_L 4.1), occurred in Geosan-gun, South Korea, on October 29, 2022, and its foreshocks and aftershocks.

Seismograms from October 21 to October 31 were obtained from 15 permanent seismic stations installed within 50 km of the epicenter, of which five are equipped with velocimeter and accelerometers and the others only with one accelerometer. All stations use a sampling rate of 100 Hz.

We used a deep neural network for picking P- and S-phase arrival times, which was trained using STEAD (Mousavi et al., 2019), INSTANCE (Michelini et al., 2021), and local data of South Korea (Kim et al., 2022). A Gaussian mixture model, GaMMA (Zhu et al., 2022) associated phases and estimated approximate earthquake locations. We found that a total of 50 earthquakes, including 25 earthquakes reported by the Korea Meteorological Administration. To provide preliminary locations for events (Figure 1), we used HYPOINVERSE (Klein, 2002) and a 1-D velocity model from Kim et al. (2011). Magnitudes of earthquakes were determined from peak amplitudes of accerlerograms by using an empirical relationship of Hong et al. (2022). Polarities for P waves were estimated by a deep neural network, which was trained SCEDC dataset of Ross et al. (2018) and local data of South Korea (Byun et al., 2022), and S/P amplitude ratios by following Yang et al. (2012). Focal mechanisms of 10 earthquakes, including the mainshock of M_L 4.1, were determined by using HASH (Hardebeck and Shearer, 2002). Solutions of all events were a strike-slip faulting mechanism. These analysis procedures took only about 75 minutes for generating a preliminary catalogue from 11-day seismograms. This shows that the automatic seismic analysis procedure presented in this study can quickly deliver valuable information for mitigating seismic hazard in the early stages of a major earthquake, followed by a large number of aftershocks.

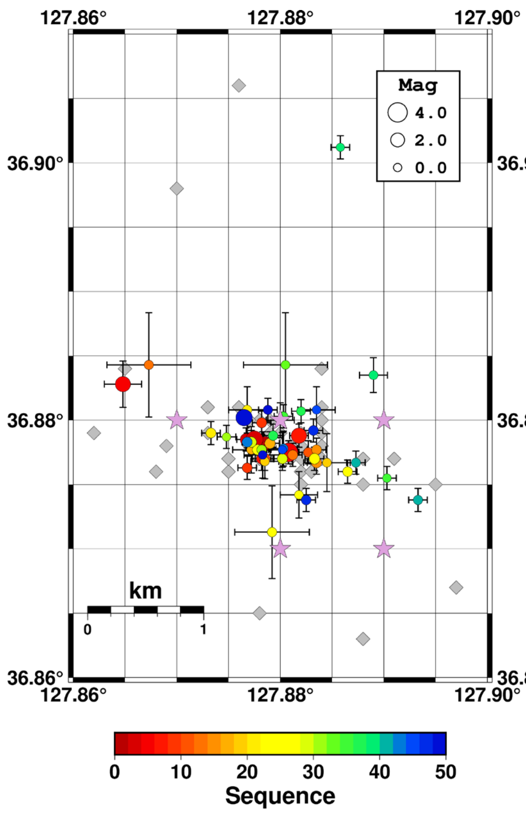

Figure 1. Epicenters of Geosan earthquake sequence. Pink starts were located by the Korea Meteorological Administration. Gray diamonds and coloured circles are epicenters obtained from association and location of this study, respectively (after from Sheen et al., 2022).

Probabilistic Forecasting and Performance Evaluation for the Aftershocks through the Scientific Investigation in China—Maduo *M*S7.4 Earthquake in May 22, 2021

Zhang, S.F., Zhang, Y.X.

Institute of Earthquake Forecasting, CEA, Beijing, China

In May 22, 2021, a M_S7.4 earthquake with focal depth of 17 km occurred in Maduo, Qinghai and broke the long-period quiescence of 3.8 years of the strong earthquakes with magnitude above 7.0 in mainland of China. Through the scientific research focused on this event using many technique means and disciplines, this event has been acknowledged that it occurred on Kunlunshankou-Jiangcuo fault and has a striking direction of NW. Several researches suggest that this earthquake has increased the stress level of Maqin-Maqu part of the Kunlunshan fault and the potential of large earthquake will be stronger in this region. In the scientific research work around this strong event, we used the temporal Epidemic Type Aftershock Sequence (ETAS) model to fit the earthquake sequence after the mainshock and described the features of the attenuation in time and the ability to trigger next offsprings. At the same time, to explore the potential of strong aftershocks after the mainshock, we conducted a short term forecasting for next 3 days and give the probability and occurrence rate of aftershocks with different target magnitude. After that, statistical method, ie. Receiver Operating Characteristic (ROC) method, was used to evaluate the performance of this forecast models. The conclusion contains: (1) ETAS model can have a good consistency with the fluctuation of observed events. The high p value suggests that the sequence has a high attenuation rate in the 30 days after the mainshock. (2) The sequence is built up mainly by the primary aftershocks and shows quiescence and activation from the homogeneous Poisson process in different state. (3) The occurrence of significant aftershocks can have impact on the forecasting for the next target events due to the high sensitivity of ETAS model to the observed earthquake. (4) The evaluation for the probabilistic forecasting for next 3-day of big aftershocks suggests that ETAS model outperforms random guess. After practice, we find that the probabilistic forecasting and performance evaluation work conducted using ETAS model can effectively provide scientific and technological support for the scientific investigation.

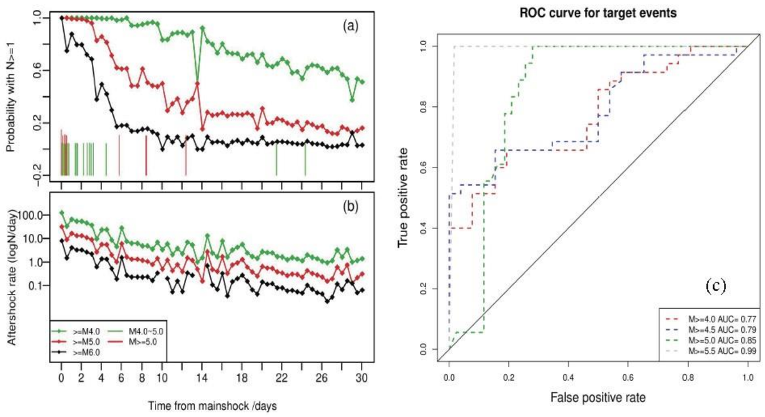

Figure 1. Forecasting result of ETAS model and its performance evaluation for the aftershocks of Maduo *M*S7.4 earthquake. (a) Occurrence probability of the aftershocks. (b) Occurrence rate of aftershocks above different magnitude level. (c) ROC test to the probability forecasting.

Nowcasting earthquakes for fault segments with similar focal mechanisms and different elapse rates: the eastern border of the Sichuan-Yunnan block in southwestern China

Zhang, S.F., Wu, Z.L., Shao, Z.G., Zhang, Y.X.
Institute of Earthquake Forecasting, CEA, Beijing, China

The eastern border of the Sichuan-Yunnan block in southwestern China is characterized by a long strike-slip fault system which consists of 18 fault segments with different elapse rates, covering almost the whole earthquake cycle. Taking the advantage of the special feature of this giant fault system, nowcasting earthquakes for different fault segments is conducted, providing a unique opportunity to understand the physical significance and practical implication of the nowcasting. To these 18 segments, Earthquake Potential Score (EPS) up to October, ~~,~~ 2022, is calculated with the circle region around the center of each ~~part~~segment, target magnitude with the level (±~~+-~~0.5) of last strong to major earthquake, radius determined by target magnitude (*M*6.0 as 100km, *M*7.0 as 200km). The elapse rate for these segments using historical earthquakes and geology data has been published. The relation between EPS and elapse rate of these segments is complex. Remarkably, the potential before the occurrence of last earthquake within each part can also be calculated using above analysis after the considering of spatial inhomogeneous of historical earthquake catalogue and temporal analysis for completeness magnitude. This presentation will introduce the analysis result in detail and discuss the implications for understanding the nowcasting method.

带格式的: 字体: 倾斜

带格式的: 字体: 倾斜

The New Zealand Community Fault Model – version 1.0: An improved geological foundation for seismic hazard modelling

Seebeck, H.[1], Van Dissen, R.[1], Litchfield, N.[1], Barnes, P.M.[2], Nicol, A.[3], Langridge. R.[1], Barrell, D. J. A.[4], Villamor, P.[1], Ellis, S.[1], Rattenbury, M.[1], Bannister, S.[1], Gerstenberger, M.[1], Ghisetti, F.[5], Sutherland, R.[6], Hirschberg, H.[6], Fraser, J.[7], Nodder, S.D.[2], Stirling, M.[8], Humphrey, J.[3], Bland, K.J.[1], Howell, A.[1,3], Mountjoy, J.[2], Moon, V.[9], Stahl, T.[3], Spinardi, F.[9], Townsend, D.[1], Clark, K.[1], Hamling, I.[1], Cox, S.[4], de Lange, W.[9], Wopereis, P.[10], Johnston, M.[11], Morgenstern, R.[1], Coffey, G.[1], Eccles, J.D. [12], Little, T.[6], Fry, B.[1], Griffin, J.[13], Townend, J.[6], Mortimer, N.[4], Alcaraz, S.[14], Massiot, C.[1], Rowland, J.V.[12], Muirhead, J.[12], Upton, P.[1], Lee, J.[1]

1. *GNS Science, Lower Hutt, Wellington*, NZ; 2. *NIWA, Wellington, NZ*; 3. *University of Canterbury, Christchurch, NZ*; 4. *GNS Science, Dunedin, NZ*; 5. *TerraGeoLogica, Ruby Bay (Mapua), NZ*; 6, *Victoria University of Wellington, Wellington, NZ*; 7. *WSP, Christchurch, NZ*; 8. *University of Otago, Dunedin, NZ*; 9. *The University of Waikato, Hamilton, NZ*; 10. *BECA, Nelson, NZ*; 11. *GNS Science (retired), Nelson, NZ*; 12. *The University of Auckland, Auckland, NZ*; 13. *Geoscience Australia, Canberra, Australia*; 14. *GNS Science, Taupo, NZ*

The New Zealand Community Fault Model (NZ CFM) is a publicly available representation of New Zealand fault zones that have the potential to produce damaging earthquakes. Compiled through collaborative engagement between New Zealand earthquake-science experts, this first edition (version 1.0) of the NZ CFM builds upon previous compilations of earthquake-source active fault models [e.g. Stirling et al. 2012; Litchfield et al. 2014] with the addition of new and modified information. Developed primarily to support an update of the New Zealand National Seismic Hazard Model [Gerstenberger et al. 2022], the NZ CFM v1.0 comprises two principal components. The first dataset is a two-dimensional map representation of the surface traces of 880 generalised fault zones. Each fault zone is assigned specific geometric and kinematic attributes (such as dip, rake, and slip rate) supplemented with a subjective quality ranking focused primarily on the confidence in assigned slip rates. The second component is a three-dimensional representation of the fault zones as triangulated mesh surfaces that are projected down-dip from the two-dimensional mapped traces to a geophysically-defined maximum fault rupture depth. We present the compilation and parameterisation of the NZ CFM v1.0, along with background on its relation to predecessor datasets, and forward applications to probabilistic seismic hazard assessment and physics-based earthquake models currently being developed for Aotearoa New Zealand. The NZ CFM v1.0 and associated report can be downloaded from https://doi.org/10.21420/NMSX-WP67.

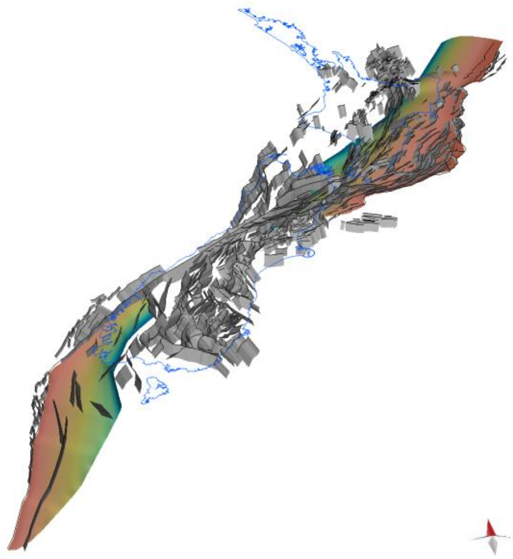

Figure 1. Oblique view of the New Zealand Community Fault Model v1.0

Spatiotemporal Variation in Low Frequency Earthquake Recurrence Along the San Andreas Fault

Allen, J.[1], and Wang, T.[1]

1. *University of Otago, Dunedin, New Zealand*

Episodic tremor sequences comprised of overlapping low frequency earthquakes (LFEs) occur frequently along the San Andreas Fault. Accompanying slow slip activity has been detected from Global Navigation Satellite System (GNSS) data (e.g. Rousset et al., 2019; Michel et al., 2022), confirming occurrence of the episodic tremor and slip (ETS) phenomenon here.

The characteristics of slow slip events (SSEs) impede comprehensive detection, making it challenging to study their occurrence patterns. We utilise extensive LFE data from a long running high resolution seismic network (Shelly, 2017) to gain insights into this more frequent and easily detectable aspect of the ETS process, with the aim to have a detailed understanding of the occurrence patterns and properties of LFEs. This will strengthen methods for the detection and modelling of SSEs.

Hidden Markov models were used to study the occurrence patterns of LFE events. Based on these models, LFE events along the San Andreas Fault can be classified into different states. Each state is a proxy for changes in the generating mechanisms that give rise to LFE events, with potential contributors including pore pressure and fault stress. We use the classification to illustrate a detailed picture of temporal changes in LFE activity - including the effects of events such as the 2004 Parkfield earthquake, and to highlight the diverse behaviours displayed across generating locations.

The evolution of LFE activity over space and time gives additional insights into how slow slip may propagate. We use clustering methods to reveal patterns in the migration of activity between spatially distinct generating locations, and identify locations with similar characteristics that are likely influenced by the same generating circumstances.

Deep Short-term Slow Slip and Tremor in the Manawatu Region, New Zealand

Fasola, S.[1], Bartlow, N.[1], and Williams, C.[2]

1. *University of Kansas, Lawrence, Kansas, USA*
2. *GNS Science, Lower Hutt, New Zealand*

Tectonic tremor is often accompanied by slow slip events (SSEs). In New Zealand, tremor is found spatially correlated with shallow SSEs as well as downdip from deeper SSEs. The Manawatu region of New Zealand is one region that experiences both deep tremor and long-term SSEs (L-SSEs), however the tremor is adjacent to, and not co-located with, the identified region of L-SSEs. While some episodes of tremor occur during deep L-SSEs, there is also a fair amount of tremor that occurs during inter-SSE periods. Observations of tremor elsewhere, including episodic tremor and slip (ETS) in Cascadia and Nankai, suggest that it is likely smaller short-term SSEs (S-SSEs) below the current geodetic network detection threshold also occur in the area where tremor is observed. We decomposed GNSS data during the period 2005-2017 using the tremor catalog of Romanet and Ide [2019] to assess the average surface displacement contributions during versus in between tremor episodes. Cumulative displacement associated with tremor periods indicated a more trenchward direction relative to inter-tremor periods in the region where we see tremor (Figure 1). Displacement associated with tremor was negligible at most far-field stations as we would expect. Directions of displacement vectors of stations near the tremor were consistent with slip along the plate interface. We performed a constrained Laplacian-smoothed least squares inversion incorporating heterogeneous elastic properties to model the displacement during tremor with the assumption that it occurs on the subduction plate interface. The slip inversion suggests that slow slip is co-located with the bursts of tremor with a cumulative displacement of about 60 mm per year (Figure 1). This study suggests that the interface below the deep L-SSEs may slip often in small ETS-like S-SSEs that are not individually detectable geodetically. The question remains as to what the nature of the strong variability in SSE behavior with depth and duration in the southern Hikurangi margin is.

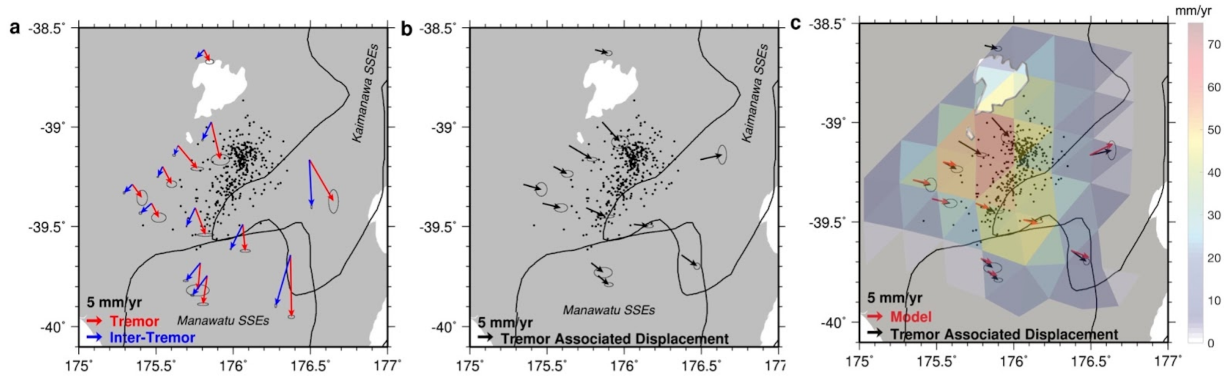

Figure 1. a) Time-averaged displacement of tremor (red arrows) and inter-tremor periods (blue arrows) obtained from decomposition of geodetic data with respect to tremor. 1-sigma errors are shown. Solid lines denote regions of SSEs [Wallace, 2020]. Black dots represent tremor from Romanet and Ide [2019]. b) Tremor associated displacement (black arrows) obtained by subtracting the inter-tremor displacement from the tremor displacement. c) Time-averaged slip associated with tremor as estimated by static slip inversion.

Seamount subduction and fluid-rich decollement control the slow earthquake activity in the Nankai Trough off Cape Muroto

Paul Caesar M. Flores[1], Shuichi Kodaira[1,2], Gaku Kimura[2], Kazuya Shiraishi[2], Yasuyuki Nakamura[2], Gou Fujie[2], Tetsuo No[2], and Yuka Kaiho[2]

1. *Graduate School of Environment and Information Sciences, Yokohama National University, Japan*
2. *Japan Agency for Marine-Earth Science and Technology (JAMSTEC), Yokohama, Japan*

Slow earthquakes occur in the Nankai Trough with varying activity along the trench. A gap in slow earthquake activity is observed between 135.4 to 135.9 °E, while a high activity is observed on both sides of the seismic gap. A dense network of multi-channel seismic reflection profiles was used to investigate the cause of this phenomenon. Two key horizons were tracked, namely, the decollement and the oceanic crust surface. The decollement was interpreted based on the geometry of the reflectors in the frontal thrust area and its continuity was traced landward. The decollement was only identifiable within 36 km from the frontal thrust. The seismicity gap between 135.4 to 135.9° E is attributed to a smoothened decollement. It is immediately bounded on both sides by a rough decollement. Another region of smooth decollement is observed west of 135°E where slow earthquakes occur, and it appears to contradict our earlier interpretation that slow earthquakes occur along the rough decollement. However, the decollement eventually came in contact or merged with the rough surface of the oceanic crust further north where the oceanic crust is characterized by the presence of numerous subducted seamounts. Previous studies have reported an overpressured decollement in the western half of the survey area. Thus, the high activity of slow earthquakes is attributed to the subducted seamounts that form the rough decollement combined with the presence of an overpressured decollement.

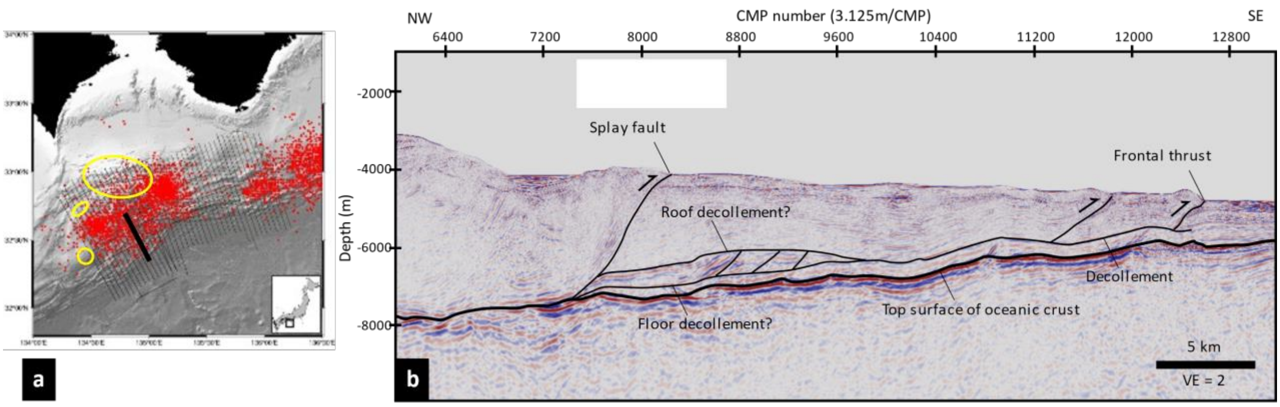

Figure 1. (a) Location of the study area showing the track lines of the seismic reflection survey (black lines), slow earthquake epicenters (red dots), and subducted seamounts (yellow circles). (b) Interpreted seismic profile indicated by the thick black line in (a).

Constructing an Earthquake Catalogue to Understand SSE Propagation Mechanisms and Their Interaction with Earthquakes on the Hikurangi Subduction Zone

Kwong, S.[1], Savage, M.[1], Jacobs, K.[2], Warren-Smith, E.[2], Wallace, L.[2,3], Mochizuki, K.[4]

1. *Victoria University of Wellington, Wellington, New Zealand*

2. *GNS Science, Lower Hutt, New Zealand*

3. *University of Texas Institute for Geophysics, Austin, Texas, USA*

4. *ERI, University of Tokyo, Tokyo, Japan*

Understanding the mechanisms that drive Slow Slip Events (SSEs) and the physical changes they cause to a fault zone, are critical for improving our forecasts of failure on large faults. The PULSE project (Physical processes UnderLying Slow Earthquakes) aims to observe and characterise the physical changes to a fault zone prior to slow earthquakes. To do this, the PULSE project deployed a network consisting of 55 onshore (48 seismic, and 7 geodetic) instruments, and 26 offshore (10 seismic and 16 geodetic) instruments, targeting the Porangahau region where SSEs occur approximately every 5 years (Figure 1). This dense network will allow us to generate a high resolution, high precision microearthquake catalogue across the SSE cycle.

To produce this catalogue, the Seisbench (Woollam et al., 2022) implementation of the automatic earthquake picker EQTransformer (Mousavi et al., 2020) will be applied over the continuous data. We have been actively testing EQTransformer's capabilities on two datasets. The first is 90 events from the GeoNet catalogue spanning June 2021 – September 2021 using both the PULSE and GeoNet on-land stations (Figure 1). The second is data from the HOBITSS deployment in 2014-2015 offshore Gisborne alongside the catalogue of events and picks produced by Yarce et al., 2019. Initial testing on the 7482 manual picks from the first dataset has shown EQtransformer performs well on the on-land stations, with results of 0.06s pick accuracy and 95% detection rates. This testing also revealed that EQTransformer's STEAD (STanford EArthquake Dataset) based model has a bias to the start of the trace, necessitating a 90-95% overlap to ensure good pick completeness. Further work is required to determine the final parameters to use over the whole PULSE dataset and whether there is a need to train EQTransformer's STEAD based model specifically for the ocean bottom seismometer data.

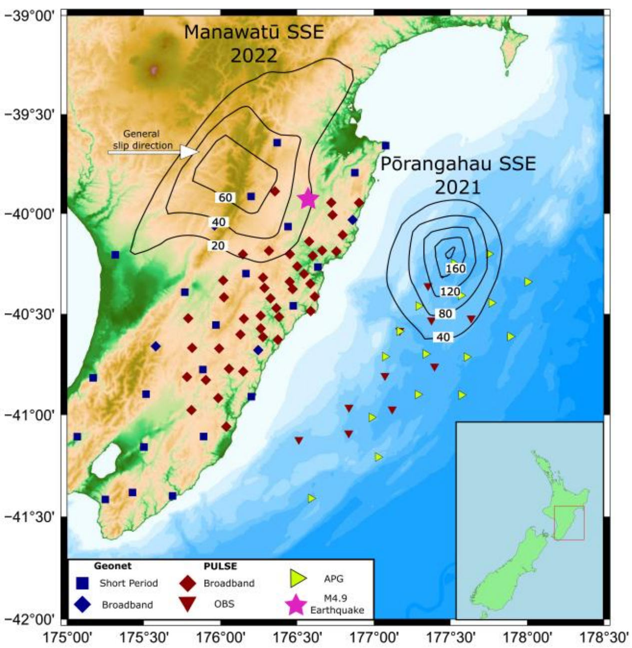

Figure 1. Map of the PULSE Network. Two SSEs that have occurred during the deployment are shown with slip contours taken from inverted onshore geodetic data (SSE slip contours from Laura Wallace). The M4.9 earthquake shown is the one of the largest events used in the initial testing stage of EQTransformer.

Interseismic coupling and Slow Slip Events along the Hikurangi subduction zone seen by geodesy

Maubant, L.[1], Frank, W.[1], Wallace, L.[2,3], Williams, C.[3], Hamling, I.[3], Doin, M-P.[4]

1. *Department of Earth, Atmospheric and Planetary Sciences, Massachusetts Institute of Technology, Cambridge*
2. *University of Texas Institute for Geophysics, Austin, Texas, USA*
3. *GNS Science, Lower Hutt, New Zealand*
4. *ISTerre, Universite Grenoble Alpes, France*

Here, we study the Hikurangi subduction zone (North Island of New Zealand) from Nov. 2014 to Jan. 2022. InSAR studies in New Zealand are particularly challenging due to the dense vegetation cover. The numerous crop fields generate strong biases in the multilooked time series results. These biases can reach several centimeters in amplitude and can be mixed with the tectonic signals. We present different strategies to mitigate these biases and correct their impact on our observations as much as possible. We correct this fading signal using a principal component analysis (PCA). This approach is applied directly to the displacement time series rather than the interferograms. We demonstrate how a PCA applied on the displacement time series can separate the spatial long-wavelength, the coherent tectonic signal from the localized biases. We observe that this latter method yield is more reliable in reducing the impact of these environmental biases than the masking method. It allows us to isolate the interseismic signal across the Hikurangi subduction zone. Using these corrected displacement time series, we then study the inter-SSE period following the Kaikoura earthquake (Nov. 2016, Mw 8.1) to observe if this crustal earthquake has impacted the long-term plate coupling. We integrate the InSAR velocity map to compute a coupling model of the inter-SSE period. We then detrend our time series to be able to extract the signal from the Slow Slip Events (SSEs) and propose a first model of slip using both InSAR and GNSS time series to obtain the slip at depth.

A Probabilistic Framework for Estimating Tectonic Vertical Land Motions for Regional Sea-Level Projections

Ng, G.[1,2], Stevens, V.L.[1], Luo, H.[3], Wang, K.[4,5], Lallemant, D.[1,2], and Hill, E.M.[1,2]

1. *Earth Observatory of Singapore, Nanyang Technological University, Singapore*
2. *Asian School of the Environment, Nanyang Technological University, Singapore*
3. *Department of Earth and Planetary Sciences, McGill University, Montreal, Quebec, Canada*
4. *School of Earth and Ocean Sciences, University of Victoria, Victoria, British Columbia, Canada*
5. *Pacific Geoscience Centre, Geological Survey of Canada, Sidney, British Columbia, Canada*

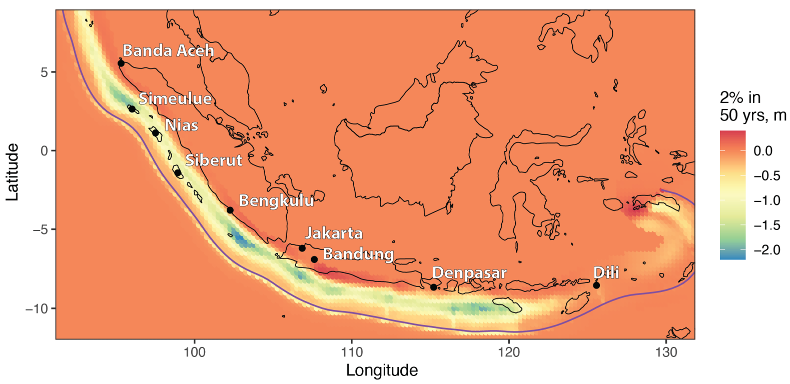

Figure 1. Total vertical land motions at Sumatra subduction zone in 50 years at 2% probability.

Vertical land motions (VLM) are large sources of uncertainties in regional relative sea-level projections. While there are many processes that contribute to VLM, VLM due to tectonics is a major cause of local spatial variability and uncertainty in relative sea-level. To address this uncertainty, we developed a model to estimate, globally, the probability of VLM due to large earthquakes that might occur in a 50-year period at subduction zones. For maintaining global self-consistency, we use globally available datasets as inputs, such as Slab2.0 fault geometries and earthquake rates from the Global Earthquake Activity Rate (GEAR) model instead of focusing on the specifics of each subduction zone. To estimate the VLM from earthquakes, we model coseismic and afterslip motion using an Okada elastic deformation model with elliptical rupture patches for coseismic slip, and afterslip surrounding the coseismic slip rupture area. The postseismic viscoelastic relaxation motion is modeled using parametric approximations of existing finite-element models. We then use a suite of simulations to find a distribution of displacements that might occur for locations around the global coastlines. At each location, we extract the probability that the location will subside more than or equal to a certain amount. Based on our models, we show spatial variability in VLM due to tectonics at various locations near each subduction zone. While some locations experience VLM changes on the order of millimeters to centimeters scale, some locations can expect changes on the order of meters in 50 years with a low probability (Figure 1). The VLM changes are non-negligible and should not be ignored for relative sea-level projections. To check that our modeling is realistic, we show that some events in our catalogue can reproduce both the coseismic and postseismic afterslip behavior of several recent large earthquakes – 2004 M_w 9.2 Sumatra-Andaman, 2010 M_w 8.8 Maule, and 2011 M_w 9.0 Tohoku-Oki events. With further improvements, our framework can be incorporated into sea-level projections that include both climate-related impacts and VLM, providing a critical next step for more accurate mitigation planning.

Evidence for Spatially Heterogeneous Megathrust Fluid Valving in the Northern Hikurangi Subduction System

Warren-Smith, E.[1]

1. *GNS Science, Lower Hutt, New Zealand*

Recent studies observe a temporal link between fluid pressure and slow slip event (SSE) cycles in subduction zones via a 'valving' model. However, it remains unclear if this is a spatially distributed process or whether discrete sites are responsible for valving fluid, and over what length scale this occurs. Spatial localisation of valving would enable specialised, targeted experiments to be designed to monitor temporal changes in physical properties occurring in these zones, and better relate their occurrence with slow earthquake cycles.

Here we consider microseismicity datasets alongside geophysical observations from New Zealand's Northern Hikurangi Margin to identify spatially heterogeneous hydrological coupling between the two plates. We identify patches of co-located, differing seismic behaviour, including: interface micro-seismicity, pre-SSE swarms, lower plate strike-slip earthquakes, upper plate swarms and elevated Vp/Vs zones. These patches correlate well with conductive interface regions constrained by magnetotelluric studies and thermal springs exhibiting mantle chemical signatures. We propose these patches represent 'valve' sites at the 10s of kilometre scale, where hydrological coupling between the plates is transiently increased, facilitating episodic fluid valving which may be linked to SSE timing.

We propose these 'valve' sites may be physically related to heterogeneities in permeability along the plate interface, most likely from entrained oceanic mafic fragments, including seamounts, or from localised fluid reservoirs linked to bending related fracturing within the lower plate. These observations contribute to a growing consensus that subduction megathrust faults are inherently heterogeneous, and these heteronegeneities in frictional and fluid related properties may play a role in their ability to host a spectrum of deformation modes.

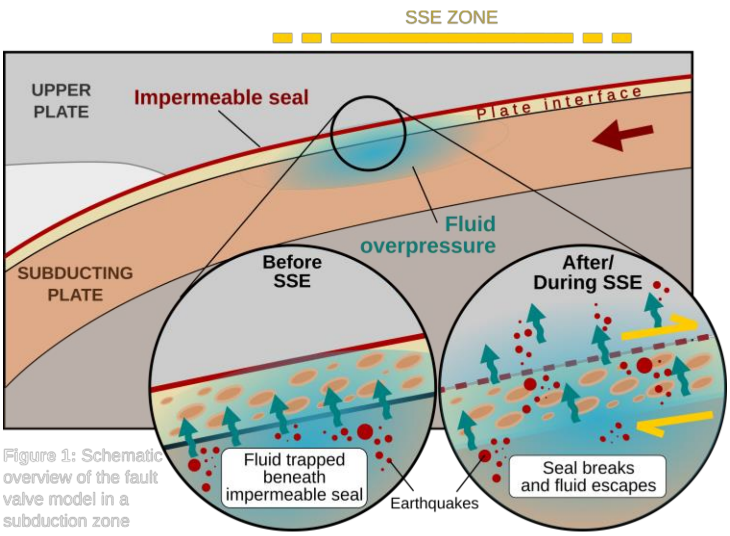

Figure 1. Schematic representation of the fault-valve model during slow slip in a subduction system.

A Compilation of Coseismic Temperature Rise and it's Application to the Earthquake Energy Budget

Coffey, G.[1], Savage, H.[2], and Polissar, P.[2]

1. *GNS Science, Lower Hutt, New Zealand*
2. *University of California Santa Cruz, Santa Cruz, USA*

Over the last two decades an increasing number of paleotemperature proxies have been developed, which have facilitated a growing dataset of coseismic temperature measurements across a variety of faults around the world. During an earthquake, temperature along a fault increases rapidly in response to frictional heating. This temperature rise exerts an important control on the chemical and mechanical behaviour of faults and can lead to dramatic weakening during coseismic slip. Furthermore, temperature rise can be used to constrain the frictional energy during an earthquake, that is, the energy dissipated as heat. As a result, understanding temperature rise across numerous faults can provide insight into the processes that may govern fault strength during sliding and it enables quantification of frictional energy for an increasing number of faults.

Here, we present a compilation of coseismic temperature and frictional energy estimates across numerous faults, which were constrained using a range of paleotemperature proxies (e.g. biomarkers, pseudotachylyte, and vitrinite reflectance). With this data we attempt to understand how coseismic temperature rise varies across different faults, place constraints on the frictional energy component of the earthquake energy budget, and explore how energy is partitioned into different sinks depending on earthquake properties such as displacement and depth.

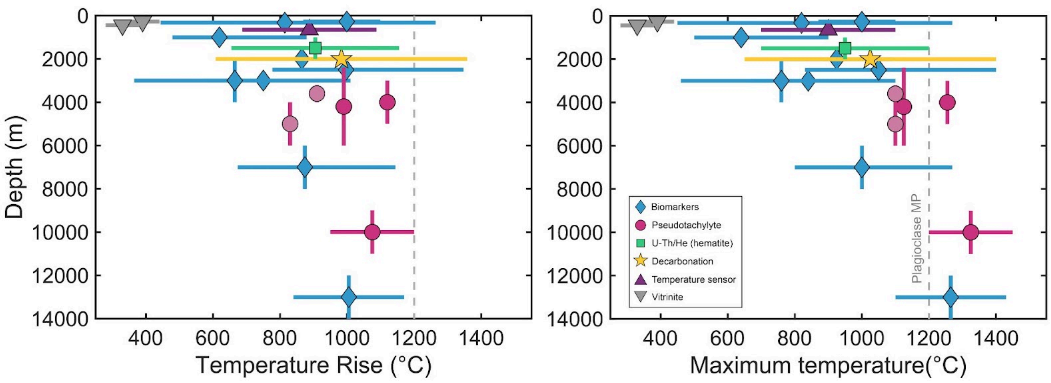

Figure 1 - Plots of compiled coseismic temperature rise (left) and maximum temperature (right) data as a function of depth and colour-coded based on temperature proxy. Pale pink points are minimum bounds on temperature.

Our compilation demonstrates that coseismic temperature rise increases with the depth of faulting until ~ 5 km after which it remains relatively constant. We also see that frictional energy across the faults included here is remarkably similar, most falling below 45 MJ/m^2. It is possible that dynamic weakening mechanisms may limit frictional energy and temperature rise during coseismic slip, particularly during large events where displacement is higher. To explore this further we compare frictional energy to other components of the earthquake energy budget and demonstrate a fundamental difference between small and large (> 3 m of displacement) earthquakes. That is, the earthquake energy budget of small earthquakes is dominated by frictional energy, while for larger earthquakes the energy involved is relatively balanced across frictional, radiated, and fracture energy.

11th ACES International Workshop, Blenheim, 28 February – 3 March, 2023

Mapping Stress Drop Variability Along the Alpine Fault

Juarez-Garfias. C.[1], Warren-Smith, E.[2], Townend, J.[1], and Abercrombie, R.[3]

1. *SGEES, Victoria University of Wellington, Wellington 6140, New Zealand*
2. *GNS Science, Lower Hutt, New Zealand*
3. *Boston University, Massachusetts, US*

The Alpine Fault is an active transform that represents the boundary between the Pacific and Australian plates. It is late in its typical cycle of large earthquakes: extensive paleoseismic research has revealed that the Central Section of the Alpine Fault ruptures in M7+ earthquakes every 249±58 years and last ruptured in 1717 AD. The paleoseismic results also reveal that some locations along of the fault, which coincide with pronounced along-strike changes in fault characteristics, act as conditional barriers to rupture. The geometry, seismicity rates and geology of the Alpine Fault change along three principal sections (North Westland, Central and South Westland Sections) but it is unclear whether source properties of near- and on-fault seismicity also vary between those fault sections, and whether these properties can elucidate, or have some influence on the conditional segmentation of the Alpine Fault during large earthquake rupture. To examine this, we calculate stress drops of moderate-magnitude earthquakes (M_L1.8–4.2) occurring on or near the Alpine Fault, using an empirical Green's function approach. We use data from dense, temporary seismometer networks, including DWARFS (Dense Westland Arrays Researching Fault Segmentation), a new two-part network designed to constrain seismogenic behaviour near key transitional boundaries on the Alpine Fault. We make separate P- and S-wave measurements of corner frequency and stress drop for 120 earthquakes occurring within 10 km of the Alpine Fault. Overall, the calculated stress drops range between 1 and 409 MPa and show good agreement with other New Zealand and global studies. We obtain median stress drop values of 12 and 14 MPa (for P- and S-waves, respectively) for the South Westland–Central section boundary zone, 23 MPa (for both P- and S-waves) for the Central Section, and 15 and 20 MPa (for P- and S-waves, respectively) for the North Westland–Central Section boundary zone. We observe no pronounced differences in stress drop along the North Westland and Central Sections, but those values are slightly higher than along the South Westland–Central section boundary.

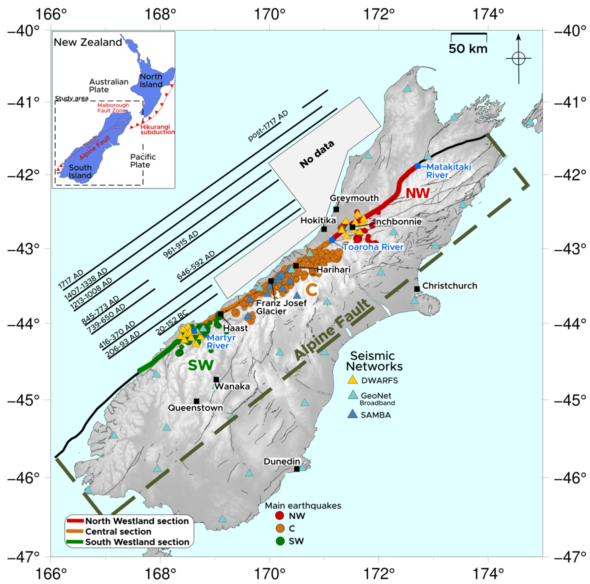

Figure 1. Earthquakes analysed using the Empirical Green's Function method. Green, orange and red circles denote earthquakes along the South Westland., Central, and North Westland Sections, respectively, scaled by magnitude. Yellow triangles are DWARFS stations deployed from 2019 to 2020. Blue triangles are broadband GeoNet stations and light blue triangles are SAMBA stations. Black lines represent the inferred rupture extents of the most recent large Alpine Fault earthquakes recognised paleoseismically.

Dynamic simulations of coseismic slickenlines on non-planar and rough faults: Towards inferring the rupture directions of paleoearthquakes

Aoki, T. [1], Kaneko, Y.[1], Kearse, J.[2]

1. *Kyoto University, Kyoto, Japan*
2. *Victoria University of Wellington, Wellington, New Zealand*

Knowing the directions of rupture propagation of paleo-earthquakes is a challenging, yet important task for our understanding of earthquake physics and seismic hazard, as the rupture direction significantly influences the distribution of strong ground motion. Recent studies proposed a relationship between the direction of rupture propagation and curvature of slickenlines formed during seismic slip [Kearse and Kaneko, 2020]. The relationship was established using a global catalogue of historic surface-rupturing earthquakes and dynamic models of idealized, planar faults. At the same time, some slickenlines previously documented on geometrically complex fault segments show their convexity opposite from the simple model prediction, which we refer to as `abnormal convexity'. To explain such observations, we perform simulations of spontaneous earthquake ruptures on non-planar and rough faults. We find that a non-planar fault model can lead to abnormal convexity of slickenlines in places where the fault geometry (e.g., dip angle) changes abruptly. In the case of strike-slip faults, abnormal convexity of slickenlines is produced when the initial along-dip stresses are larger than, and are opposite in direction to, the dynamic stresses imparted by the mixed-mode rupture. Such results are also confirmed in our rupture simulations with a rough fault. Our results also show that the parameter space for which abnormal convexity of slickenlines occurs near Earth's surface is narrow, especially when the fault strength and initial shear stresses increase with depth. Nevertheless, slickenlines on geometrically complex faults need to be carefully interpreted and investigation of rupture direction using curved slickenlines should focus on structurally simple parts of faults.

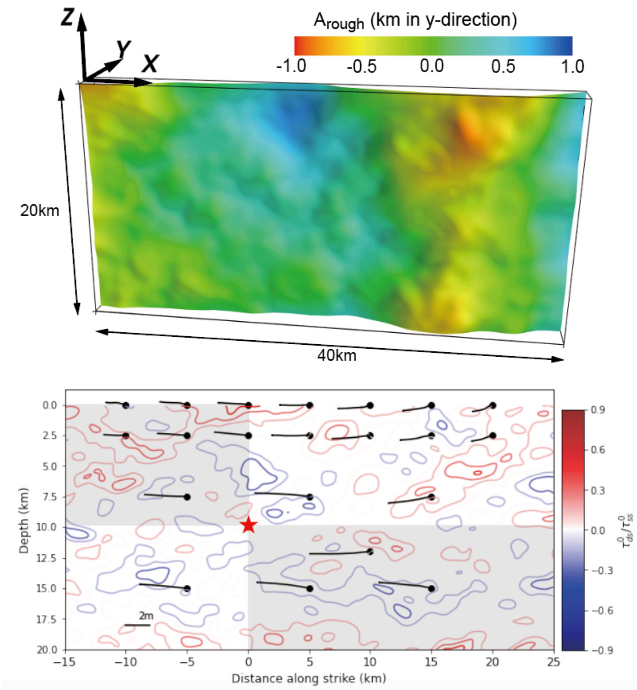

Figure 1. Model of a rough fault (top) and the corresponding synthetic slickenlines (bottom). The convexity of slickenline curvature is affected by the change in local dip angle.

Seismotectonics of the 27 July 2022 M_w 7.0 Northwestern Luzon Earthquake: Insights from field investigation, seismicity and InSAR analysis

Llamas, D.C.E.[1,2], Perez, J.S.[1], Constantino, R.C.C.[1], Dizon, M.P. [1], Buhay, D.J.L. [1], Grutas, R.N. [1], Lagunsad, K.D.B. [1], Legaspi, C.J.M. [1], De Leon, R.J.B. [1], Quimson, M.M.Y. [1], Pitapit, R.S.D. [1], Rocamora, C.G. H. [1], and Pedrosa, M.G.G. [1]

1. *Department of Science and Technology - Philippine Institute of Volcanology and Seismology (DOST-PHIVOLCS), Quezon City, Philippines*

2. *National Institute of Geological Sciences, University of the Philippines, Quezon City, Philippines*

On 27 July 2022, a magnitude (M_w) 7.0 earthquake struck Northwestern Luzon, Philippines – a region traversed by the northern splays of the Philippine Fault (Figure 1B), an ~1,500 km-long sinistral fault, traversing the entire Philippine archipelago. The occurrence of this earthquake provides a rare opportunity to understand how these faults accommodate the deformation derived from plate motion (Figure 1A). Here we attempt to assess the seismotectonics of the earthquake based on the surface deformation observed from InSAR, seismicity analysis and post-earthquake field investigation.

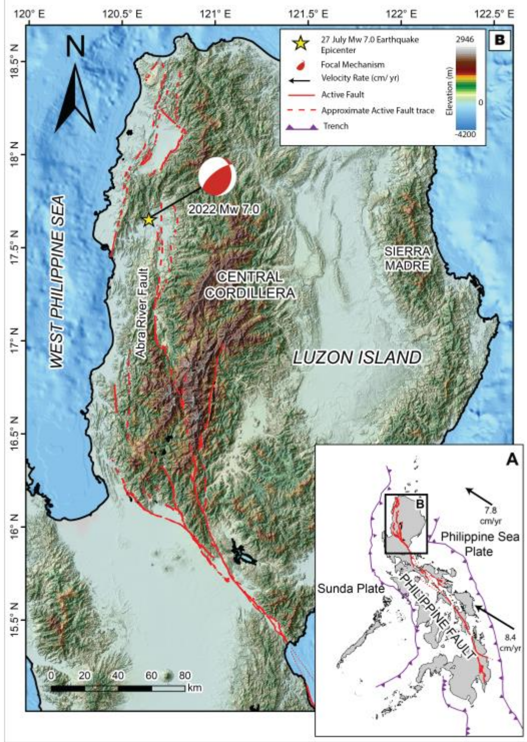

Figure 1. Tectonic setting of the 2022 Mw7.0 Northwestern Luzon earthquake. The Philippine Faut bifurcates into several splays in northern Luzon.

Earthquake data, including focal mechanism solution and aftershock distribution, indicate that the earthquake was generated by an almost north-south striking reverse left-lateral oblique fault that is gently dipping to the east. Surface deformation, with peak line-of-sight displacement of 14 cm, observed from InSAR is concentrated on the east side of the Abra River Fault (which is the hanging wall), a typical characteristic of thrust motion as this earthquake has a significant amount of reverse slip component. We interpret that the causative fault is a part of the positive flower structure at a depth that connects to the steeply dipping Abra River Fault (steepening upward) - which can explain the gentle dip and oblique-slip of the preferred fault plane at depth. The spatial distribution of geologic impacts, such as earthquake-induced landslides and liquefaction, suggests a southward direction of rupture propagation, consistent with southward increase in peak ground acceleration (PGA) values. The transpressive nature of the fault contributes to the continuous uplift of the Central Cordillera. Although earthquake, geodetic and field data suggest that the Abra River Fault is the probable causative fault, the derived geometry and kinematics challenge our understanding of the nature of the Abra River Fault, as well as the other segments of the Philippine Fault. The need to understand these earthquake sources in the country is needed for a better seismic hazard and risk assessment.

11th ACES International Workshop, Blenheim, 28 February – 3 March, 2023

Source fault characteristics of the 21 June 2022 M_W6.0 Afghanistan earthquake

Marfito, B.[1,2], Salman, R.[1,2], Way, L.[1,2], Liang, C.[3], Wang, K.[4], Bürgmann, R.[4], and Yun, S.H.[1,2,5]

1. *Earth Observatory of Singapore, Nanyang Technological University, Singapore*
2. *Asian School of the Environment, Nanyang Technological University, Singapore*
3. *Institute of Remote Sensing and Geographic Information System, Peking University, China*
4. *Earth and Planetary Science, University of California, Berkeley, United States of America*
5. *School of Electrical and Electronic Engineering, Nanyang Technological University, Singapore*

An M_W 6.0 earthquake struck 55 km west of Khöst, Afghanistan on 21 June 2022 with a depth of 4.0 km (USGS [2022]). The earthquake's epicenter is within the North Waziristan-Bannu Thrust Fault System (Ruleman et al. [2007]). This earthquake also triggered numerous landslides and damaged houses which caused more than 1,500 injuries and at least 1,000 deaths in Paktika and Khöst provinces (Aljazeera [2022]).

We produced Sentinel-1 line-of-sight displacements (InSAR) (Figure 1) and ALOS-2 along-track displacements (Multiple Aperture Interferometry) and study the source characteristics of the earthquake. We performed non-linear modeling to estimate the fault geometry, and linear modeling to estimate the coseismic slip distribution. Our preliminary models indicate that the earthquake was generated by a NE-SW trending, NW-dipping left-lateral fault. Our models also show that most of the coseismic slip occurred above a depth of 8 km, with a peak slip of 2.3 to 2.5 m at a depth of 3 km.

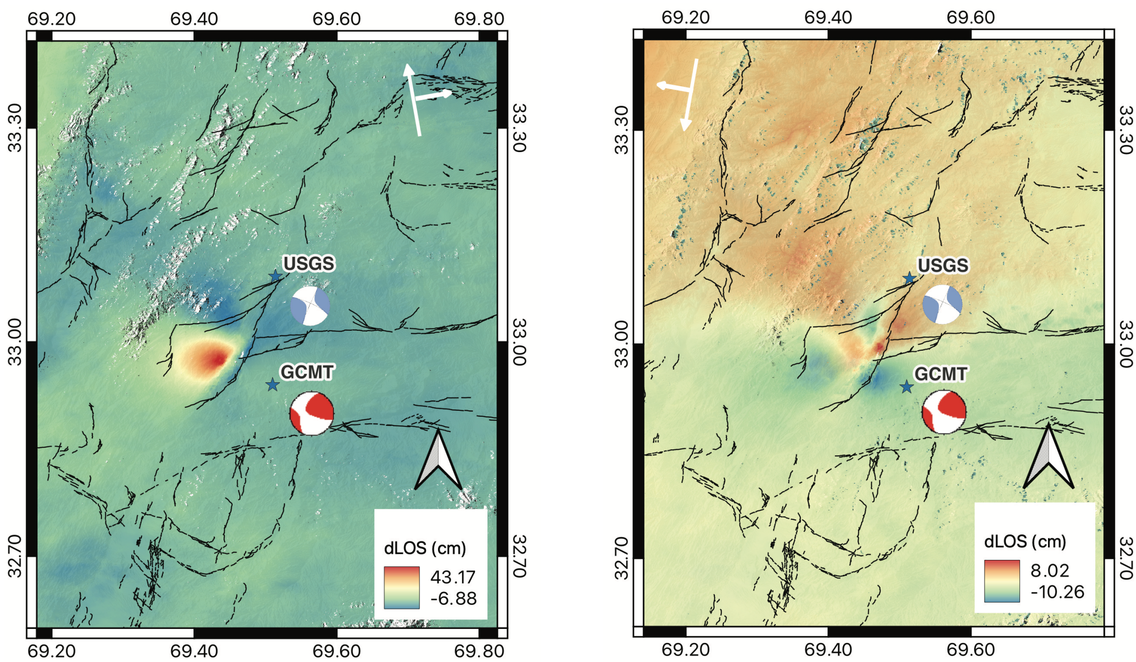

(A) (B)

Figure 1. (A) Sentinel-1 ascending, and (B) descending line-of-sight deformation maps of the 21 June 2022 M_W6.0 Afghanistan earthquake. The black lines are the mapped faults from Ruleman et al. [2007], and the two blue stars are the epicentral locations from USGS and GCMT.

Understanding fault roughness effects on microearthquake rupture behavior through 3D dynamic rupture simulations

Palgunadi, K. H.[1], Vyas, J. C.[1], Gabriel, A.-A.[2,3], Tinti, E.[4,5], Cocco, M.[5], and Mai, P. M.[1]

1. *Physical Science and Engineering, King Abdullah University of Science and Technology, Thuwal, Saudi Arabia*
2. *Department of Earth and Environmental Sciences, Geophysics, Ludwig-Maximilians-Universität München, Munich, Germany*
3. *Institute of Geophysics and Planetary Physics, Scripps Institute of Oceanography, University of California, San Diego, California, USA*
4. *Department of Earth Sciences, Universitá La Sapienza, Rome, Italy*
5. *Instituto Nazionale di Geofisica e Vulcanologia, Rome, Italy*

Geometric fault complexity (e.g., fault curvature, fault roughness, fracture networks) affects the spatio-temporal evolution of earthquake rupture. Fault roughness causes rupture front acceleration/deceleration leading to strong high frequency energy radiation. These effects have generally been studied using 3D dynamic rupture simulations for large earthquakes, but remain poorly investigated for small events ($M_w < 4$). Laboratory experiments have shed light on rupture evolution on rough faults (e.g., Ohnaka, 2013; Ji and Wu, 2020; Ji et al., 2022) for miniature “lab-quakes”, where it remains unclear how to upscale these findings to natural earthquakes. Therefore, physics-based simulations of microearthquake are needed to bridge the gap between large natural earthquakes and the laboratory scale. For this purpose, we perform 3D dynamic rupture simulations on planar and rough-fault geometries to understand rupture behaviour for small-magnitude earthquakes ($M_w \sim 1$).

Our simulations use laboratory-based rate-and-state friction law with rapid velocity weakening to resolve rupture on small faults (50m x 50m) targeting $M_w \sim 1$. Rupture dynamics and wave propagation are computed using SeisSol (https://github.com/SeisSol/SeisSol). We parameterize fault roughness using a band-limited self-similar (Hurst exponent H=1) fractal surface with an amplitude-to-wavelength ratio α that ranges from 0.005 to 0.01. Our assumed initial stress conditions follow Andersonian faulting theory for a normal to strike-slip regime. Preliminary results show that rupture remains confined to the nucleation area in case of unfavorably oriented horizontal maximum stress SHmax, whereas runaway rupture occurs if SHmax is aligned on both the planar and the rough fault. Qualitatively, ruptures on the planar or rough fault show minimal differences. This suggests that fault roughness on the scale considered in these preliminary simulations has little influence on the rupture process. If this observation is confirmed with further refined simulations for varying stress, friction, and roughness parameterizations, the result may shed light on differences in rupture initiation and propagation on immature fault zones compared to well-developed mature faults.

The earthquakes (1929-1991) in the northwestern part of the South Island, New Zealand, and their relationship with the stress field

Tagami, A.[1], Matsuno, M.[1],Okada, T.[1], Matsumoto, S.[2], Kawamura, Y.[2], Iio, Y.[3], Sato, T.[1], Hirahara, S.[1], Kimura, S.[1], Bannister, S.[4], Ristau, J.[4], Townend, J.[5], Savage, M.[5], Thurber, C.[6], and Sibson, R.[7]

1. *Research Center for Prediction of Earthquakes and Volcanic Eruptions, Graduate School of Science, Tohoku University, Sendai, Japan*
2. *Institute of Seismology and Volcanology, Faculty of Science, Kyushu University, Shimabara, Japan*
3. *Disaster Prevention Research Institute, Kyoto University, Uji, Japan*
4. *GNS Science, New Zealand*
5. *Victoria University of Wellington, New Zealand*
6. *University of Wisconsin - Madison, United States of America*
7. *University of Otago, New Zealand*

Stress fields of ESE-WNW oriented compression are widely distributed in the northern part of South Island [Townend et al., 2012]. Also, many old normal faults developed due to the old extensional stress fields widely distributed in this region, and tectonic inversion under compressional stress, in which the normal faults have been re-activated as reverse faults, has been confirmed [Ghisetti et al., 2014].

In this study, we focused on five large to moderate-sized earthquakes. We investigated the relationship between the fault planes of these earthquakes and the stress field. First, we estimated the stress field using the focal mechanisms obtained by temporal and permanent stations [Okada et al., 2019; Lanza et al., 2019; Matsuno et al., 2022] and the GeoNet moment tensor solutions. Then, using the Slip Tendency analysis [Morris et al., 1996] we evaluated the likelihood of slip for fault planes. For ST analysis, we use the nodal planes of the focal mechanisms estimated by Anderson et al. [1993] and Doser et al. [1999] for the fault plane data.

Results

The 1929 Buller earthquake (BUL-1, Mw 7.3): The eastward-dipping plane shows a large ST value (>0.7). This is consistent with the White Creek Fault, on which the earthquake occurred [e.g., Doser et al., 1999].

The 1962 Westport earthquake (WES, Mw 5.6): The eastward-dipping plane, which shows a large ST value (>0.7), is a possible fault plane from the ST analysis.

The 1968 Inangahua earthquake （INA, Mw 7.2）: Both planes show a large ST value (>0.7). Note that Anderson et al. [1994] estimated that the westward dipping plane might slip in this event.

The 1971 Maruia Springs earthquake (MAR, Mw 5.7): Both nodal planes have small ST values (<0.7)and are unlikely to slip. The stress change by the previous earthquakes (BUL-1 and INA) might affect this earthquake.

The 1991 Hawks Crag earthquake (HC2, Mw 6.0): We focused on a foreshock (HC1, Mw 5.8) and an aftershock (HC2, Mw 6.0). In the case of HC1, the low dip angle plane, which has a large ST value (>0.7), is a possible fault plane from the ST analysis. In the case of HC2, both nodal planes show a large ST value (>0.7).

Foreshock Sequences in Western Yunnan, Southwest China

Gaohua Zhu[1,2], Hongfeng Yang[2]

1. CAS Key Laboratory of Marine Geology and Environment, Center for Ocean Mega-Science, Institute of Oceanology, Chinese Academy of Sciences, Qingdao 266071, China

2. Earth and Environmental Sciences Programme, Faculty of Science, The Chinese University of Hong Kong, Shatin, Hong Kong, China

Although the physical mechanism of earthquake nucleation processes is under debate and it is still challenging to distinguish foreshocks during an ongoing seismic sequence, foreshocks may still provide unique and valuable information for earthquake nucleation process. Investigating the temporal and spatial evolution of foreshock sequences with high resolution and monitoring *b*-values in real time may shed light on these key issues.

Many foreshock and aftershock sequences accompanying moderate mainshocks have been reported in the west of Yunnan Province, China, such as the 2016 Eryuan (blue dots in Fig.1b) and 2021 Yangbi (green dots in Fig.1b) earthquake sequences. The nice coverage of seismic network in western Yunnan provides the opportunity to investigate how the foreshock sequence evolved and establish the temporal transient in *b* values. We built comprehensive earthquake catalogs using a machine-learning phase picker and the template matching method, and then investigated the space-time evolution and key source parameters of the foreshocks. The observed spatial patterns of 2021 Yangbi sequence suggest a triggered cascade of stress transfer. The results can contribute to decoding the role of foreshocks in earthquake nucleation.

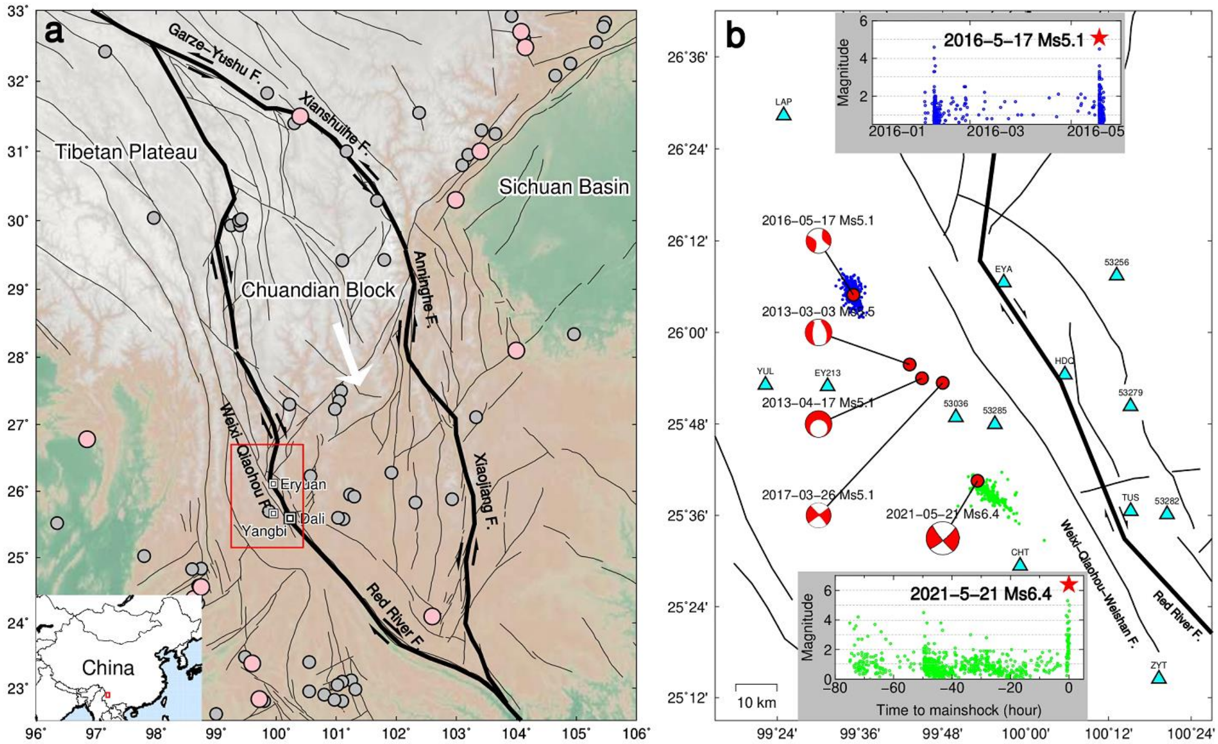

Fig. 1 The tectonic map and historical large earthquakes (pink dots: M>7.0; gray dots: 7>M>6) surrounding the study region. (b) The seismic stations (triangles) and two example foreshock sequences.